공학박사 학위논문

Cyclic Shear Behaviors of Geosynthetic-Soil Interface considering Chemical Effects

화학적 영향을 고려한 토목섬유-흙 접촉면의 동적전단거동

2014 년 8 월

서울대학교 대학원

건설환경공학부

곽 창 원

Cyclic Shear Behaviors of Geosynthetic-Soil Interface considering Chemical Effects

지도 교수 박 준 범

이 논문을 공학박사 학위논문으로 제출함

2014년 7월

서울대학교 대학원

건설환경공학부

곽 창 원

곽창원의 공학박사 학위논문을 인준함

2014년 6월

위 원 장 _____ **(인)**

부위원장 _____ **(인)**

위 원 _____ **(인)**

위 원 _____ **(인)**

위 원 _____ **(인)**

Abstract

Cyclic Shear Behaviors of Geosynthetic-Soil Interface considering Chemical Effects

Kwak, Changwon

Department of Civil & Environmental Engineering

The Graduate School

Seoul National University

Geosynthetics have been widely applied in waste landfill site for reinforcement, filtration, drainage, protection, and separation. Geosynthetics inevitably contact soil particle directly, composing a geosynthetic-soil interface corresponding to the external forces and conditions. The differences in the intrinsic material characteristics at the interface induce complicated stress-strain behaviors and nonlinear responses. Recent studies have presented the behaviors of geosynthetic-soil systems are subjected to the interface shear strength degradation, which is affected by ambient factors such as the magnitude of normal stress, type of external loading and chemical conditions.

In this study, particularly, the effects of chemical aggressors such as acidity and basicity from the leachate on the geosynthetic-soil interface were intensively investigated under cyclic shear loading to consider the dynamic condition, based on the experimental approach. The Multi-purpose Interface

Apparatus (M-PIA) which is able to simulate the cyclic simple shear conditions of the interface was newly manufactured and modified for better performance. 72 sets of cyclic simple shear tests were conducted to inspect the effects of the *p*H values of leachate on the shear behavior of the geosynthetic-soil interface. Both geosynthetics and Jumunjin sand were submerged in acid, neutral, and basic solutions for 30 days and 850 days, representing relatively short-term and long-term behaviors of the interface, respectively. Test results displayed remarkable distinction in chemical degradation trends according to the *p*H values. The Disturbed State Concept (DSC) and disturbance function were introduced and employed to estimate shear stress degradation based on the experimental study, quantitatively. New disturbance functions and parameters that determine the characteristics of shear strength at the interface were mathematically evaluated. Furthermore, microscopic observation by Focused Ion Beam (FIB) was introduced and utilized to clarify the reason of the variation of interface damage subjected to the chemical conditions. As a result, the variation of the cyclic shear behavior at the geosynthetic-soil interface was due to the different damage patterns of the soil particle surface.

Based on the experimental approach, the numerical back-prediction based on the DSC parametric study of the cyclic shear stress-strain behavior was performed to verify the accuracy and applicability of the DSC parameters. The back-prediction utilized the numerical interpolation from the test results and enabled to consider the shear stress degradation as load cycles, successfully. The shear strains were obtained from the average shear strain increment from the disturbance function curve and updated according to the

load cycles. The comparison results between the experimental data and back-predicted results were found to be in good agreements. Consequently, a general methodology to estimate the cyclic shear stress degradation of geosynthetic-soil interface considering chemical effects has been established and verified.

Keywords : Geosynthetic-Soil interface, Chemical conditions, Multi-Purpose Interface Apparatus (M-PIA), Cyclic simple shear tests, Disturbed State Concept (DSC), Focused Ion Beam (FIB), Numerical back-prediction

Student Number : 2010-30237

TABLE OF CONTENTS

LIST OF TABLES

LIST OF FIGURES

1. Introduction

1.1 Background

Majority of earth structures involve the combination of different medium due to the diversity of construction area, method, and materials. The area formed between adjacent materials is called as “interface”. In engineering systems, discontinuities exist at the interface and overall system shows discontinuous behavior due to the discontinuities. Therefore, the theoretical approaches based on continuum mechanics may exhibit limitations to characterize the response of an interface. Furthermore, the difference of intrinsic material properties at interface entails complicated problems; therefore this subject has been treated as an important issue and studied for a long time.

Coulomb’s law of friction can be considered to be the first formal constitutive model to describe the response of two bodies in contact (Desai, 2001). The tangential or shear force parallel to the plane of contact, F can be expressed as the multiplication between the coefficient of friction, μ, and normal force to the contact. This law is only valid for dry friction between rigid bodies and assumes μ to be constant. Practically, as shown in Figure 1.1, the contact surface involves asperities, and the material body deforms due to external loads. Then, Oden and Pires (1983) presented modified equation considering the limitation of Coulomb’s law in Equation 1.1,

$$F = A_r\, s \tag{1.1}$$

where, s is the average shear strength of the interface and A_r is the weighted actual contact are given by,

$$A_r = A_1 + A_2 + \cdots = \frac{N_1}{p_0} + \frac{N_2}{p_0} + \cdots = \frac{N}{p_0} \tag{1.2}$$

where, $A_1, A_2, \cdots$ are the contact areas of individual deforming asperities, $N_1, N_2, \cdots$ are the normal loads on the asperities, and p_0 is the approximately constant local plastic yield pressure. Combining Equation 1.1 and 1.2 yields,

$$F = \frac{s}{p_0} N = \mu N \tag{1.3}$$

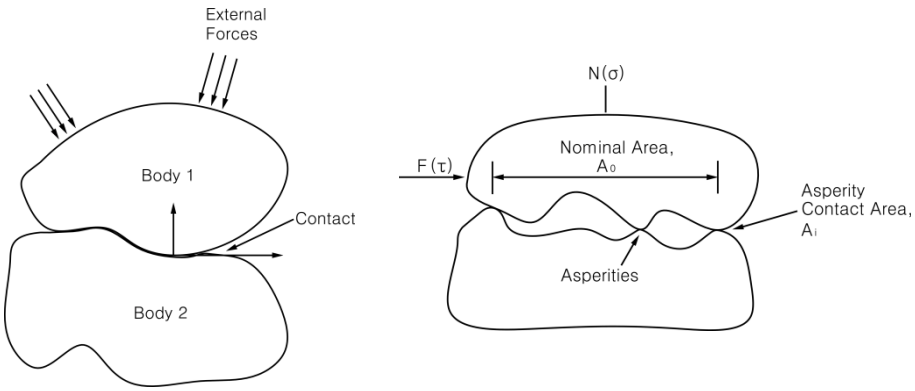

(a) Contact between two bodies (b) Contacts at asperities

Figure 1.1 Schematic of contact and asperities (modified after Desai, 2001)

Afterward, there have been diverse ways based on the strength, limit equilibrium, elastic and elasto-plastic theories to define the force at the interface (Desai, 1981).

In geotechnical engineering field, the interface displays various types as shown in Figure 1.2.

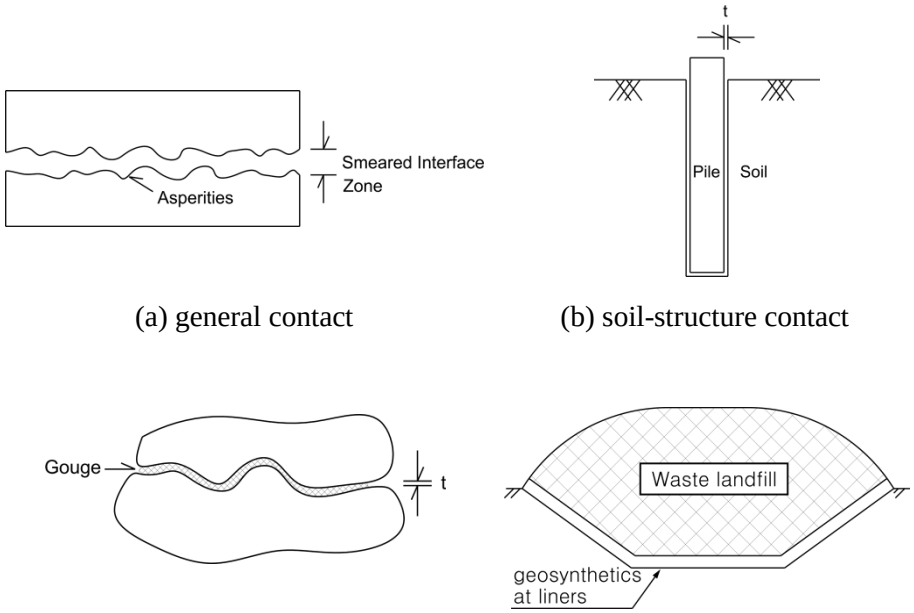

(a) general contact (b) soil-structure contact

(c) rock joint with or without gouge (d) geosynthetic-soil contact

Figure 1.2 Types of interfaces (modified after Desai, 2001)

With rapid industrialization, the quantity of waste has increased, continuously. Waste shows different forms and may degrade into harmless products, or be nondegradable, or even be hazardous. Hazard wastes have potential risks to human health and ecosystem; therefore, waste should be classified and treated according to its physical and chemical characteristics. Worldwide, landfilling is the most popular means of hazardous and municipal waste disposal because it can be a relatively safe and cost effective if conducted based on precise design and managed with sufficient care (Orloff and Falk, 2003). However, landfills were also identified as one of major threats to groundwater resources (Mor et al., 2006), therefore, hazardous and

municipal waste landfill facilities require lining and covering systems that are mainly organized by geosynthetics and soils. All types of geosynthetics in all identified functions such as reinforcement, filtration, drainage, protection, and separation have used in the facilities. These geosynthetic systems are nowadays an accepted and well established component of the landfill industry (Bouazza et al., 2002). Geosynthetic-soil interface inevitably appears at the waste landfill site (see Figure 1.2 (d)).

An important characteristic of these liner systems with respect to their stability is the shear resistance along the interface between the various liner or cover system components (Stark et al., 1996). The behaviors of geosynthetics are strongly related to the characteristics of the geosynthetic-soil interface because the geosynthetic comprises an interface area around itself corresponding to the external forces, friction, stiffness, etc. Therefore, various studies on the shear behavior of the interface have been performed (Seo et al., 2007; Seo et al., 2004; Ling et al., 2002; De and Zimmie, 1997; Gilbert et al., 1997; Fishman and Pal, 1994).

Recently, a number of researches have focused on a few important factors such as chemical substances, dynamic load and their effects on the behavior of the interface. Leachate generated through the chemical and biological process possesses aggressive chemical substances and affects the behavior of the interface by leaching or combination with other substances in the interface material, and this effect has not been studied intensively yet. In addition, the effect of dynamic loading on the geosynthetic-soil interface can be very significant because dynamic loading can induce various modes of motion such as slip, loss of contact or de-bonding, and re-contact or re-

bonding at the interface (Navayogarajah et al., 1992). Moreover, the failure of the waste containment facilities requires high cost of recovery due to the transportation, deposit, treatment of the refuse. Therefore, seismic stability is very important in the design and analysis of the waste landfills. Figure 1.3 displays a few pictures of the seismic failure in the waste landfill sites, reported in USA.

(a) Superficial cracking of cover soils at Sunshine Canyon Landfill

(b) Tear in Chiquita Canyon Landfill geomembrane

Figure 1.3 Seismic failure in waste landfill sites liner (Northridge earthquake, M=6.7, 1994) (Matasovic et al., 1998)

Experimental approach is most critical and vital because the shear behavior of the interface is affected by many practical factors and shows complex response under specific conditions. Stessel and Hodge (1995) performed chemical resistance tests of geomembrane liners and showed that the chemical aggressor caused no significant change in the physical characteristics of the geomembrane, however, cyclic loads were able to accelerate the manifestation of the effects of chemical attack. In the previous researches, the chemical agents showed a particularly severe effect on raw materials of geosynthetic because the chain scission leads to a decrease in molecular weight and makes the material brittle and more prone to environmental cracking (Hawkins, 1984; Tisinger and Giroud, 1993). However, recent technologies of material, antioxidants and chemical additives to alleviate chemical decay have been advanced and verified. Koerner et al. (1988) confirmed the chemical stability of polyethylene containing antioxidants over a wide range of *p*H solutions. Jeon et al. (2006) conducted an experimental study to confirm the chemical resistance of a nonwoven geotextile made of polypropylene and its composite. The results reported the polypropylene geotextile maintained about 95 % of its initial strength in waste landfill leachate.

Even though these experimental results and theoretical development are valuable, there are still some limitations because these studies only focused on the geosynthetic material itself, not on the geosynthetic-soil interface. Furthermore, the dynamic response of the geosynthetic-soil interface under the chemical conditions was not investigated minutely in most studies.

Therefore, the main object in this study is the geosynthetic-soil interface

in the waste landfill site, as shown in Figure 1.4. Chemical conditions of leachate were also considered by *p*H solutions because submerged soil interacts with ion sources of oxides and hydroxides. The soil conditions under various substances which are rendered soluble and removed through leaching or combination with other substances appear to depend mainly on the *p*H of the surround liquid (Gidigasu, 1976). Moreover, the *p*H in leachate is considered to be the most significant parameter affecting leachate concentration (Rafizul and Alamgir, 2012). Therefore, *p*H values of the solutions are one of the mainly governing factors to characterizing leachate and can represent the chemical conditions.

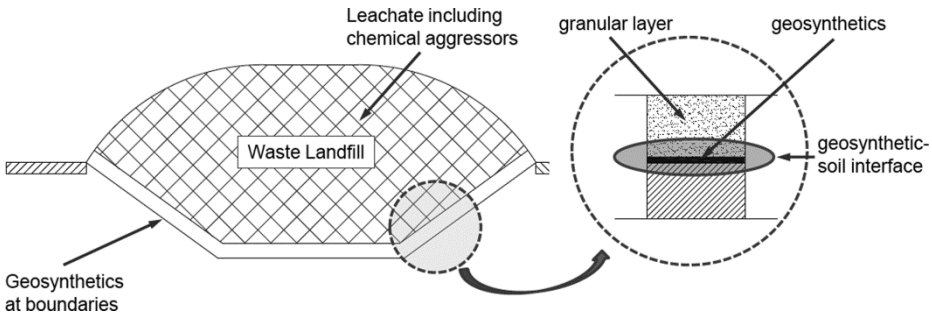

Figure 1.4 Main object of the present study

Cyclic simple shear tests were performed to investigate dynamic shear response of the interface because the seismic stability must be considered in accordance with the Article 35 of Waste Management Enforcement Regulations and in Korea. A Multi-Purpose Interface Apparatus (M-PIA) was newly manufactured and modified for the experimental approach. 72 sets of cyclic simple shear tests were performed to investigate the effects of the *p*H

values of leachate on the shear behavior of the geosynthetic-soil interface. Both geosynthetics and Jumunjin sand were submerged in acid, neutral, and basic solutions for 30 days and 850 days, representing relatively short-term and long-term behaviors of the interface, respectively. The Disturbed State Concept (DSC) and disturbance function were introduced and utilized to estimate shear stress degradation based on the experimental study, quantitatively. The convenience and reliability of the DSC have been successfully verified in the previous research (Armaleh and Desai, 1990; Ma, 1990; Rigby and Desai, 1995; Park et al., 2000).

Furthermore, microscopic observation by the Focused Ion Beam (FIB) was conducted to clarify the reason of the variation of interface damage subjected to *p*H of 4.0, 7.0, and 10.0. Based on the experimental and microscopic approach, the numerical back-prediction of the cyclic shear stress-strain relationship was accomplished based on the parametric study. The numerical back-prediction results were compared with the experimental data obtained by the cyclic simple shear test in all chemical conditions to verify the accuracy and applicability of the DSC parameters.

The overall scope and procedures of the present research was displayed in the form of a flowchart in Figure 1.5.

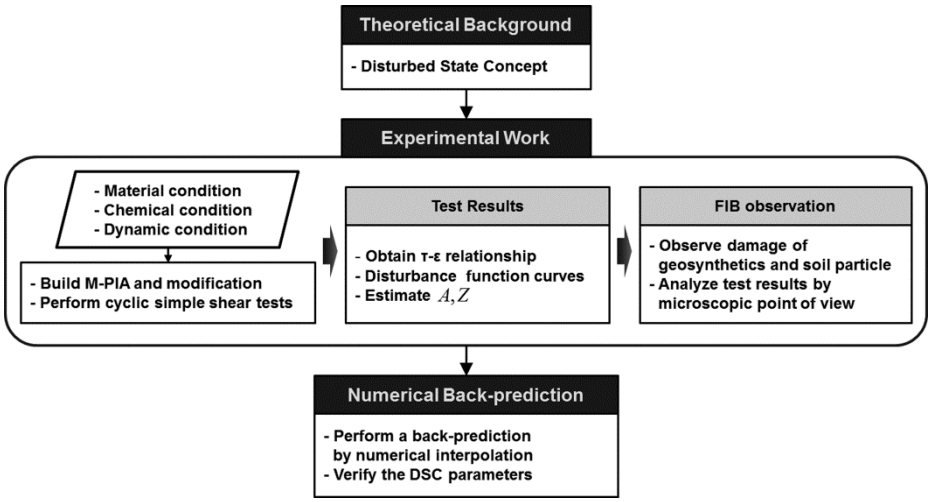

Figure 1.5 Scope and procedures of the present study

1.2 Objective

The comprehensive objective of this research is to investigate cyclic shear behaviors of geosynthetic-soil interface considering chemical effects. A new test apparatus is built and modified to perform cyclic simple shear tests. Both geosynthetics and Jumunjin sand are submerged in acid, neutral, and basic solutions for 30 days and 850 days, representing relatively short-term and long-term behaviors of the interface, respectively. 72 sets of cyclic simple shear test are performed and the shear stress degradation is estimated by the Disturbed State Concept and disturbance functions. As a result, new disturbance function parameters are suggested to characterize each chemical condition mathematically.

Microscopic observation is conducted to clarify the reason of variation of

shear stress responses at the interface subjected to the *p*H values by Focused Ion Beam (FIB). Based on the experimental approach, the numerical back-prediction of the cyclic shear stress-strain relationship is accomplished based on the parametric study to validate the obtained DSC parameters with the test results.

Consequently, a general methodology to estimate the cyclic shear stress degradation of geosynthetic-soil interface considering chemical effects is established and verified.

1.3 Dissertation organization

This research mainly focuses on the experimental data from newly developed apparatus and microscopic observation. It consists of six chapters:

Chapter 1. Introduction – background, comprehensive objective, and the organizational summary of the dissertation were presented.

Chapter 2. Literature Review – contained a brief review of the previous studies on the geosynthetic-soil interface. Firstly, the basis of geosynthetics and waste landfill was reviewed. Secondly, the chemical characteristics of leachate and chemical resistance of the geosynthetics were surveyed. Then, the previous studies on the cyclic simple shear test and apparatus were presented including the test conditions such as loading frequency, strain

range, and boundary conditions, etc. Finally, the Disturbed State Concept and the disturbance function were introduced. A few experimental studies on the interface by the Disturbed State Concept were also analyzed.

Chapter 3. Experimental Work – described building a new interface apparatus with some modification and performing cyclic simple shear tests. A newly developed Multi-Purpose Interface Apparatus (M-PIA) was introduced and major modification for better performance was also presented. Then, the test conditions of material, chemical, dynamic, and boundary were explained. Test results were displayed and analyzed, then, the damage of interface was estimated by the disturbance function with new parameters, quantitatively. Additionally, the prototype test results considering thermal effect were demonstrated to present the recent advance in this study.

Chapter 4. Microscopic Observation – were conducted by Focused Ion Beam (FIB) to clarify the reason of the variation of interface damage subjected to the *p*H values. Geosynthetics and soil particle after the cyclic simple shear test were observed according to the submerging period and chemical conditions. Then, the effect of chemical attack was confirmed and the reason of the variation of interface damage was also clarified by FIB

Chapter 5. Back-prediction based on Parametric Study – was accomplished to reproduce and validate the obtained DSC parameters. The back-predicted cyclic shear stress-strain relationship considering chemical conditions displayed good agreements with the test results.

Chapter 6. Conclusions and Recommendations – at the end, summarized the main conclusions from the present study described in the dissertation and suggested directions for future researches.

2. Literature Review

2.1 Introduction

Even though the interface has been treated as an important issue and studied for a long time, it is still difficult to understand its behavior in depth. Most problems associated with interface are the shear resistance between adjacent materials comprising the interface. In this study, the main object is the geosynthetic-soil interface which appears inevitably in all waste landfill sites. Shear behavior of the geosynthetic-soil interface is known to be affected by some practical factors, and the dynamic and chemical conditions were considered simultaneously in this study. Due to the frequent occurrence of strong earthquakes worldwide and regulations in Korean law, the dynamic responses of the interface should be considered in the design and analysis of the waste landfill site. Additionally, the chemical substances in the leachate contact with geosynthetics and soil particles directly, therefore, the chemical effects on the interface shear behavior play an important role and need to be investigated in detail.

This chapter contains a brief review of the previous studies on the geosynthetic-soil interface in four categories. Firstly, the basis of geosynthetics and waste landfill are reviewed since they are the main object of this study. Secondly, the chemical characteristics of leachate and chemical resistance of the geosynthetics were surveyed. Then, the previous studies on the conventional cyclic simple shear test and apparatus were presented

because it is necessary to simulate the behavior relevant to various modes of deformation and derive parameters from appropriate laboratory tests in order to identify the influence of relative motions at interfaces. Various test results according to the test conditions such as loading frequency, strain range, and boundary conditions, etc. were presented. Additionally, the cyclic shear device in the previous studies were also introduced and reviewed. Finally, the Disturbed State Concept and the disturbance function, as useful means of estimating the interface damage were explained.

2.2 Geosynthetics and waste landfill site

2.2.1 Geosynthetics - overview

According to the ASTM D4439, a geosynthetic is defined as follows: a planar product manufactured from polymeric material used with soil, rock, earth, or other geotechnical engineering related material as an integral part of a human-made project, structure, or system. Since 1970s, geosynthetics have emerged as universal engineering materials having wide array of civil engineering applications e.g., geoenvironmental, geotechnical, structural systems. Geosynthetics perform five major functions: (1) separation, (2) reinforcement, (3) filtration, (4) drainage, and (5) containment (of liquid and/or gas). The use of geosynthetics has basically two aims: better perform of target object and economic advantages against the traditional materials

(Koerner, 2005). Waste landfill site is ideal to utilize geosynthetics because the geosynthetics encompass the entire range of functions listed above in the mixture of soil, solid, i.e., waste, and liquid.

There are seven specific types of geosynthetics: (1) geotextiles, (2) geogrids, (3) geonets, (4) geomembranes, (5) geosynthetic clay liners (GCL), (6) geofoam, and (7) geocomposites. Figure 2.1 displays the typical types of geosynthetic products.

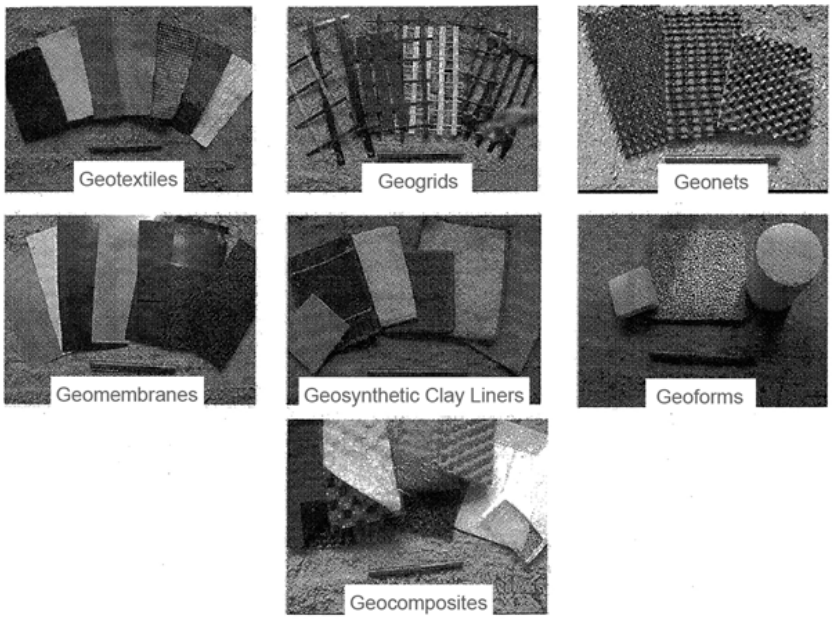

Figure 2.1 Collage of the basic types of geosynthetic products (Koerner, 2005)

Among those types of geosynthetics, geocomposites are most common in the waste landfill site in Korea. Geocomposites represent a combination of geosynthetics whereby two or more individual geosynthetics are utilized together, hence, various shapes of geocomposites can be produced.

The vast majority of the geosynthetics are made from synthetic polymers;

therefore, the composition, structure, and identification of polymer were briefly reviewed. The basic feedstock for the polymers used to make geosynthetics is ethylene gas. Ethylene is reacted by a catalyst to produce polyethylene (PE), polyester (PET), polypropylene (PP), polyvinyl chloride (PVC), etc. Figure 2.2 shows the major substances to manufacture the geosynthetics.

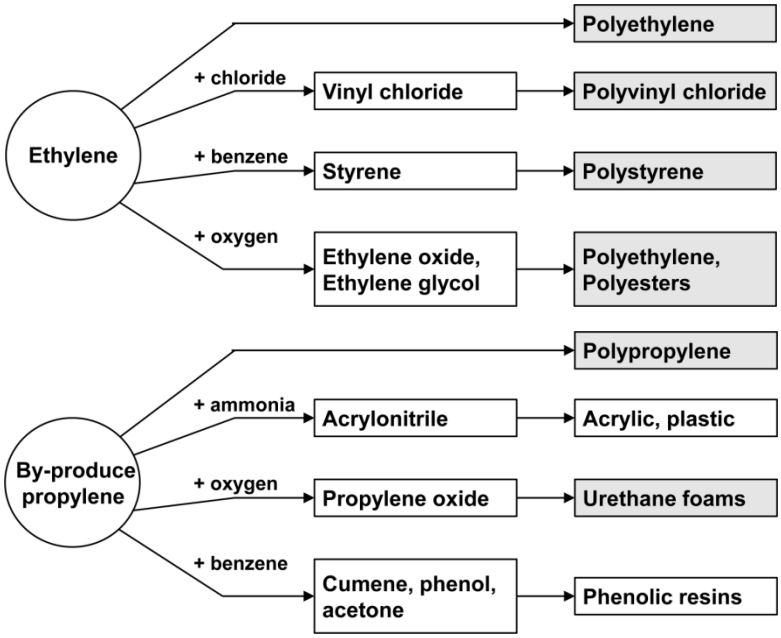

Figure 2.2 Major polymeric products (modified after Koerner, 2005)

Bonding mechanism between polymer molecules and their chains is remarkably important to understand the behavior and performance of the geosynthetics. The bonding between polymer molecules is van der Waals forces and hydrogen bonds, or permanent dipoles. Sometimes, the bonds can be weaken and supplemented by some form of cross-linking by means of

covalent bonds. Table 2.1 presents the repeating molecular units of polymers and structure used in manufacture of geosynthetics.

One of the important concerns on the characteristics of geosynthetics is the degradation because the degree of degradation may determine the durability of geosynthetics. It is known that all the degradation mechanisms result in some form of molecular chain scission, bond breaking, cross-linking, or the extraction of formulated components (Koerner, 2005). Table 2.2 summarized the types of degradation.

Table 2.1 Molecular structure of polymers (Koerner, 2005)

Polymer	Repeating unit	Types of gosynthetics
Polyethylene (PE)	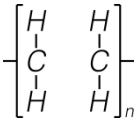	geotextiles, geomembranes, geogrids, geonets, geopipe, geocomposites
Polypropylene (PP)	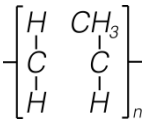	geotextiles, geomembranes, geogrids, geocomposites
Polyvinyl chloride (PVC)	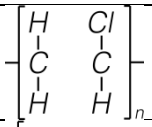	geomembranes, geocomposites, geopipe
Polyester (PET)	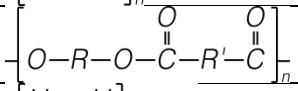	geotextiles, geogrids
Polystyrene (PS)	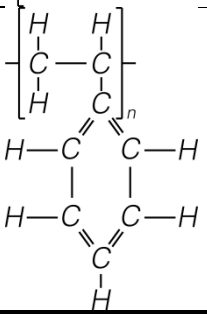	geocomposites, geofoam

Table 2.2 Types of degradation of geosynthetics

Types	Feature
Sunlight (ultraviolet)	- An important cause of degradation to all organic materials including polymers - Ultraviolet (UV), with wavelengths shorter 400 nm causes main damage - Actual degradation is caused from the breaking of the polymer's chemical bonds by photons of light
Temperature	- Extremely high temperature causes all polymer Degradation at an accelerated rate - An accelerating factor acting with other degradation mechanisms
Oxidation	- All types of polymers react with oxygen - Polypropylene and polyethylene are generally considered to be the most susceptible to oxidation - At ambient temperatures and in the absence of sunlight, the rate of oxidation of polymers is very slow
Hydrolytic (chemical)	- Hydrolysis can cause degradation via either internal or external fiber and yarn reactions - Geosynthetics manufactured using polyester resins are particularly affected - Degradation can occur when immersion liquid has a very high (pH > 10) or very low (pH < 3) alkalinity - Can be considered as a kind of chemical degradation
Chemical	- A wide range of chemicals can cause degradation - Depends on the manufacturer, chemical concentration, temperature, period of exposure
Biological	- Generally, the biodegradation is highly unlikely - The additives to the polymer, processing aids, plasticizers may be vulnerable, but not clear
Aging	- Depends on the manufacturer and field conditions - Normally, the lifetime of the structure is less than the lifetime of geosynthetics, so the aging hardly involves functional problems

As shown in Table 2.2, there are a few important types of degradation of geosynthetics; however, the process is extremely slow in a buried environment (Koerner, 2005). Moreover, the recent improvement of the materials science and manufacturing technology, the degradation of geosynthetic itself has been under control and does not be involved with significant problems.

2.2.2 Waste landfill site

With increasing industrialization, the amount of waste continuously increases. Waste takes various forms such as solids, liquids, sludges, gases, or any combination thereof. Depending on the source of generation, some wastes may degrade into harmless products whereas others may be nondegradable and hazardous (Oweis and Khera, 1998). Therefore, waste should be managed in accordance with its physical and chemical characteristics. Table 2.3 displays the type and disposal method of waste. As displayed in Table 2.3, landfilling is the most popular means of hazardous and municipal waste disposal because it can be a relatively safe and cost effective if conducted based on precise design and managed with sufficient care (Orloff and Falk, 2003). Hence, waste landfill site has also increased worldwide. However, waste landfills were also identified as one of major threats to groundwater resources (Mor et al., 2006), therefore, hazardous and municipal waste landfill facilities require lining and covering systems. Geosynthetics are the appropriate and ideal material to function such as reinforcement, filtration,

drainage, protection, and separation in the facilities.

Table 2.3 Type and disposal method of waste (Oweis and Khera, 1998)

Disposal method	Waste type				
	Municipal	Industrial	Dredged	Mineral	Agricultural
Landfilling	○	○	○	○	
Ocean disposal	○		○		
Incineration	○		○		
Recovery	○	○			
Sewer system	○				
Septic tanks	○				
Surface impoundment		○	○	○	○
Land application	○	○	○		○
Construction application	○	○	○	○	

Geosynthetics are applied at the bottom and layers, then, comprise geosynthetic-soil interface, therefore, the overall stability of waste landfill site depends on the shear resistance at the interface. Figure 2.3 shows the example of waste landfill site in Korea and Figure 2.4 demonstrates the typical section of the waste landfill site. According to the Waste Management Act (Article 29) and Waste Management Enforcement Regulations (Article 35), sand layer should be placed on the geosynthetics with minimum thickness of 30 cm.

In the waste landfill, heat is one of the primary byproducts. Heat is generated as a result of biological and chemical decomposition or hydration of

incinerated residues in wastes. The decomposition of waste occurs both aerobically and anaerobically with the aerobic decomposition phases starting before the anaerobic decomposition phase. The chemical reactions that occur during the microbial decomposition of a major component of solid waste (e.g., glucose) are shown in Equation 2.1 and 2.2, respectively (Rowe and Islam, 2009).

$$C_6H_{12}O_6 + 6O_2 \rightarrow 6CO_2 + 6H_2O + 1770\ {}^{kJ}/_{mol} \quad \text{(aerobic)} \qquad (2.1)$$

$$C_6H_{12}O_6 \rightarrow 3CH_4 + 3CO_2 + 100\ {}^{kJ}/_{mol} \quad \text{(anaerobic)} \qquad (2.2)$$

High temperature is accelerating factor acting with other degradation mechanisms such as chemical, which plays an important role for the shear stress degradation in geosynthetic-soil interface.

Nowadays, seismic stability of waste landfill site has been a subject of intense research, primarily due to the severe environmental impact of a potential failure. Damage on geosynthetics of three landfills (namely Chiquita Canyon C, Chiquita Canyon D, and Lopez Canyon) reported during the 1994 Northridge earthquake (Zania et al., 2010). Note that the dynamic shear behavior of the geosynthetic-soil interface is one of the most important factors in the stability issues of waste landfill sites.

Figure 2.3 Sample view of waste landfill site (Multifunctional Administrative City Construction Agency, 2013)

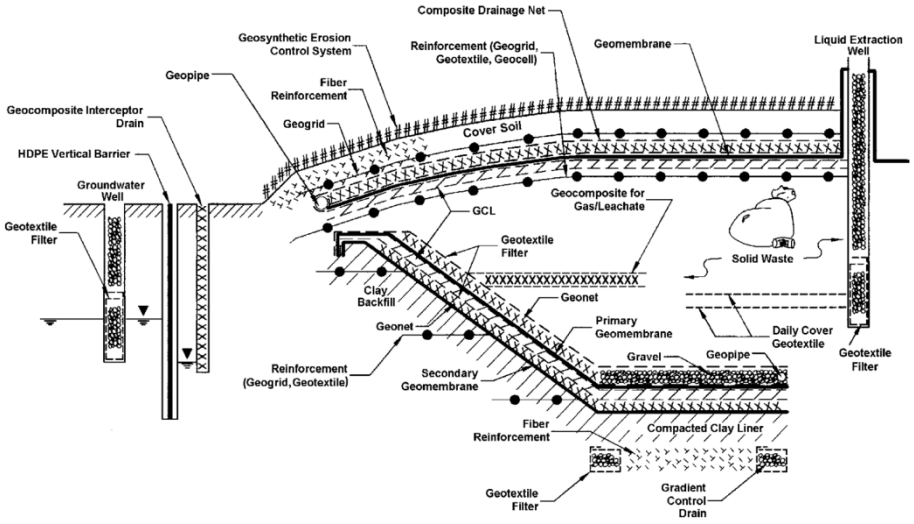

Figure 2.4 Typical section of waste landfill site (after Zornberg and Christopher, 1999)

2.3 Leachate and chemical characteristics

Chemical substances in the leachate may affect the response of geosynthetic-soil interface, therefore, the knowledge of leachate and its chemical characteristics should be reviewed to progress the present study. In this chapter, chemical characteristics of leachate and chemical resistance of the geosynthetics were surveyed through the previous researches.

2.3.1 Leachate generation

Waste placed in landfills or open dumps are subject to either groundwater underflow or infiltration from the outside. The dumped wastes gradually release its initial interstitial water, and some of its decomposition by-products get into water moving through the waste deposit. Such liquid containing innumerable organic and inorganic compounds is called ‘leachate’ (Mor et al., 2006).

Since the waste in a landfill is a mixture of various organic material such as food, paper, plastics, rubber, wood, ash, etc. and inorganic substances. An organic body undergoes decomposition and oxidation in the presence of oxygen, moisture, and microorganism under appropriate temperature (Oweis and Khera, 1998). The percolation of water through the landfill generates leachate. The source of water could be precipitation, irrigation, groundwater, or leachate recirculated through the landfill as shown in Figure 2.5. The

amount of leachate generated mainly is subjected to the available water, landfill constituents, and structure of landfill.

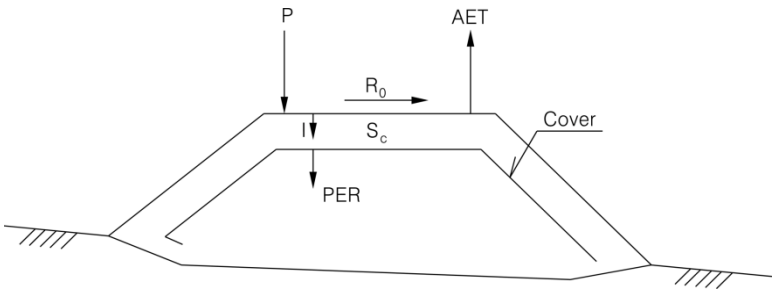

Figure 2.5 Leachate generation and parameters (redrawn after Oweis and Khera, 1998)

In Figure 2.5, P is the input water from precipitation, recirculation, irrigation, or surrounding surface runoff, I is the infiltrating liquid, and R_0 is the surface runoff. S_c is the landfill cover, and PER_s is the remainder which will percolate into the refuse. Some portion of the infiltrating liquid (I) lost by evaporation is described as AET.

2.3.2 Chemical characteristics

Leachate in a landfill retains a range of inorganic and organic substances as given in Table 2.4. Those substances may affect the chemical properties of the leachate.

Table 2.4 Constituents of leachate from municipal waste landfills (summarized after Oweis and Khera, 1998)

Types	Concentration (mg/l)
Total organic carbon	50-45,000
Total solids	1-75,000
Total dissolve solids	725-55,000
Total suspended solids	10-45,000
Volatile suspended solids	20-750
Total volatile solids	90-50,000
Fixed solids	80-50,000
Alkalinity (as C_aCO_3)	0.1-20,350
Acidity	2,700-6,000
Total coliform bacteria	0-10 (c.f.u./100 ml)
Iron	200-5,500
Zinc	0.6-220
Sulfate	25-500
Sodium	0.2-79
Total volatile acid	70-27,700
Ammonium nitrogen	0-1,106
Fecal coliform bacteria	0-10 (c.f.u./1,000 ml)
Chlorine	30-5,000
Copper	0.1-9
Lead	0.001-1.44
Magnesium	3-15,600
Potassium	35-2,300
Total phosphorus	0.1-150

Biodegradation of waste occurs in the presence of oxygen by aerobic bacteria, in the absence of oxygen by anaerobic bacteria, or with very little oxygen by facultative anaerobic bacteria. The quantity of oxygen inside the landfill changes with the process of the decomposition.

Previous studies reported that the *p*H value changes dramatically because

of the complicated biological and chemical reactions in the leachate. Kjeldsen et al. (2002) reviewed on the long-term composition of landfill leachate focused on the *p*H change with the decay process in the waste. Generally, it is accepted that landfills undergo at least four phases of decomposition, (1) an initial aerobic phase: decomposition occurs and produces CO_2 and H_2O; accordingly, *p*H decreases slightly, (2) active aerobic phase: the activities of acid former and facultative fungus increase; then, *p*H decreases significantly and most of the leachate volume is generated at this stage, (3) anaerobic putrefaction phase: as oxygen sources are depleted, anaerobic decomposition occurs due to the deoxidation state inside the landfill and the decomposition of the amino acids produces NH_3; hence, there is a meaningful increase in *p*H, (4) initial and stable methanogenic phase (Christensen and Kjeldsen 1995): the methanogens convert the endproducts of the acetogenic reactions to methane and carbon dioxide (Zehnder et al. 1982). This procedure continues efficiently over a relatively narrow *p*H range around neutral. In the second phase, the hydrolytic fermentative and acetogenic bacteria dominate, resulting in the accumulation of carboxylic acids and a decrease in *p*H. As the *p*H is acidic, the acid phase leachate is chemically aggressive and will increase the solubility of many compounds (Kjeldsen et al. 2002).

Based on this process, the *p*H values vary dramatically. During the acid phase, the leachate may show low *p*H values and high concentrations of many compounds. In the later stable methanogenic phase, the *p*H increases since the degradability of the organic carbon is lowered significantly (Ehrig 1988). Oweis & Khera (1998) reported the *p*H values of leachate from municipal waste landfills were at 3.5 to 8.5, and Bilgili et al. (2007) demonstrated the

variation of *p*H values according to the buried period in the landfill site (Figure 2.6). Therefore, the geosynthetics and soils in the waste landfills are exposed to neutrality, acidity and basicity (Kwak et al., 2013[a]).

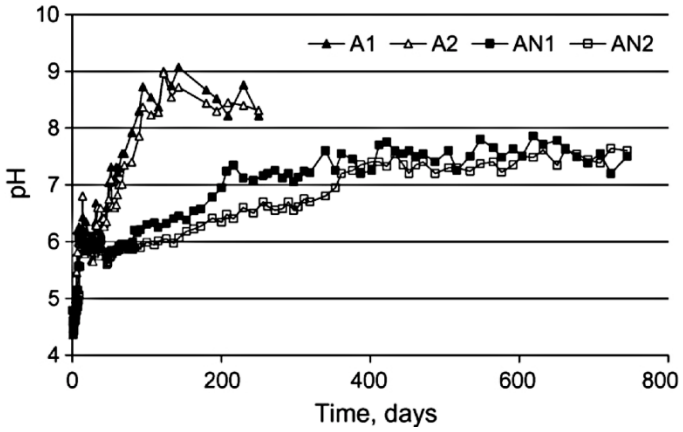

Figure 2.6 The change of *p*H in landfill site (Bilgili et al., 2007)

2.3.3 Chemical resistance of geosynthetics

As mentioned before, geosynthetics provide various design functions necessary for construction of waste landfill site. Since the environmental impact in case of the failure is enormous, geosynthetics must retain resistance to chemical degradation while in contact with chemical aggressors and maintain physical strength to meet up their design specifications.

Decades ago, the US Environmental Protection Agency (EPA) suggested standards to certify the minimum requirements of geosynthetics for safe landfill design. EPA Method 9090 which is originally developed in the early

1980s, provided a basis for determining the resistance of geomembranes with waste liquids by artificially simulating field conditions. Rectangular geomembrane samples are immersed in a chemical environment representative of the waste liquids or leachates to be contained. Minimum periods of 120 days at room temperature (22℃) and elevated temperatures (50℃) are used. Samples are immersed in exposure tanks filled with the leachate, then sealed to prevent the loss of volatile leachate components. Physical properties of the geosynthetic samples are monitored before immersion and every 30 days thereafter to estimate the resistance of geosynthetics. Cassidy et al. (1992) reviewed on this method and summarized a few test methods; however, there were no standardized methods for analyzing the durability of geosynthetic materials upon exposure to the aggressive chemicals. Afterward, ASTM D5322 and D5496 were built and presented the standard practice for immersion procedures for evaluating the chemical resistance of geosynthetics and for field immersion testing of geosynthetics. ASTM D5747 suggested the standard practice for tests to evaluate the chemical resistance of geomembranes to liquids. After Vandervoort (1992), general chemical resistance guidelines were announced as shown in Table 2.5. Even though there are no established rules on the allowable variation from the original test properties, a few researchers also suggested the criteria of resistance for HDPE in Table 2.6. From Table 2.5, high-density polyethylene (HDPE) shows generally good resistance, accordingly, is the material of choice for most landfill liners.

Table 2.5 General chemical resistance guidelines (After Vandervoort, 1992)

Chemical	Types of geosynthetics			
	HDPE	PVC	CSPE-R	EPDM-R
General:				
aliphatic hydrocarbons	V			
aromatic hydrocarbons	V			
chlorinated solvents	V			V
Oxygenated solvents	V			V
crude petroleum solvents	V			V
alcohols	V	V		
Acids:	V			
organic	V	V	V	V
inorganic	V	V	V	V
Heavy metals	V	V	V	V
Salts	V	V	V	

* V = generally good resistance

In general, HDPE geomembranes consist of 96 - 97.5 % of polyethylene resin, 2 - 3 % of carbon black and 0.5 - 1.0 % of other additives such as antioxidants and stabilizers (Hsuan and Koerner, 1995). The additives in HDPE play an important role to improve the chemical resistance, therefore, majority of researches on the chemical interaction indicates the robust performance of HDPE.

Table 2.6 Criteria of resistance for HDPE (Koerner, 2005)

Property	O'Toole (1986)		Little (1985)		Koerner (2005)	
	R	N.R	R	N.R	R	N.R
Permeation rate (g/m^2-hr)	-	-	< 0.9	≥ 0.9	< 0.9	≥ 0.9
Change in weight (%)	< 0.5	> 0.1	< 3	≥ 3	< 2	≥ 2
Change in volume (%)	< 0.2	> 0.5	< 1	≥ 1	< 1	≥ 1
Change in yield strength (%)	< 10	> 20	< 20	≥ 20	< 20	≥ 20
Change in yield elongation (%)			< 20	≥ 20	< 30	≥ 30
Change in modulus (%)					< 30	≥ 30
Change in tear strength (%)					< 20	≥ 20
Change in puncture strength (%)					< 30	≥ 30

* R = Resistant, N.R = Not resistant

Schmidt et al. (1984) conducted a series of physical index tests (examining tensile and tear properties) on polyethylene liner samples from exposed and submerged geomembranes that had been in use for up to 16 years. The results displayed a stiffening of polymers and some decline in elongation; however, those were less significant for buried geomembrane. The major cause of failure to the liners was from physical damage, rather than weathering/aging effects.

Hsuan et al. (1987) analyzed the degradation behavior of geosynthetics under extremely high *p*H values. In the study, the specific mechanisms and extent of the degradation are dependent on many factors such as the type of

polymer, additives, heat, sunlight, moisture, oxygen, radiation, bacteria, and the magnitude of the mechanical stress. Especially, polyethylene is susceptible to the hydrolytic reaction, and then the molecular weight is able to be reduced via chain scission. The hydrolytic reaction can cause degradation of fabric or yarn of the geosynthetics and be accelerated substantially by basic environments.

Hsuan et al. (1991) performed experimental research on an HDPE geomembrane after 7-year use for solid waste leachate storage in a surface impoundment. The samples were obtained from four different locations in the lagoons, ranging from areas continuously exposed to the leachate continuously. The results showed no meaningful microscopic change in the geomembrane sheets or seams after 7 years of exposure. No significant changes in the internal structure of the geomembrane was also confirmed, and no effects on the hydraulic/engineering containment properties of the geomembranes.

Eith and Koerner (1997) presented a case in which an HDPE geomembrane was used as part of a double liner system for a landfill. After 8 years of service, the geomembrane had been exposed to chemical substances of leachate. The physical, mechanical and durability test results demonstrated no evident damage of the HDPE geomembrane properties.

Jeon et al. (2006) performed the experimental study to evaluate the long-term performance of geosynthetics. Drawn, knitted, junction bonded types of geomembranes, geocomposite, and strip-type reinforcement were compared by the laboratory tests. The resistance factors of chemical degradation, biological degradation, creep deformation, and installation damage were

estimated and the results showed the geocomposite exhibited the best long-term design strength among samples, implying the best overall long-term performance, however, the variation of resistance factors were not so considerable.

In summary, the advance of recent technology enhanced the durability and resistance of the geosynthetics against chemical aggressors.

2.4 Laboratory testing of interface

Most of the previous researches ensure the material stability of geosynthetics against chemical attack in the waste landfill site. The critical portion of the whole stability of landfill site is the geosynthetic-soil interface and the shear resistance along the interface is an important characteristic of the stability of the whole landfill system (Stark et al., 1996). The interface is affected by many practical factors and conditions; therefore, appropriate laboratory test is inevitably required to understand the shear behaviors in depth. Especially for the dynamic condition which is the main concern of the present study, cyclic simple shear test is engaged in the experimental study because it is able to simulate the closest conditions of the field during dynamic loading at a reasonable cost (Amer et al., 1986). Cyclic simple shear tests can be conducted for a wider range of strain amplitude, that is, 10^{-2} % to about 5 %, and this range is the general range of strain encountered in the ground motion during seismic activities (Das, 1993).

Several tests and apparatus have been suggested to investigate the shear behavior at the interface. Testing methods can be classified into 3 categories as shown in Table 2.7. As mentioned before, cyclic simple shear test is widely available and most appropriate means to reproduce the seismic conditions of the interface, among those testing methods.

In this chapter, the concept of laboratory shear tests and the history of shear devices were introduced and various types of the devices were reviewed. Basic theories and conditions of simple shear test were also surveyed and the cyclic shear behavior of interface was analyzed based on the test results.

Table 2.7 Interface testing methods

Method	Advantages	Disadvantages
Direct shear (static)	- commonly available - simple sample preparation and operation	- progressive failure occurs along the interface - physical boundaries influence results - relative displacement along interface cannot be obtained independently - sectional area of interface changes during shear
Ring torsion (static and dynamic)	- available to large strain - no end effects - constant area of interface	- difficult sample preparation - complicated system and test procedure - displacement gradient across the interface, and as a result, shear strain variation in the sample occurs - solid overlaying the soil
Simple shear (static and dynamic)	- simple sample preparation and operation - easy operation - displacement components can be measured independently	- stress concentration at the ends

2.4.1 Direct shear tests

The direct shear test has been very popular for the laboratory testing of soils due to its simplicity. After Martin et al. (1984), the direct shear test has been widely used for geosynthetic interfaces and test standards were suggested (ASTM D5321). ASTM D5321 (2008) recommended square or rectangular shear container and they should have a minimum dimension that is greater than 300 mm. The depth of each container which contains soil must be a minimum of 50 mm. Figure 2.7 shows the schematic of the conventional direct shear test apparatus.

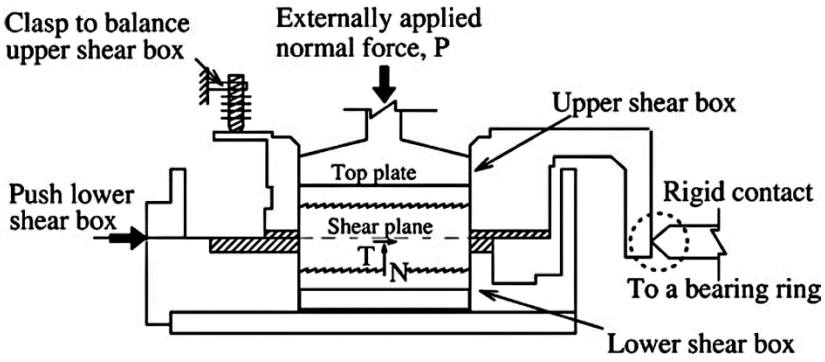

Figure 2.7 Schematic of direct shear test apparatus (Liu et al., 2005)

Lee and Manjunath (2000) described large-size direct shear tests on soil-geotextile interfaces. Medium-grained, uniform sand and three varieties of woven and nonwoven geotextiles were utilized to investigate the interface friction coefficient. A large-size apparatus specifically designed were

introduced and the results were compared with those obtained from the conventional direct shear apparatus. It was known that the test results were significantly affected by the boundary and testing. The inherent drawbacks in the conventional direct shear box equipment were also mentioned. These include the followings: (1) The interface test results markedly affected by sagging of the geosynthetics caused the application of normal force; this could result in nonuniform stress distribution acting on the testing surface, then nonplanar shear surface between soil and geosynthetics may appear. (2) The absence of an effective support and anchoring facility for geotextiles may lead to slippage and distortion during relative shear displacement. (3) The surface area of contact between soil and geotextile decreases as shearing progresses. (4) The residual shear strength cannot be evaluated due to the limit on traveling distance. Additionally, drainage control is not applicable. Even though those drawbacks, it is still utilized due to simple procedure and convenient operation, especially for granular soils.

Seo et al. (2007) briefly reviewed on direct shear test and performed direct shear test for interfaces between a nonwoven geotextile, two types of geosynthetic clay liners (GCL), and two types of geomembranes (smooth and textured). The hydrated condition was considered to examine the effects of interface wetting in detail. The direct shear tests on large (300 X 300 mm) rectangular device were performed with a maximum traveling distance of 100 mm and no loss in the shearing area. The test results showed that the normal stress level, interface water presence dominated the interface shear strength and behavior. The friction angle decreased with increasing normal stress as shown in Figure 2.8, therefore, it is suggested that the shear strength should be

determined under the maximum normal stress condition expected during the lifecycle for safe design.

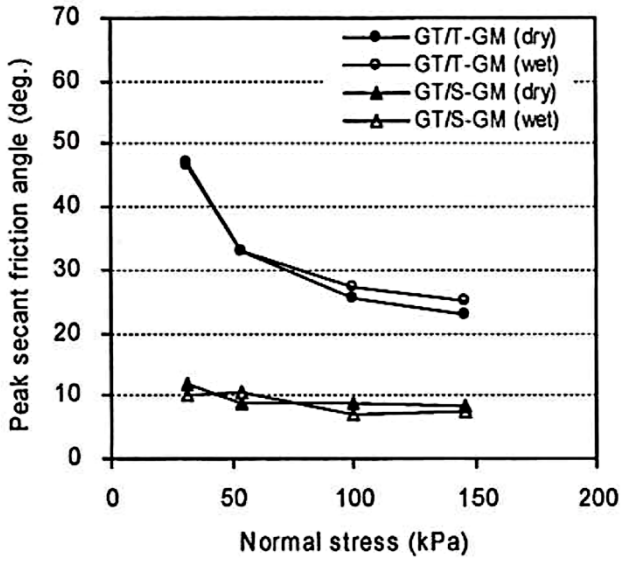

Figure 2.8 Decrease of friction angle with normal stress (Seo et al., 2007)

It is a common practice to investigate the shear strength behavior of geosynthetics using a large direct shear box with a minimum specimen size of 300 X 300 mm (ASTM D5321, 2008; ASDM D6243, 2008). However, note that many researchers (e.g. Takasumi et al., 1991; Gilbert et al., 1997; Koerner et al., 1998) verified that small specimens exhibited acceptable results.

2.4.2 Torsional shear tests

Stark and Poeppel (1994) presented the use of a torsional ring shear

apparatus to measure the shear strength of geosynthetic-geosynthetic and geosynthetic-soil interfaces. Figure 2.9 displays the sketch diagram of the torsional ring shear test principle and Figure 2.10 shows the structure of typical ring shear apparatus.

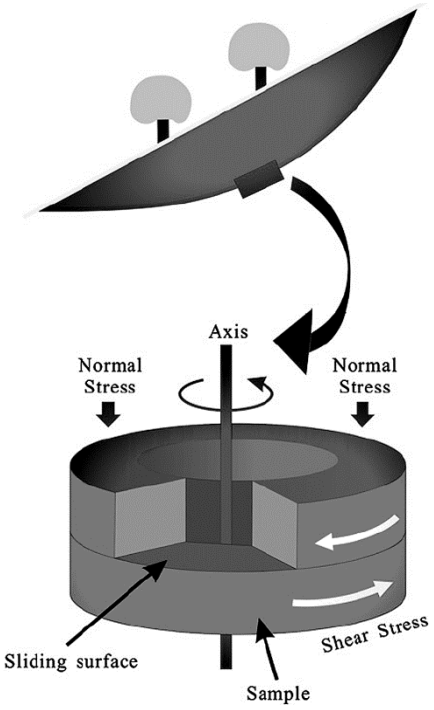

Figure 2.9 Torsional ring shear test principle (modified after Sassa et al., 2004)

The torsional ring shear apparatus allows: (1) unlimited continuous shear displacement in one direction and the development of a residual or minimum interface strength condition, (2) the same interface to be sheared throughout the test, i.e., the specimen maintains constant cross-sectional area, (3) shear failure does not occur through a pre-determined plane, (4) no machine friction over the full range of normal stresses, (5) no eccentric shear loading.

Disadvantages of the apparatus include a small specimen size and difficulty in preparation of specimen and system operation. Shear strain variation in the specimen may occur due to the displacement gradient across the interface.

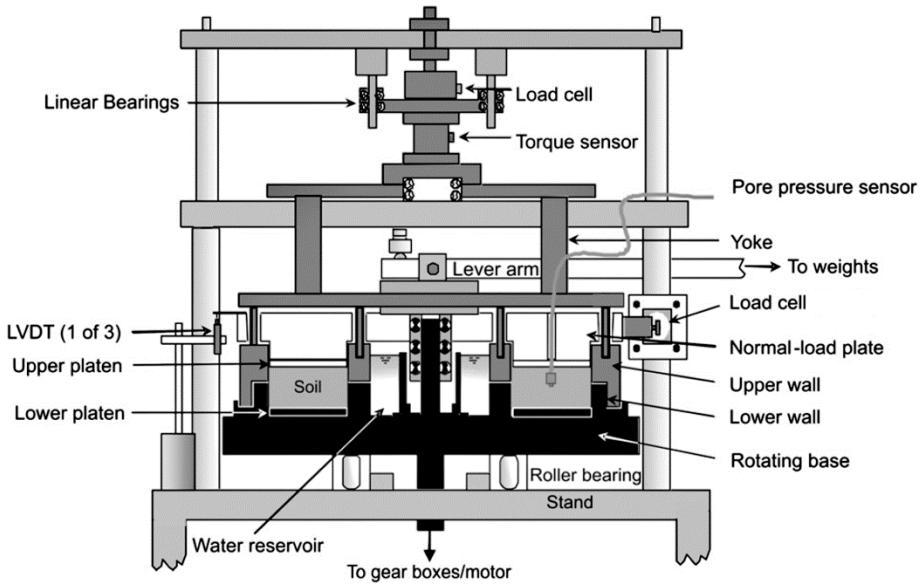

Figure 2.10 Structure of typical ring shear apparatus (modified after Iverson et al., 2010)

Stark et al. (1996) performed torsional ring shear tests on interfaces comprised of HDPE geomembranes-nonwoven geotextiles and a drainage geocomposite. The effects of geotextile fiber type, fabric style, polymer composition were also investigated. The textured HDPE geomembrane-nonwoven geotextile and drainage geocomposite interfaces exhibited a large post-peak strength loss. This strength loss was attributed to pulling out or tearing of filaments from the nonwoven geotextile and, at high normal stresses,

the loss can be caused by damage to or removal of the texturing on the geomembrane surface.

Tan et al. (1998) described the evaluation of the soil-geotextile interface shear strength using the torsional ring shear test. Dry sand and nonwoven polypropylene geotextile were used and the results showed that the peak friction angle and residual friction angles were not greatly influenced by the rate of shear. The results also indicated that the friction angle of the sand-geotextile interface decreased as the overburden pressure increased, which showed consistent with the results performed by direct shear tests by Seo et al. (2007). A set of direct shear tests was conducted and the results were compared with those of torsional ring shear tests. As a result, the measurements of sand-geotextile interface friction angle gauged by both equipments were almost identical at small shear displacement of less than 3 mm. Beyond 3 mm of displacement, the direct shear test showed higher friction angle than the ring shear test, and the direct shear test was unable to measure interface shear strength at a displacement large than about 15 mm, whereas the ring shear test could measure residual interface shear strength at a displacement of more than 200 mm.

2.4.3 Cyclic simple shear tests

Simple shear is defined as the shear stress which is created by a direct action of the forces in trying to cut through the material (Gere and Timoshenko, 1991). Practically, shear force is applying only one direction, as

shown in Figure 2.11 below. Simple shear test closely simulates plane strain condition and allow for the principal axes of stresses and strains to rotate. Section area, A remains constant during shear, and the shear strain, γ is defined as follows in case of small shear displacement, a,

$$\gamma \cong \tan\gamma = \frac{a}{h} \tag{2.3}$$

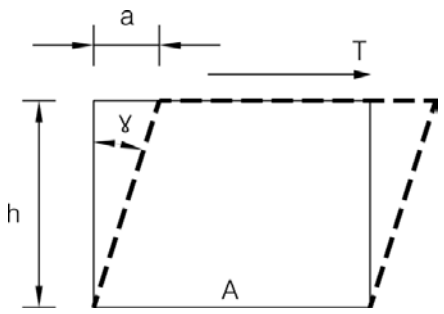

Figure 2.11 Schematic of simple shear state

Cyclic simple shear testing simulates the stresses which applied to a soil element under the earthquake loading. The stress conditions under cyclic simple shear test were demonstrated in Figure 2.12. The soil specimen in the shear box is first consolidated by a normal stress, σ_0', then a lateral stress, $K_0\sigma_0'$ is developed in the specimen because of lateral confinement, where K_0 represents the coefficient of earth pressure at-rest. One of the stacked shallow rings, reinforced rubber membrane, and rigid walls are normally utilized as lateral confinement system in the apparatus. The soil specimen is subjected to

cyclic shear stress, τ at the top and bottom surface, accordingly, exhibits the stress state shown at the lower diagram in Figure 2.12. The directions of the major principal stresses rotate smoothly, as in the in-situ condition (Hazirbaba, 2005). Seed and Peacock (1971) pointed out that the applied shear stress, τ, is not the maximum shear stress in the sample. The maximum shear stress, τ_{max}, can be calculated by:

$$\tau_{max} = \tau^2 + \left[\frac{\sigma_0' (1 - K_0)}{2}\right]^2 \quad (2.4)$$

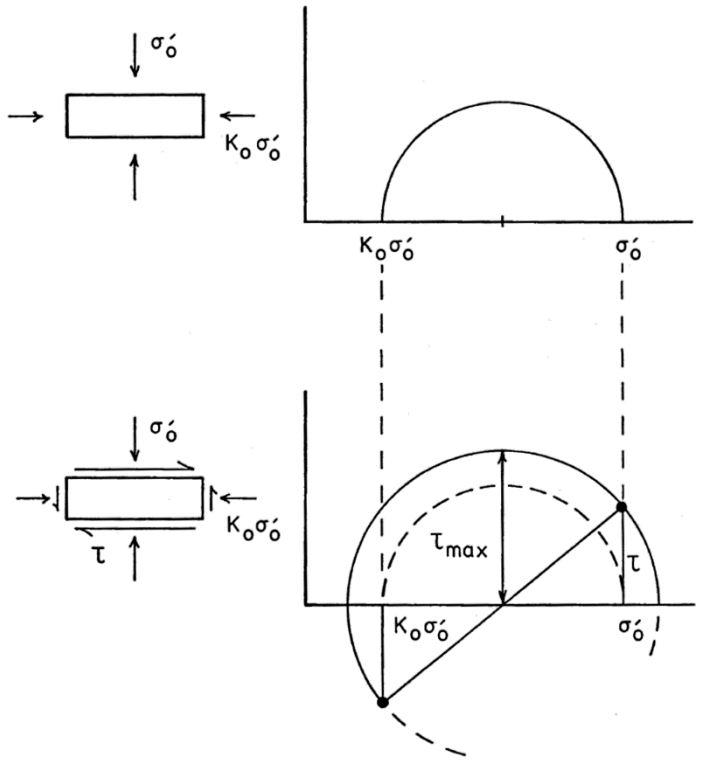

Figure 2.12 Simple shear stress conditions (after Seed and Peacock, 1971)

The historical background of cyclic simple shear devices was summarized by Amer et al. (1986). The use of the cyclic simple shear device goes back approximately 80 years. Kjellman (1951) described the Royal Swedish Geotechnical Institute (SGI) direct-shear apparatus built in 1936. In this apparatus a cylindrical specimen of 6 cm in diameter and 2 cm in height was set between two grooved plates. A rubber membrane was applied to maintain constant section area and a stack of aluminum rings confined the outside of membrane. Figure 2.13 displays the schematic of the SGI-type device.

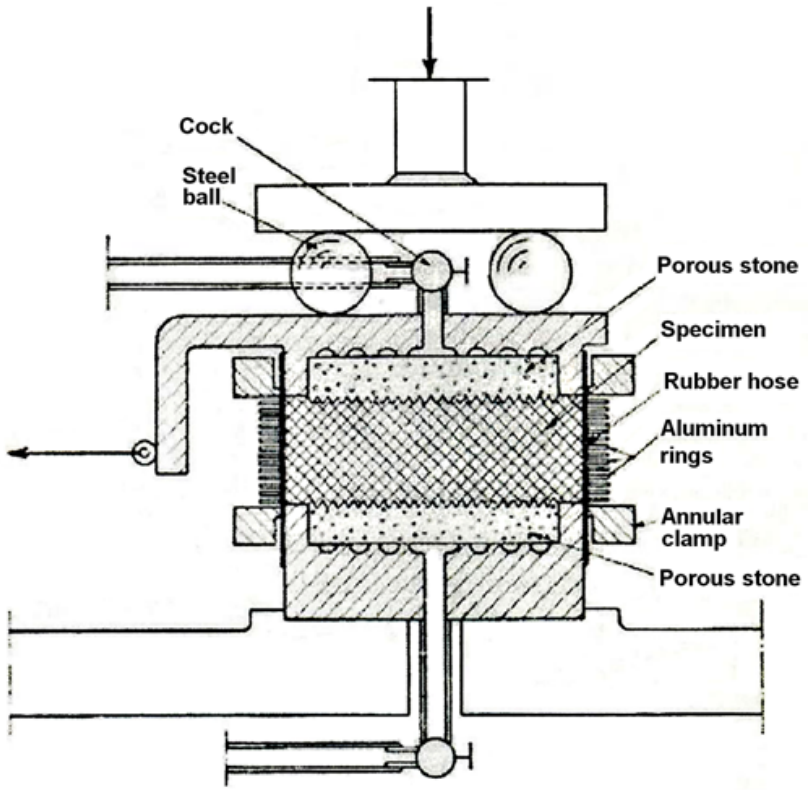

Figure 2.13 Schematic of the SGI-type device (Kjellman, 1951)

Roscoe (1953) introduced the Cambridge type simple shear apparatus, which shows a square 6- by 6-cm specimen that is 2 cm thick. The device has two fixed sides and two hinged end walls that rotate simultaneously in order to uniformly deform the soil specimen. However, one of the major problems with this apparatus is how to prepare a uniform square specimen. The Roscoe type apparatus has been utilized by many researchers (Peacock and Seed, 1968; Seed and Peacock, 1971; Finn et al., 1971).

The Norwegian Geotechnical Institute (NGI) developed a simple shear device that is basically a transformation of the SGI device in 1961. The NGI simple shear apparatus also utilized a cylindrical specimen and nonrigid vertical boundaries. While the SCI apparatus uses stacked rings to confine the specimen, the NGI apparatus applied a wire-reinforced rubber membrane. The standard size of a specimen is up to 2 cm height and 8 cm in diameter and has been used by many researchers (Amer et al., 1986; Chu and Vucetic, 1992; Song et al., 2004; Mortezaie and Vucetic, 2012). Figure 2.14 demonstrates the configuration of the NGI-type device and Figure 2.15 displays the specimen secured with membrane and O-rings

Amer et al. (1986) surveyed the advantages and limitations of the cyclic simple shear test. Though cyclic triaxial testing is the most widely used laboratory method for evaluating dynamic characteristics of cohesionless soils while the cyclic simple shear test is still used quite modestly for evaluating the same properties. As discussed by many investigators, , the cyclic simple shear test becomes the closest way to approximate the level ground field conditions during cyclic loadings at a reasonable cost, considering the cost of equipment and cost associated with the complexity of the specimen

preparation technique. Shaking tables for unidirectional and multidirectional loading is also an excellent way to simulate the dynamic conditions, but the cost in these special tests becomes quite high. One specific matter of permanent concern is the stress concentrations and the nonuniformity of stress-strain distribution within the soil specimen. In case of the soil element in the field is far from the influence of any boundaries that may cause a nonuniform stress-strain distribution. Therefore, it was recommended that a large-scale of specimen to avoid the size effect of the test, however, it is note that the size effect was only verified in the NGI-type of apparatus.

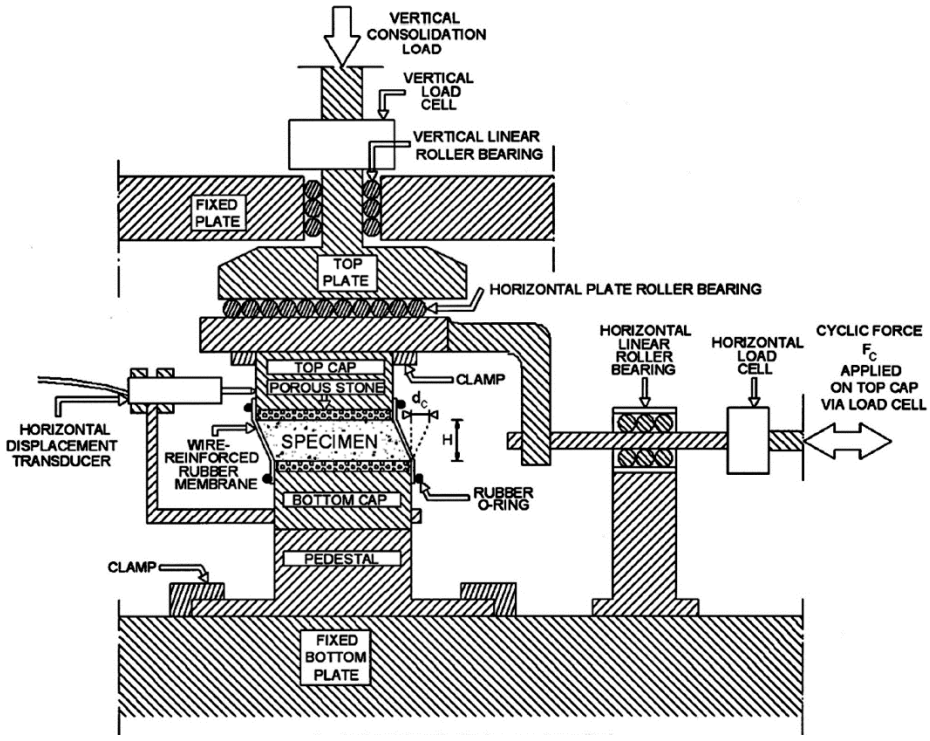

Figure 2.14 Configuration of the NGI-type device at UCLA (Mortezaie and Vucetic, 2012)

Figure 2.15 Specimen secured with membrane and O-rings (Chu and Vucetic, 1992)

Chu and Vucetic (1992) conducted 36 cyclic strain-controlled direct simple shear tests on low-plasticity compacted clay. NGI-type apparatus was utilized and the strains between 0.008 to 4.6 % were applied. The test results showed a very consistent behavior of the clay at different moisture contents. At small cyclic shear strains below 0.1 %, the stress-strain response was slightly nonlinear, i.e., close to linearly elastic, and the vertical settlement was negligible. At larger strain level, the cyclic stress-strain behavior became nonlinear and a continuous settlement with loading cycle occurred. Figure 2.16 shows typical load-displacement curves, however, the strains were not controlled precisely because a variation of peak displacement was observed at each cycle.

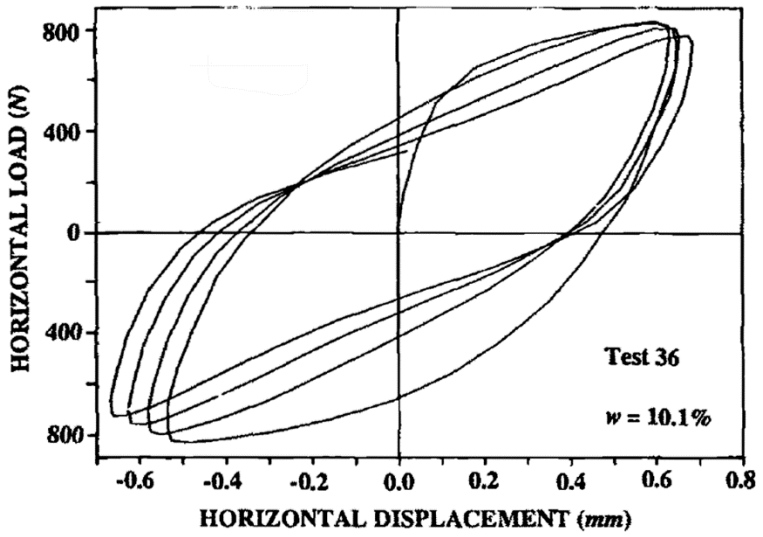

Figure 2.16 Load-displacement curves (Chu and Vucetic)

Desai and Rigby (1997) investigated the cyclic shear behavior considering a number of important factors such as pore water pressure, direct and simple shear deformations, drained conditions, and static and cyclic loading. New laboratory test equipment called cyclic multi-degree-of-freedom device (CYMDOF-P), which is able to consider the effect of pore water pressure was introduced. It involved a number of improvements and modifications including circular specimens, testing under direct and simple shear conditions, and inclusion of the effect of pore water pressure. The device also allows for translational, normal, and rotational motions. Figure 2.17 shows the details of the test box. For simple shear testing, the simple shear deformations are allowed by laterally confining the specimen of geologic material by thin and smooth Teflon-coated rings.

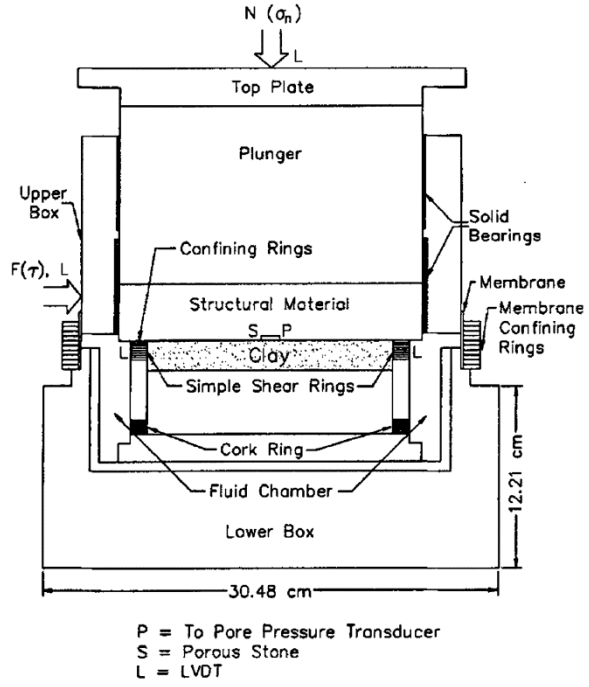

Figure 2.17 Details of CYMDOF-P test box (Desai and Rigby, 1997)

Direct shear and simple shear behavior was compared with respect to the types of materials and loadings. Figure 2.18 displays the shear stress-displacement relationship under quasi-static load condition of soft rock-clay interface. In case of the direct shear test, the peak shear stress was observed and the shear stress decreased after the peak showing a softening behavior, were observed, while the maximum shear stress showed the tendency of continuous yielding or hardening because of the redistribution of stresses in the simple shear condition as the soil can deform.

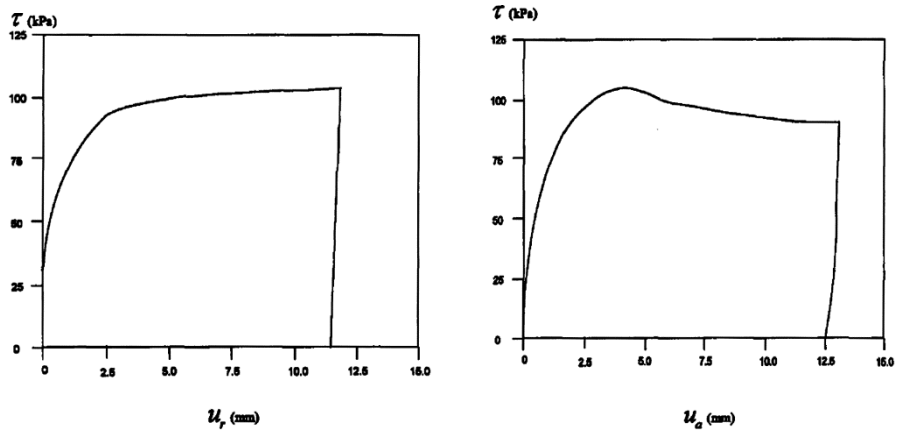

(a) simple shear test (b) direct shear test

Figure 2.18 Results of quasi-static test (Desai and Rigby, 1997)

The shear behaviors of clay-steel interface were also compared under cyclic loading. As similar to the quasi-static test result, the peak shear stresses from the direct shear tests were somewhat higher than those from the simple shear tests. The difference could be due to the fact that the direct shear test involved shear behavior at the junction decided in advance, while the simple shear test involved participation of the soil in the response. For the pore water pressure, the direct shear test showed slight higher value, but the difference was not significant. The small differences may be due to the fact the deformation gradients and strains as well as pore water pressures appeared to concentrate in a rather narrow zone in the soil. Figure 2.19 shows the shear displacement curves at different cycles.

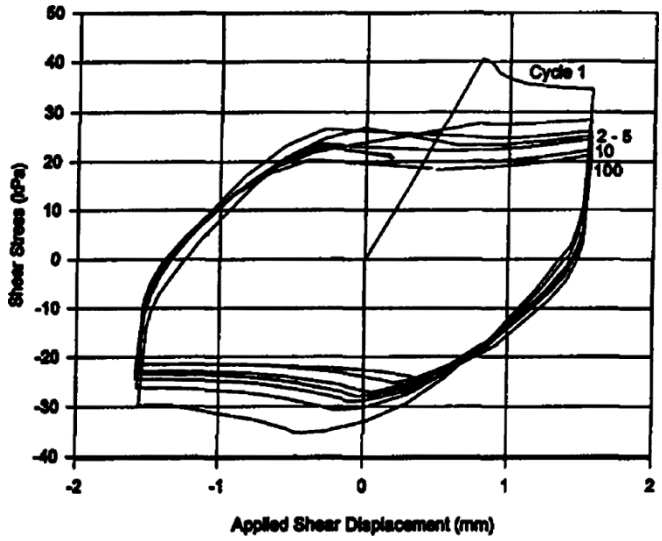

Figure 2.19 Shear stress-displacement curves (Desai and Rigby, 1997)

2.4.4 Test conditions of cyclic tests

Based on the previous studies, several conditions such as the amplitude of strain, the frequency of cyclic loading, and the boundary conditions of the cyclic tests are known to be important factors because they affect the test results significantly.

Pestana et al. (2000) performed a series of strain controlled cyclic simple shear tests for initially consolidated clays with symmetric (single side) strain amplitudes of 1 and 5 %, respectively. In both cases, the secant shear modulus decreased, the excess pore pressure increased, and the maximum shear stress decreased with increasing number of cycles, which represented the cyclic shear stress degradation. As the cyclic strain amplitude increase, the specimen

generated a higher pore pressure, thus a larger degradation of the secant shear modulus, for a given number of cycles. The tendency of cyclic shear behavior close to the failure was observed continuously in case of applying larger strain. Figure 2.20 shows the shear stress-strain curves according to the amplitude of strain.

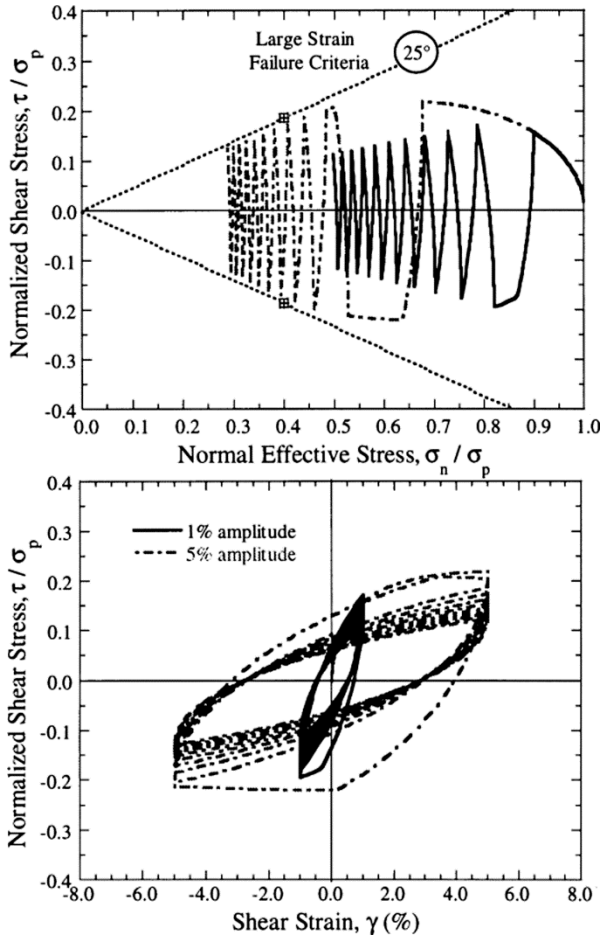

Figure 2.20 Effect of cyclic strain amplitude in cyclic simple shear tests (Pestana et al., 2000)

As the structures are expected to be exposed to earthquakes with various frequency of dynamic loading, therefore, the frequency of loading affects the shear behavior of the material in the laboratory tests. The literature review announced loading frequency in typical dynamic situation as shown in Table 2.8.

Table 2.8 Loading frequency in dynamic situation (modified after Araei et al., 2012)

Sources	Frequency (Hz)	Reference
Earthquake	0.1 - 10	Shibuya et al. (1995)
	0.5 - 13	Araei et al. (2009)
	< 15	Silva et al. (1988)
Traffic	< 20	O'reilly and Brown (1991)
Sea wave	0.05 - 0.07	O'reilly and Brown (1991)
Machine foundation	10 - 100	Ishihara (1996)
Storm	0.01 - 0.1	Shibuya et al. (1995)

Araei et al. (2012) analyzed the effects of loading frequency on shear stress-strain behavior of rockfill materials under cyclic loading conditions. Figure 2.21 displays the stress-strain hysteresis loop at almost the same amplitude of deviatoric stress and strain at effective confining pressure of 1,000 kPa, at the 10^{th} cycle under loading frequency of 0.1 and 10 Hz. Some differences in the hysteresis loop were found that an elliptical shape was observed at high loading frequency. The obtained hysteresis loop indicates the importance of loading frequency on damping ratio, which is calculated by the

geometrical shape of the hysteresis loop. Namely, the increase in loading frequency caused the increase in Young's modulus, however the test results exhibited the rate of increase in Young's modulus due to increase of loading frequency decreased at the strain higher than 0.005 %, which implied that the Young's modulus is slightly affected by loading frequency. Therefore, it is induced that the strength of the specimen is not affected by loading frequency seriously. Shibuya (1995) also announced that soil behavior was often assumed to be independent of the frequency of seismic loading of 0.1 to 10 Hz, as a common practice in geotechnical engineering.

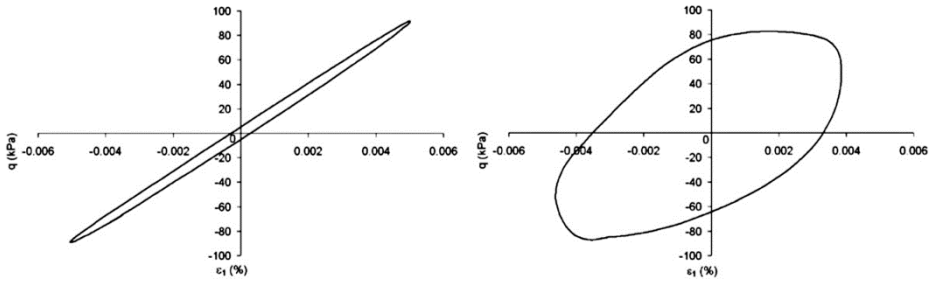

(a) 0.1 Hz (b) 10 Hz

Figure 2.21 Effect of frequency of cyclic loading (Araei et al., 2012)

Another topic to review in this chapter is about the boundary condition of cyclic simple shear test because the boundary condition of the specimen may represent the in-situ states at shear deformation. Fakharian and Evgin (1997) summarized the three typical boundary conditions and conducted an experimental research to investigate cyclic simple shear behavior of sand-steel interfaces. The stiffness in the normal direction to the interface is commonly denoted by K, and it is defined as the ratio of the variation in the normal

stress to the variation in the normal displacement at the upper boundary of the sample, as follows:

$$K = \frac{d\sigma_n}{d\nu} \tag{2.3}$$

where, σ_n is the normal stress and ν is the normal displacement at the interface, respectively. Three typical boundary conditions are generally used in laboratory experiments:

$$\text{Case Ⅰ.}\quad K = 0, \text{ i.e., } d\sigma_n = 0; d\nu \neq 0 \tag{2.4}$$

$$\text{Case Ⅱ.}\quad K = \infty, \text{ i.e., } d\sigma_n \neq 0; d\nu = 0 \tag{2.5}$$

$$\text{Case Ⅲ.}\quad K = \text{constant, i.e., } d\sigma_n \neq 0; d\nu \neq 0 \tag{2.6}$$

Case Ⅰ, i.e., the 'constant normal stress' is a representation of the condition in which the normal stress does not change during the process of shearing as demonstrated in Figure 2.22 (a). In this case, the interface may compress or dilate freely ($d\sigma_n = 0; d\nu \neq 0$). In simple shear or torsional shear device, it is usual for a constant normal stress to be applied across the interface while the behavior under steadily increasing shear load or relative

shear displacement is observed. Tests under this boundary condition provide useful strength data for certain types of engineering problems such as slope stability. In the field, blocks of soil or rock may slide upon discontinuities by gravity and in many cases it is reasonable to assume that the stress acting normal to the shearing plane remains constant during shear. However, there exist practical problems where the normal stress on the interface may not remain constant as shear occurs. If dilation or contraction were to take place, the normal stress could change during the shear (Ooi and Carter, 1987).

Case Ⅱ is the condition of 'constant volume.' No displacement is allowed at the upper boundary of the sample in the direction normal to the interface plane as illustrated in Figure 2.22 (b). During the test, the normal stress increases or decreases depending on the tendency of the soil to dilate or compress ($d\sigma_n \neq 0; dv = 0$). This condition may simulate the situation that abrupt displacement of materials above or beneath the interface occurs, therefore, it was considered in the present study.

Case Ⅲ is the condition of 'constant normal stiffness.' Normal stress and normal displacement vary proportionally where the proportionality constant is denoted by K ($d\sigma_n/dv = K$), as shown in Figure 2.22 (c). Therefore, Case Ⅰ and Case Ⅱ are the lower and upper bounds of Case Ⅲ, respectively. A few researchers built a machine capable of shear testing an interface under condition of constant normal stiffness. Fakharian and Evgin (1996, 1997) developed an automated apparatus for three-dimensional monotonic and cyclic testing of interfaces, named C3DI, and investigated the cyclic simple shear behavior of sand-steel interfaces, which represented the situation such as a pile-soil interface. Dry medium crushed silica sand and a

rough steel plate were selected as the testing material, and cyclic simple shear test was performed. It was concluded that the reduction in maximum shear stress was not only due to the reduction in normal stress, but also to a greater extent due to the increased amount of mobilized sliding displacement at the interface with an increasing number of cycles. The reduction in maximum shear stress with cycles was dramatic when failure was experienced at the interface, i.e., when the shear stress-normal stress ratio reached a peak value and subsequently approached a residual value. Figure 2.23 displays the schematic of C3DI, and the variations of shear stress, stress ratio, and normal stress with time are also shown in Figure 2.24.

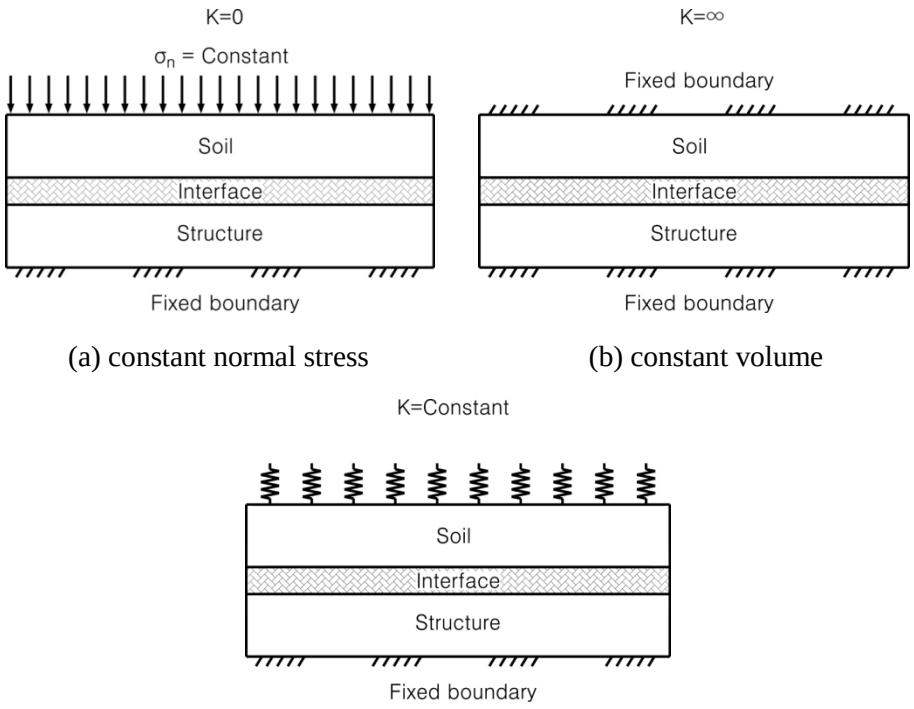

(a) constant normal stress (b) constant volume

(c) constant normal stiffness

Figure 2.22 Boundary conditions of cyclic simple shear test (Fakharian and Evgin, 1997)

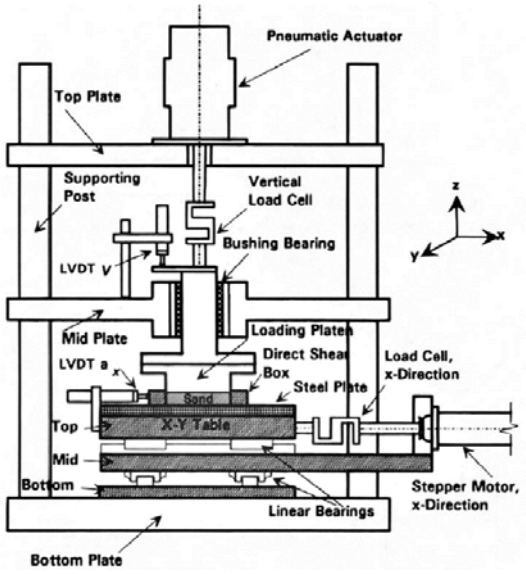

Figure 2.23 Schematic of C3DI (Fakharian and Evgin, 1996)

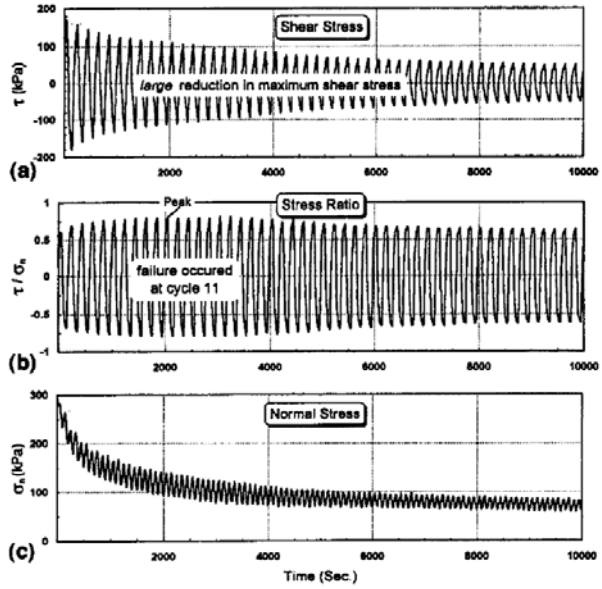

Figure 2.24 Variations of (a) shear stress; (b)stress ratio; (c) normal stress with time (Fakharian and Evgin, 1997)

However, there have been a few problems to reproduce the constant normal stiffness condition in the laboratory. Since the normal displacement should be controlled by feedback of normal stress, complexity and sensitivity of the apparatus increase, hence, the likelihood of mechanical errors also increases. Furthermore, the vertical friction between the shear device and plunger of the normal controller may affect the ability of maintaining the normal stiffness of the boundary constant. Based on the previous studies, the constant normal stiffness apparatus has been utilized mainly in the field of rock mechanics (Leichnitz, 1985; Ooi and Carter, 1987; Jiang et al., 2004).

2.5 Disturbed State Concept (DSC)

An understanding of the engineering behavior of the interfaces between structural and geological materials subjected to cyclic earthquake-type loading is important for safe and improved analysis and design of many geotechnical structures. Especially for the waste landfill site in the present study, it is also important to utilize the appropriate constitutive model in order to obtain more precise solutions of geosynthetic-soil interface behavior. In the geotechnical engineering field, many advanced constitutive models such as Mohr-Coulomb, Ramberg-Osgood, HiSS model, etc., have been introduced, however, these conventional models are not enough to predict or simulate the realistic damage progress at the geosynthetic-soil interface (Park, 1997; Kwak et al., 2013[b]).

The Disturbed State Concept (DSC) and disturbance function have been employed to understand the chemical effects on the interface in this study. The disturbance function is a key factor of DSC to define dynamic shear stress degradation quantitatively. The convenience and reliability of DSC have been successfully verified by previous researches (Armaleh and Desai, 1990; Ma, 1990; Rigby and Desai, 1995; Park et al., 2000), and it also showed the valuable accomplishment in the numerical formulation of dynamic interface behavior (Seo et al., 2004). Table 2.9 summarized the previous verifications of DSC with respect to various interfaces.

Table 2.9 Verification of DSC

Interfaces / Materials	Type of loading	References
Sand-concrete	cyclic	Desai & Nagaraj (1988)
Rock joints	monotonic	Ma (1990)
Dry sand	monotonic	Almaleh & Desai (1990)
Rock joints	monotonic	Desai & Ma (1992)
Sand-steel	cyclic / monotonic	Alanazy (1996)
Sand-steel	cyclic	Navayogarajah et al. (1992)
Sand-geosynthetics	monotonic	Pal & Wathugala (1999)
Geosynthetics	monotonic	Seo et al. (2004, 2007)
Sand-geosynthetics	cyclic	Kwak et al. (2013)[a]
Sand-geosynthetics	cyclic	Kwak et al. (2013)[b]

2.5.1 Overview

The early theory of DSC was originated by Desai (1974) to characterize the softening behavior of an overconsolidated soil using its behavior in normally consolidated state as reference state. This initial concept was later developed and unified as Disturbed State Concept (DSC) to model the behavior of a wide range of materials (Desai and Ma, 1992; Desai, 1995).

The Disturbed State Concept is based on the physical principle that the behavior exhibited through the interacting mechanisms of components in a mixture can be expressed in terms of the responses of the components

connected through a coupling function, called the disturbance function (Desai, 2001), which will be explained later in detail. Accordingly, there are two reference states, relative intact (RI) and fully adjusted (FA) state, which express the initial and final condition of material in the DSC. The initial condition is defined as RI state and the material continuously approaches to the FA state by the external force. The observed state which exists in the middle of RI and FA states can be expressed in terms of RI and FA state. Self-adjustment occurs during this procedure and the disturbance increases in the material's microstructure. Figure 2.25 describes the fundamental of RI and FA states.

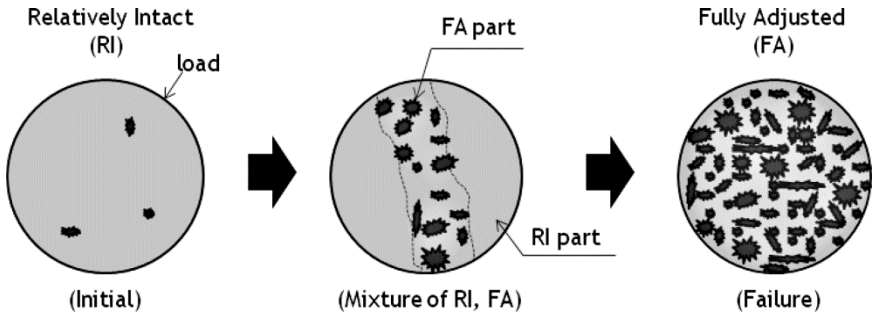

Figure 2.25 Relatively intact (RI) and fully adjusted (FA) states in DSC (Kwak et al., 2013[b])

Though dynamic or static loads cause the different shapes of shear stress-strain response, the overall trend is identical to each other. Shear stress degradation due to the accumulation of internal damage can be observed on both load conditions. Figure 2.26 shows the typical shear stress-strain behavior under the static and dynamic load conditions.

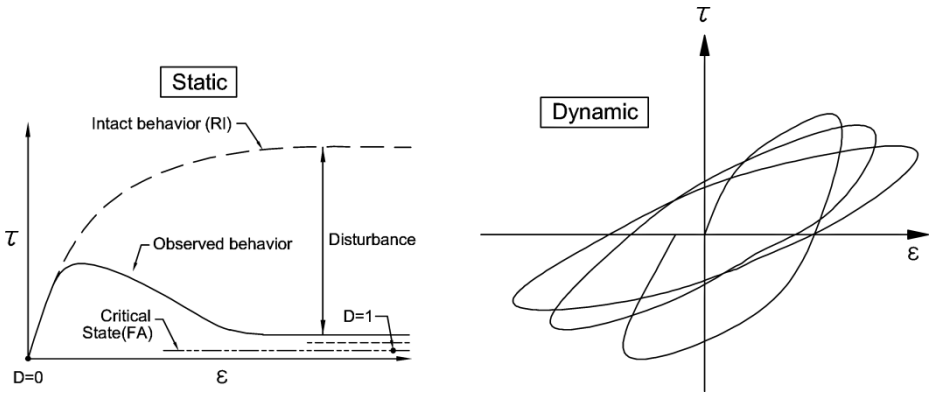

Figure 2.26 Typical shear stress-strain curves (Kwak et al., 2013[b])

2.5.2 Disturbance function and parameters

The disturbance D, represents the deviation of the current state with respect to the initial and final states of the material and it can be expressed by the disturbance function. Therefore, the disturbance function is strong and convenient tool to express the degree of damage quantitatively. The direct way to estimate the disturbance is to measure the total volume of failed region and calculate the ratio to the total volume of intact region. However, it is not practically possible to define the disturbance D based on such physical measurements because there is no way to measure the internal volume of fully adjusted material directly. In lieu of direct measurements, a few equations to define disturbance in terms of variables such as mechanical energy, accumulated plastic strains, normal or shear stresses, etc. have been suggested and verified (Desai, 2001). Those equations are based on the idea that the

degradation in a material is similar to the degradation trend in natural systems and as a result, mathematical functions which express the degradation can be adopted to describe material damage (Kwak et al., 2013[b]).

The disturbance D is known to be the function of certain internal factors which affect the constitutive behavior in a broad sense. In this study, the internal microstructural damage is assumed to be mainly affected by the deviatoric plastic strain trajectory, ξ_D, hence,

$$D = D[\,\xi_D,\ (t, \alpha_i)] \tag{2.7}$$

where, t is time or the number of loading cycles, and α_i means the environmental factors. The physical meaning of deviatoric plastic strain trajectory is the accumulated plastic strain in stress-strain loops through each loading cycles. In the functional form based on the modification of the Weibull (1951) function is:

$$D = D_u \left[\, 1 - e^{(-A\,\xi_D^Z)} \right] \tag{2.8}$$

where, A, Z are intrinsic material parameters decided by the degree of damage, and D_u is the ultimate disturbance which asymptotically approaches 1.0, but can never reach 1.0. Equation (2.8) is commonly accepted for a growth and decay processes (Armaleh and Desai, 1990). D has the value between 0.0 and 1.0 at each strain but many materials fail before D reaches

1.0 (Park and Desai, 2000).

The disturbance can be considered as the deviation of the current (observed) behavior with respect to its behavior in the two reference states, RI and FA, and defined on the basis of the stress-strain, volumetric (void ratio), and nondestructive (velocity or attenuation) behavior. Figure 2.27 displays the typical test data and disturbances from each test.

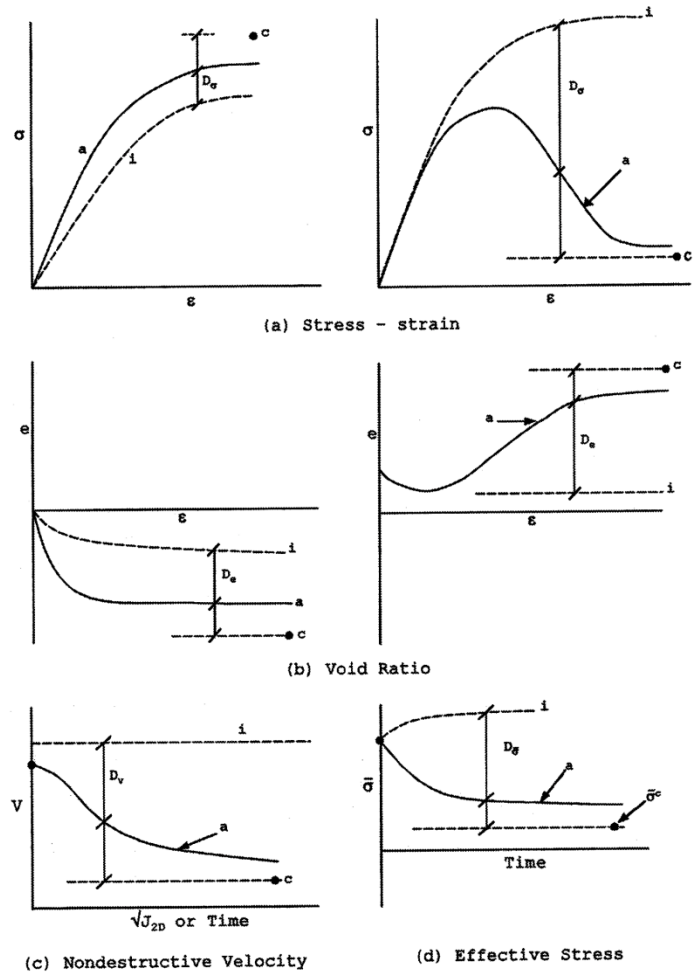

Figure 2.27 Disturbance from static test result (Desai, 2001)

In the cyclic shear test, D value can be defined based on the shear stresses at the RI, FA and the observed cycle as,

$$D = \frac{\tau^{i} - \tau^{a}}{\tau^{i} - \tau^{c}} \tag{2.9}$$

where, $i, a,$ and c denote the RI, observed, and FA states, respectively and the equation evaluates the normalized shear stress degradation, D from each hysteretic loop. ξ_D is the deviatoric plastic shear strain trajectory as mentioned before, then the following equations can be derived from Figure 2.28 to calculate D and ξ_D values directly from the cyclic simple shear test results. The deviatoric plastic shear strain trajectory at the 1st (ξ_{D_1}) and Nth (ξ_{D_N}) cycle can be calculated by:

$$\xi_{D\_1} = \overline{ob} + \overline{bo} + \overline{oa} \tag{2.10}$$

$$\xi_{D\_N} = \overline{cd} + \overline{de} + \overline{ed} + \overline{dc} + \sum_{N=2}^{N} \xi_{D\_N-1} \quad (N \geq 2) \tag{2.11}$$

Note that the positive permanent plastic strain of the hysteretic loop, d_{ε}^{p} is the length of the intercept of strain axis inside the loop as shown in Figure 2.29. By combining the Equation 2.9 through 2.11 and Figure 2.28, the disturbance D and plastic strain trajectory ξ_D can be estimated and expressed as a D function curve.

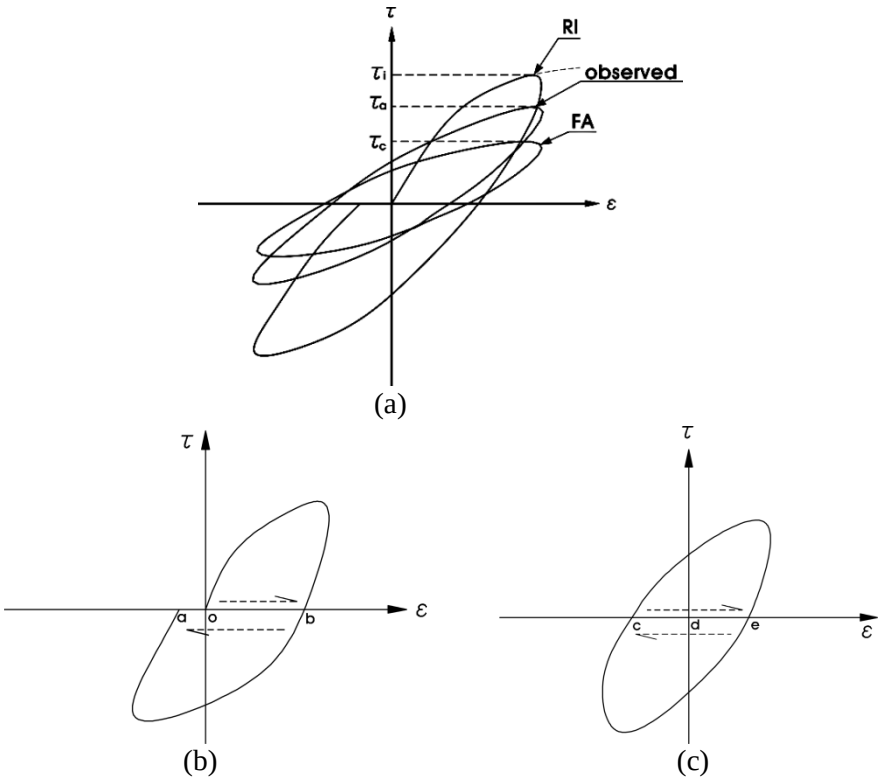

Figure 2.28 Calculation of D and ξ_D

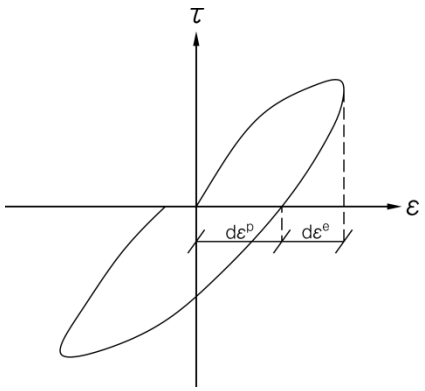

Figure 2.29 Plastic strain of hysteretic curve

Figure 2.30 illustrates the typical shape of D function curves. The degree of damage of a material is determined by the shape of the D function curve, quantitatively. The damage of a material at a certain plastic shear strain trajectory, ξ_1, indicate A or B, depending on the shape of the D function curve. In this example, the variation of the degree of damage can be estimated by ΔD. After obtaining the curve, the disturbance function can be mathematically defined by the intrinsic material parameters A, and Z. Those parameters can be estimated via linear regression of the disturbance function curve. Taking the logarithm twice on both sides of Equation (2.8) yields:

$$\ln\left[-\ln\left(1-\frac{D}{0.99}\right)\right] = \ln A + Z\ln\xi_D \tag{2.12}$$

Note that D_u is 0.99 in Equation (2.8) based on the previous researches (Desai, 2001).

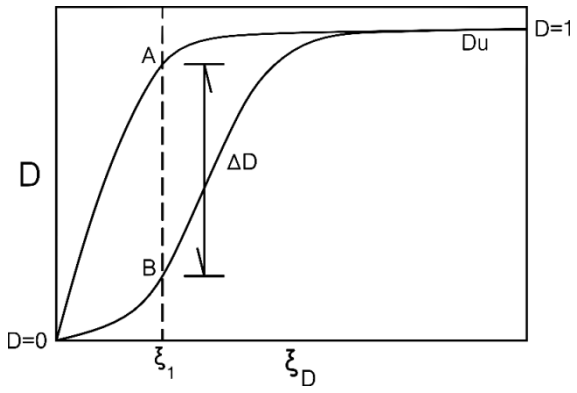

Figure 2.30 Typical D function curves

An example of the result of linear regression is displayed in Figure 2.31. Z is the slope of the line, and the intercept of the vertical axis represents $\ln A$.

The mathematical sensitivity of A, Z parameters was analyzed in Figure 2.32. In case where A increases the curve moves left, which means the material undergoes more damage at small plastic strain level, namely the material approaches the failure in spite of small plastic strain. If Z increases the slope of curve grows, which means the rapid increase of the material damage, namely, the damage significantly grows with small increment of plastic strain. Accordingly, the shear strength characteristics of geosynthetic-soil interface can be defined using the disturbance function visually and quantitatively (Kwak et al, 2013[b]).

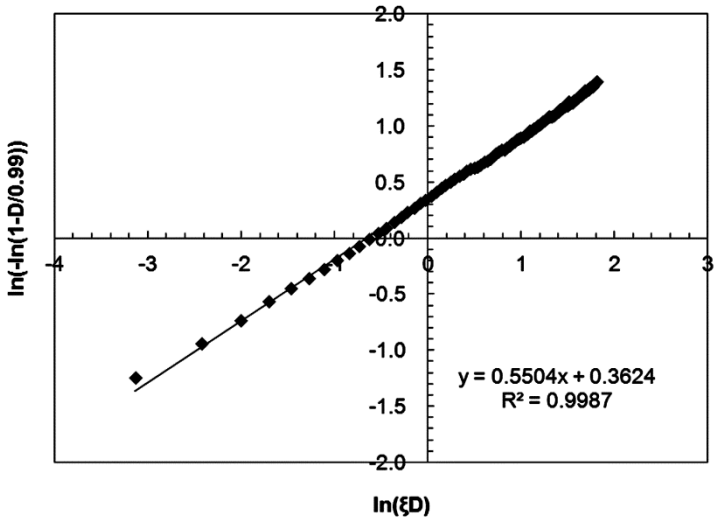

Figure 2.31 Representative plot of linear regression

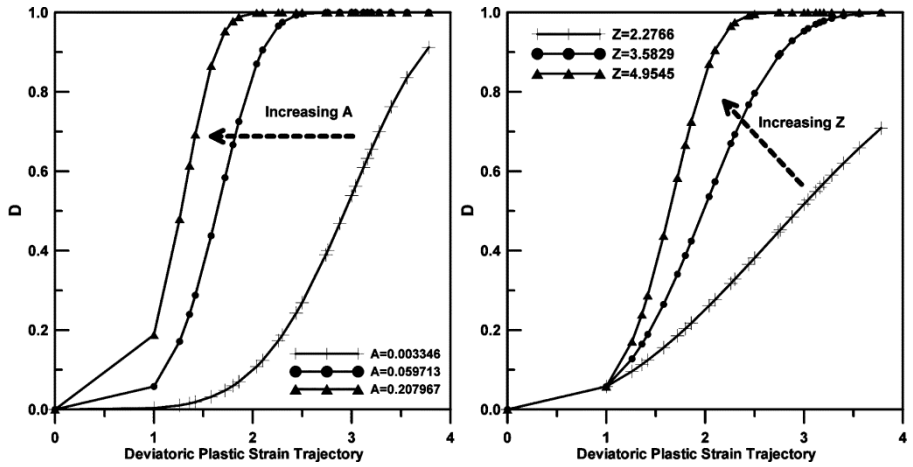

Figure 2.32 Mathematical sensitivity of A, Z parameters (Kwak et al., 2013[b])

2.5.3 Interface studies based on DSC

The Disturbed State Concept and the disturbance function provide appropriate and convenient methodology to investigate the monotonic or cyclic shear behavior of interfaces. Desai et al. (2005) presented one of the studies based on DSC and the disturbance function. Sand-concrete interfaces were tested by cyclic multi-degree-of freedom device and the disturbance function parameters were determined. A series of interface shear test were performed with medium roughness under different normal pressure of 35, 70 and 207 kPa, and two relative densities of 60 and 45 % for Ottawa sand. A typical result for cyclic shear stress versus relative displacement of interface, and the variation of effective normal stress versus time for normal stress of 207 kPa are presented in Figure 2.33. The prediction result by constitutive

modeling is also shown.

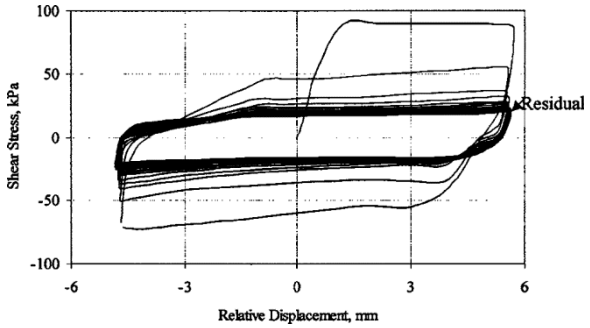

(a) shear stress versus relative displacement

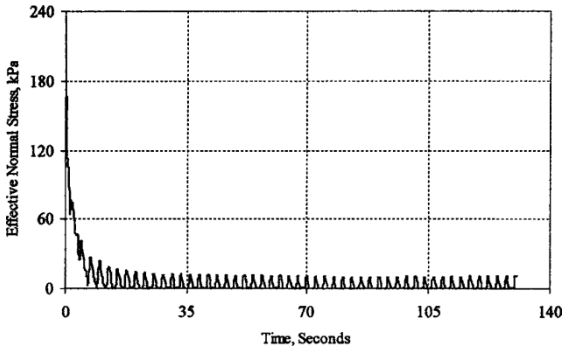

(b) effective normal stress versus time

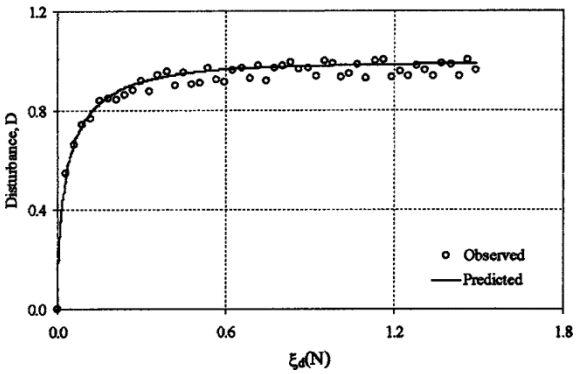

(c) prediction of the disturbance

Figure 2.33 Cyclic simple shear results (Desai et al., 2005)

3. Experimental Works

3.1 Introduction

Shear stress and deformation behaviors of the waste landfill systems under dynamic (earthquake) loading are significantly influenced by the response of interfaces composed of geosynthetics and soil. Chemical aggressors in the leachate may affect the dynamic shear behavior of the interface, however, it has not been investigated yet in detail. Therefore, it is required to develop an appropriate testing device and perform an experimental study considering the chemical effects on the interface to overcome some limitations in theoretical approach.

After the experimental research by Martin et al. (1984), direct shear tests for geosynthetic-soil interface have been recommended and used by many researchers for decades (Seo et. al., 2007). The standard test method to determine the coefficient of soil and geosynthetics under the static condition are well described in ASTM D5321. The test procedures to find interface shear resistance of geosynthetic clay liner by direct shear method are defined in ASTM D6243-09. However, it is still insufficient to test the cyclic shear behavior of the various kinds of interfaces under chemical and dynamic conditions, hence, the development of new apparatus and performing the cyclic simple shear test are the most important portion in the present study.

This chapter was classified into 3 parts. A new interface apparatus and major modifications for better performance were introduced in the first part.

After that, in the second part, tests conditions including test material, chemical, dynamic, and boundary condition were explained. Then finally, the results of cyclic simple shear tests were presented and analyzed. Based on the test results, the degree of damage of geosynthetic-soil interface subjected to chemical conditions was estimated as a form of the disturbance function curves with newly determined parameters, quantitatively.

3.2 Multi-purpose interface apparatus (M-PIA)

3.2.1 Initial model of M-PIA - 1st generation

General

A new apparatus, named as M-PIA (multi-purpose interface apparatus) to investigate the chemical effects on the geosynthetic-soil interface under cyclic loading was manufactured in 2010. This was the 1st generation of the apparatus. Figure 3.1 and 3.2 illustrate the schematic and photograph of the experimental setup of the M-PIA. The apparatus is comprised of the testing device and two peripheral systems: (1) load and displacement application, (2) data acquisition. The testing device is also divided into two modules; the upper and lower module as shown in Figure 3.1. Basically, the M-PIA is devised to perform the strain-controlled test of the interface because the shear stress degradation is to be observed and utilized to estimate the degree of

damage through the DSC theory and Equation 2.9. Generally, an abrupt failure of the specimen occurs in a stress-controlled test, then, it is difficult to observe the shear stress-strain behavior around the failure, or even after the failure. Figure 3.3 compared typical stress-strain relationships under strain and stress controlled conditions.

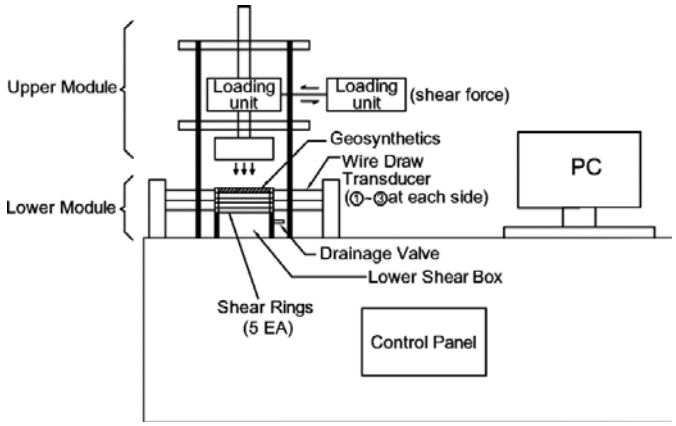

Figure 3.1 Schematic of overall M-PIA (Kwak et al., 2013[b])

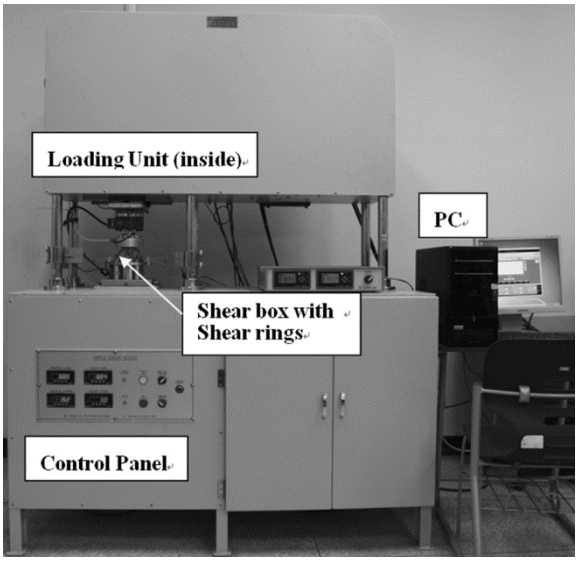

Figure 3.2 Experimental setup (Kwak et al., 2013[b])

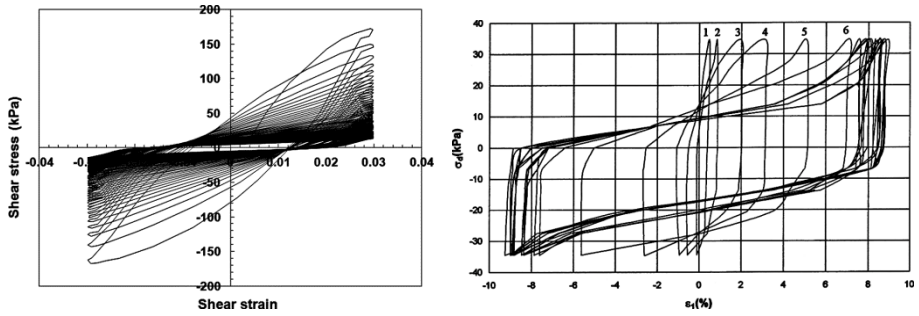

(a) strain-controlled (b) stress-controlled (Park, 1997)

Figure 3.3 Typical stress-strain relationships

External reaction frame

The external reaction frame carries the normal load and transfers the shear load. 4 vertical shafts are connected to the loading plate and exert the normal forces on the upper surface of the specimen. Steel slab is placed at the upper side of the vertical shafts and support the shear load application unit. Maximum vertical load of 50 kN is able to be applied by mechanical motor system.

Shear device

The circular-shaped shear device consists of two components: shear box and shear rings. The geosynthetics and soil specimen are set in the circular shear box of the lower module. The geosynthetic sample is placed on top of the soil and rubber membrane encapsulates the soil and geosynthetic specimen, creating a whole specimen with a volume of 628 cm^3 ($D = 100$ mm, $H = 80$ mm). Five independent shear rings that are 2 mm in thickness were Teflon-

coated to avoid the frictional resistance between rings which may cause inaccuracy in the test results. The schematic with the detailed dimensions of the shear box are presented in Figure 3.4, and photography of the components is shown in Figure 3.5.

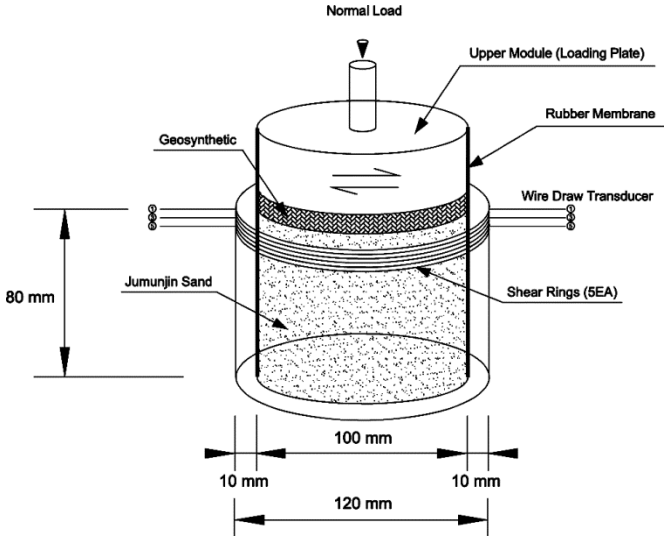

Figure 3.4 Schematic of shear device

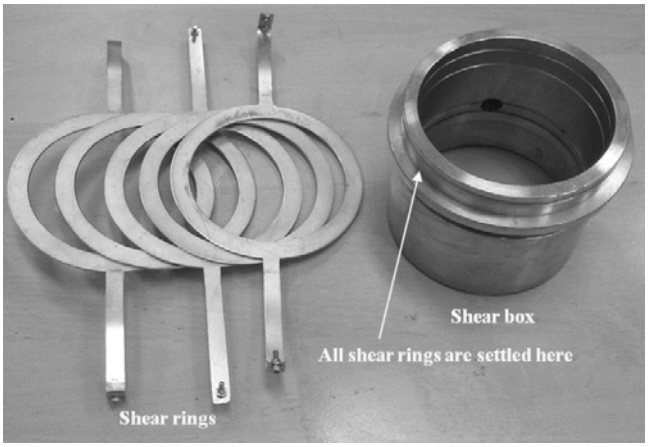

(a) shear box and shear rings (continued)

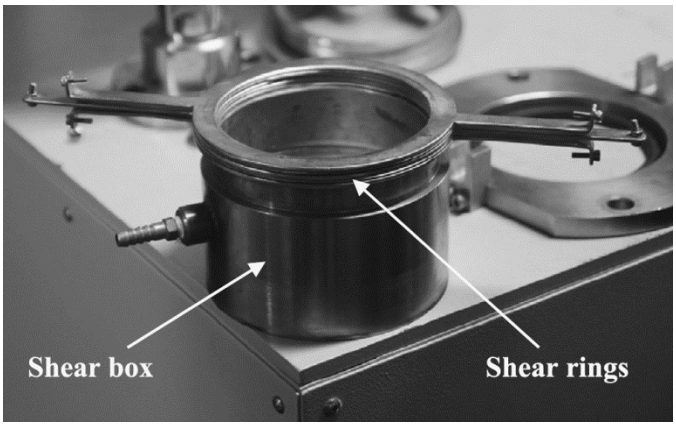

(b) shear rings on the shear box

Figure 3.5 Shear device (Kwak et al., 2013[a,b])

Load and displacement application system

Normal load and shear displacement apply through two independent systems: one controls the normal load applied at the loading plate which contacts the top surface of the geosynthetic specimen, and the other controls the shear displacement with maximum frequency of 1.0 Hz. After reaching the target normal force, then shear displacement is given by a pneumatic actuator. Both two systems consist of an electric servo controller unit which is connected to a precise helical structure. Linear motion slides that are directly connected to the horizontal servo motor are equipped for applying shear displacement and maintain a desired constant rate or frequency of shear displacement. Two separate load and displacement application systems allow the independent measurement of variation of normal force, shear force, and shear displacement. Note that, even though the systems for applying normal load and shear displacement are separated, however, the normal force and

shear displacement are generated by the upper module at once.

Data acquisition system

Wire draw transducers with maximum resolution of 0.01 mm are directly linked with the first, third, and fifth shear rings from the top of the specimen to record the shear displacement during the cyclic shear test, as demonstrated in Figure 3.6.

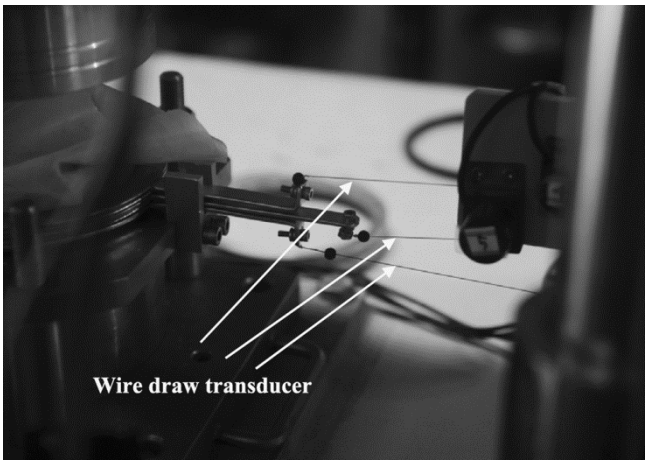

Figure 3.6 Wire draw transducers (Kwak et al., 2013[a])

The data acquisition system contains the software package built by Dong-Ah Testing Machine Co., and minimum data logging interval is 0.3 second. All measured forces and displacement are automatically stored by the embedded software.

Figure 3.7 displays the specimen setup, and Table 3.1 summarized the specifications of M-PIA in 1st generation.

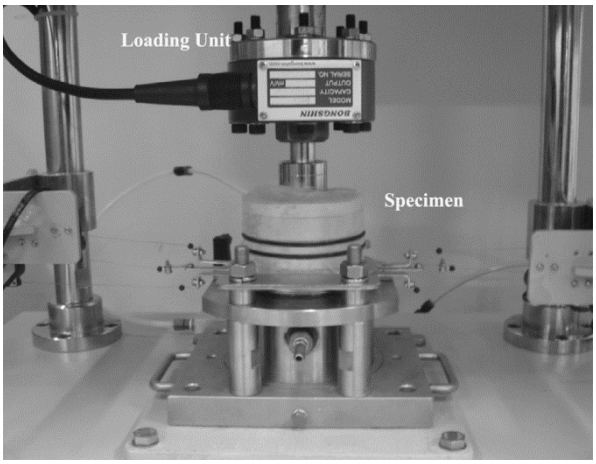

Figure 3.7 Specimen setup (Kwak et al., 2013[a])

Table 3.1 Specifications of M-PIA (1st generation)

Component	Specifications
Specimen Size	- 100 (Dia.) X 80 (H) mm
Loading system	- Max. load : 50 kN, horizontal
	- Max. load : 50 kN, vertical
	- Max. traveling dist. : 150 mm, horizontal
	- Max. traveling dist. : 150 mm, vertical
	- Precise helical structure
	- Linear motion slides
Servo motor	- Horizontal : helical servo motor system
	- Vertical : helical servo motor system
Range of horizontal vibration	- 1.0 Hz
Data acquisition system	- Data logging interval : 0.3 s
Power	- 220 V, 60 Hz
Resolution of wire draw transducer	- Horizontal : 0.01 mm

3.2.2 Minor modifications of M-PIA - 2nd generation

Though a few successful accomplishments (Kwak et al., 2013[a]; Park et al., 2010) some items to be improved was found. First of all, the cyclic shear force exerted by the upper module was able to induce a bending moment at the normal loading axis because direction of the lateral force to create the shear displacement of the specimen and normal force are perpendicular. When the moment is generated, the initial M-PIA model showed a rocking movement of the loading plate (see Figure 3.8).

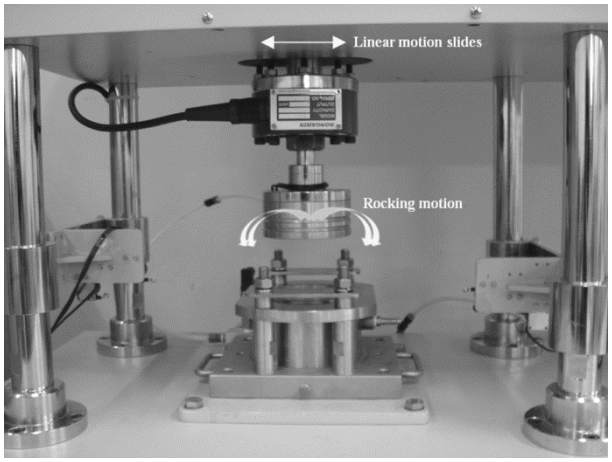

Figure 3.8 Rocking problems in M-PIA of 1st generation (Kwak et al., 2013[b])

Two pairs of railways were welded on top and beneath of the slab to guide the liner motion sliders, and the railways successfully minimized the effect of the moment. Figure 3.9 illustrated the modified slab with railways.

Figure 3.9 Modified M-PIA with railways (Kwak et al., 2013[b])

Another problem was the rough data acquisition system. 0.3 second was not a sufficiently small interval to readout the shear stress-strain responses in detail. Figure 3.10 displays the raw data before the improvement. The optimization of the embedded software package made it possible for data logging interval to be reduced to 0.1 second, then the smooth shear stress-strain curves were able to be obtained due to the minimizing of data missing as shown in Figure 3.11.

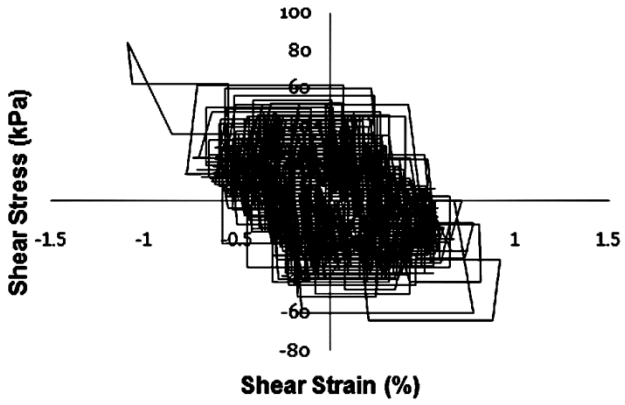

Figure 3.10 Rough data acquisition

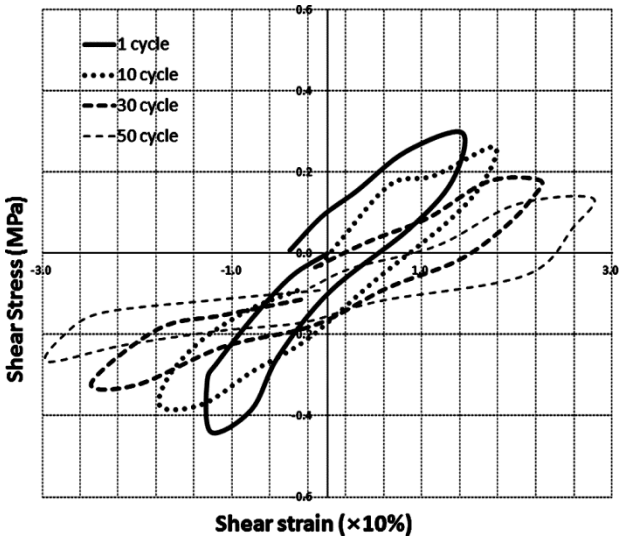

Figure 3.11 A modified shear stress-strain curves after software optimization

3.2.3 Major modifications of M-PIA - 3rd generation

Though a few successful accomplishments by M-PIA of 2nd generation (Kwak et al., 2013[a]; Park et al., 2010), some limitations of the performance were found. Four major improvements to overcome the limitations in the previous versions of M-PIA were presented.

Separation of loading systems

First improvement was the re-design of the basic structure in the load and displacement application systems. The load and displacement application systems were separated into the upper and lower module, as shown in Figure

3.12. Normal load set to be only applied by the upper module and preset lateral displacement set to be exerted by the lower module to avoid the effect of the non-horizontal resultant force. In the previous versions, normal load and shear displacement were exerted by the upper module at once, accordingly, the direction of the resultant of those force vectors was diagonal and generated unintended bending moment in the specimen. By dividing the loading unit into each independent module, the effect of non-horizontal resultant force became negligible. This seemed to be the most important modification of the apparatus.

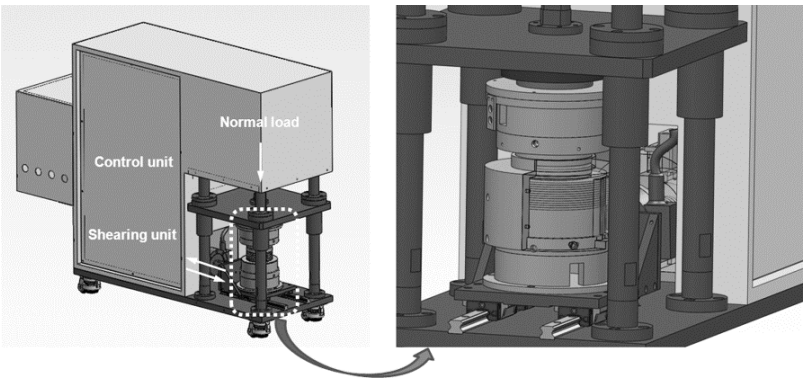

(a) schematic of structure

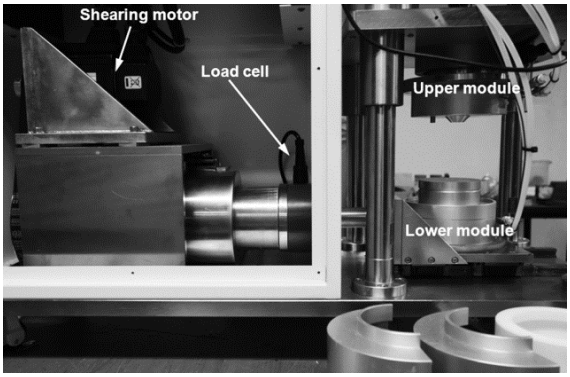

(b) separation of load and displacement application systems

Figure 3.12 Structural modification of M-PIA (3rd generation)

Teflon shear rings

Second improvement was that the raw material of shear ring changed from steel to Teflon for minimizing the frictional resistance between each ring, which may cause inaccuracy in shear force and displacement readouts. The number of shear ring increased from 5 to 12 as well. It is known that the coefficient of friction of Teflon is from 0.2 to 0.04, which is the smallest value in all solid materials. Additionally, the thickness increased from 2.0 mm to 3.0 mm due to secure the stiffness of shear ring itself and prevent from tearing the membrane during shearing. As Teflon also shows good dimensional stability and chemical resistance, hence, it is considered as an appropriate material comprising the shear ring. Entire soil and geosynthetic specimen set to be encircled by 12 independent shear rings, with 2 mm of dummy thickness at top and bottom of the outer mold to avoid the leakage of sand or liquid, therefore the total height of the geosynthetic-soil specimen is 40 mm. The inner diameter of the shear ring is 100 mm, same as the previous versions and the outer diameter is 140 mm. Figure 3.13 and 3.14 display the schematic and photography of shear box and shear rings, respectively.

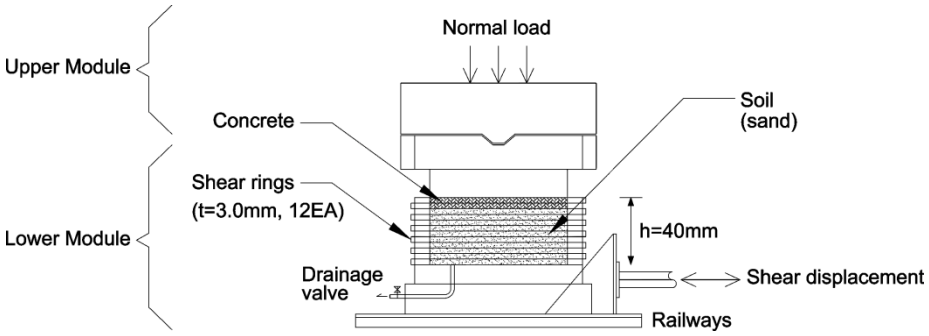

(a) modified shear box (continued)

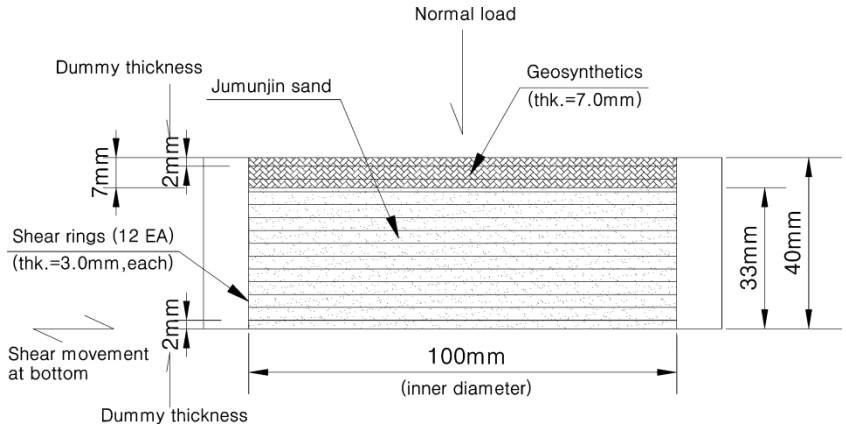

(b) section of specimen in shear box

Figure 3.13 Schematic of shear device (Kwak et al., 2014)

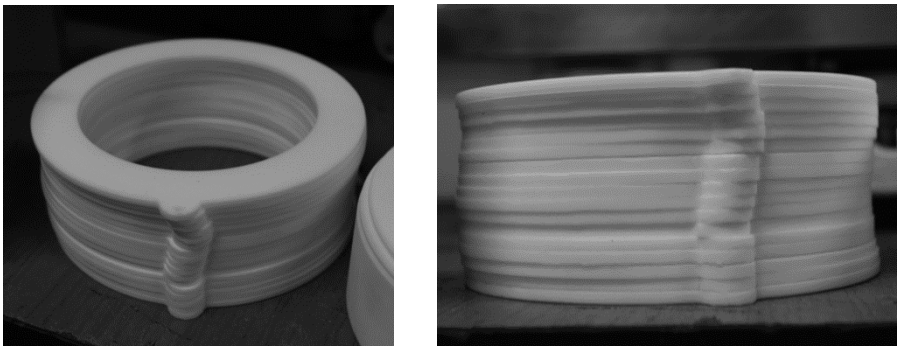

(a) isometric view (b) side view

Figure 3.14 Shear rings

Outer mold

Third modification is the invention of the outer mold for easy set-up of the specimen. Shear rings and specimen are set up inside the mold and the whole mold moves on top of the lower module. Then, the outer mold is split into half-and-half and removed with minimum disturbance of the

geosynthetic-soil specimen. The outer mold enables easy and rapid set-up of the specimen without inceptive displacement of shear rings, accordingly, the reliability of the test increases. Figure 3.15 demonstrates the procedures of the specimen set-up and Figure 3.16 shows the test-ready state of the specimen.

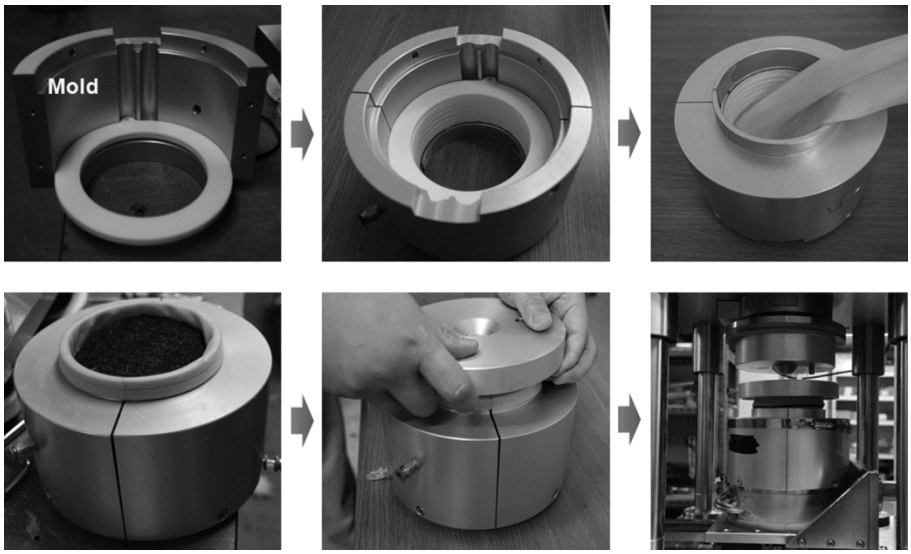

Figure 3.15 Specimen set-up procedures using outer mold

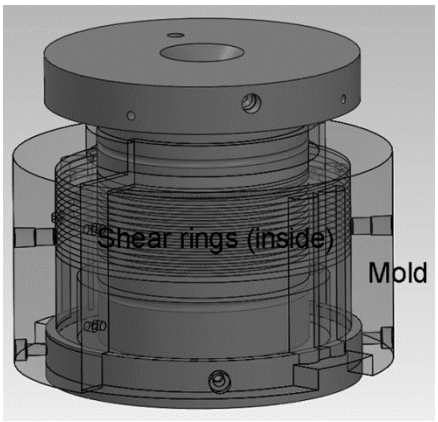

(a) specimen in outer mold

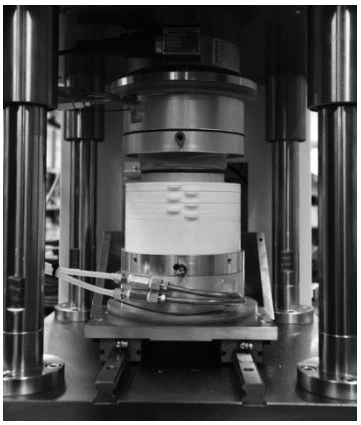

(b) after mold removal

Figure 3.16 Test-ready state of the specimen

Load control system

Last major modification is the adoption of a closed loop controlling algorism in the load control system while the previous versions utilized an open loop control system. The closed loop controlling is able to consider the feedback from the output of the system during the test. An open-loop controlling, also called a non-feedback controlling, is a type of controlling that computes its input into a system using only the current state and its model of the system, therefore, the system does not observe the output of the processes and may not balance the output of the processes. In the loading process, the open controlling cannot adjust the inertia force at the inflection point of load or displacement phases. On the other hands, the closed loop controlling continuously monitors the output of the processes and compensates the errors of the system automatically.

A proportional-integral-derivative (PID) controller was employed as a closed-loop controlling system to manifest the sinusoidal shear displacement in the apparatus. Figure 3.17 illustrates the output signals from the open and closed cycle, and Figure 3.18 displays a typical readout of the system response in the present apparatus.

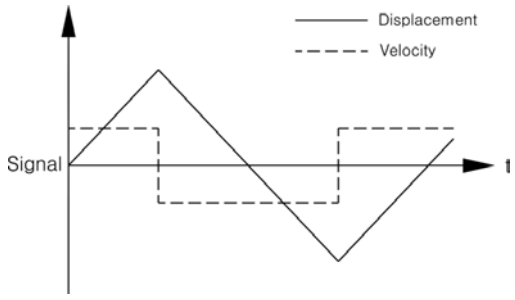

(a) open loop signal readout (continued)

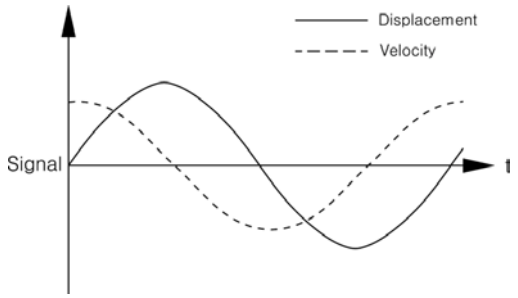

(b) closed loop signal readout

Figure 3.17 Signal response of the open and closed loop

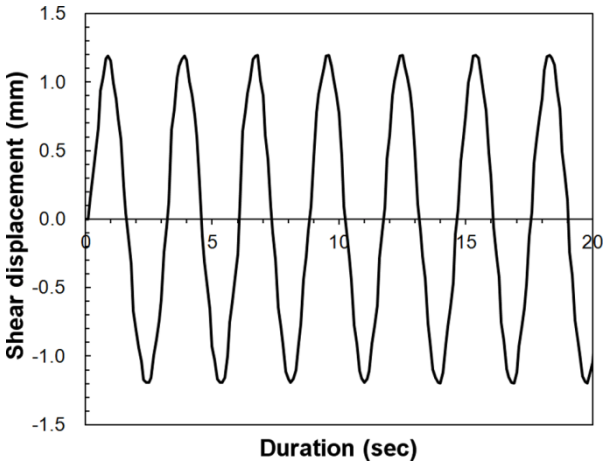

Figure 3.18 A typical readout of the system response

Four major improvements such as the separation of loading application systems, Teflon shear rings, the invention of outer mold, and the modification of the load control system were reviewed in this section. Based on the improvements, Table 3.2 integrated the overall specifications of the present apparatus

Table 3.2 Specifications of M-PIA (3rd generation)

Component	Specifications
Device Size	- 1,300 (L) X 600 (W) X 1,00 0 (H) mm
Loading system	- Max. load : 10 kN, horizontal
	- Max. load : 10 kN, vertical
	- Max. traveling dist. : 150 mm, horizontal
	- Max. traveling dist. : 150 mm, vertical
	- Precise helical structure
	- Linear motion slides
Servo motor	- Horizontal : helical servo motor system
(SB04A 60D)	Max. velocity : 5,000 r/min
	- Strain-controlled test : velocity range of
	0.001 to 100 mm/min
	- Vertical : helical servo motor system
	Max. velocity : 5,000 r/min
	- Screw jack : SJ32 Traveling shaft type
	▪ Traveling distance : 100 mm
	▪ Traveling velocity : 5 to 200 kN/min (by load)
	0.1 to 100 mm/min (by displ.)
	▪ Max. load : 10 kN ± 10 %
Range of horizontal vibration	- 0.01 to 1.0 Hz
Data acquisition system	- 4 Ch. Of PID output
	- Data logging interval : 0.1 s
Power	- 220 V, 60 Hz, 15 kW
Load cell resolution	- Horizontal : 0.1 N
	- Vertical : 0.1 N

3.3 Test conditions

A series of cyclic simple shear tests were conducted in accordance with the chemical conditions, submerging periods, and the normal stress applied to the specimen. In this study, all laboratory tests were performed at room temperature of 23±2 ℃ for the geosynthetic-soil interface. Each test condition was presented and the specifications of the geosynthetic material and soil were also described.

3.3.1 Test materials

The materials in the test of the geosynthetic-soil interface are literally the geosynthetics and granular soil. Jumunjin sand is used as the typical type of a granular soil in the present study. The particle size of Jumunjin sand is uniform and the grain-size distribution was presented in Figure 3.19 (a) and the physical characteristics were summarized in Table 3.3. Note that this research is limited to the Jumunjin sand in the viewpoint of the test material, and the behavior of the in-situ sand (SM) may display different response. However, the particle-size distribution curve of the poorly-graded sand (SP) spread on the geosynthetics based on the waste management regulations shows similar trend to the curve of Jumunjin sand as shown in Figure 3.19 (b).

The types and characteristics of geosynthetics were already reviewed in Chapter 2.2. Among the various geosynthetics, a composite type of

geosynthetics, i.e., geocomposite has been the most commonly applied to the waste landfill site in Korea, because it exhibits the vigorous chemical resistance and diverse combination of geosynthetic materials enables the waste landfill design subjected to the in-situ condition. Figure 3.20 demonstrates the cross-section and surface of the geocomposite utilized in the present experimental study.

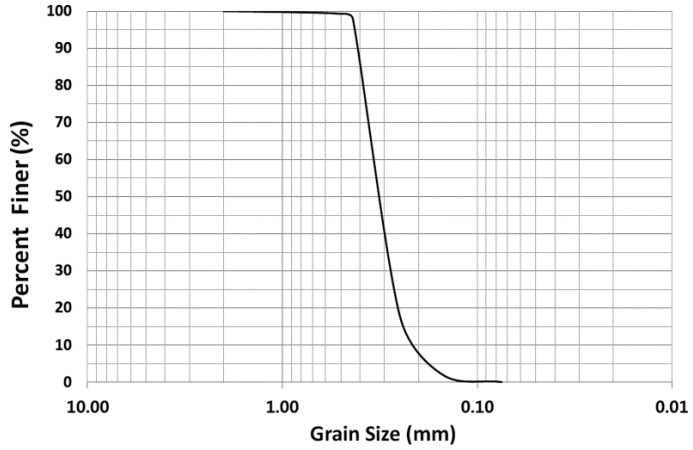

(a) Jumunjin sand

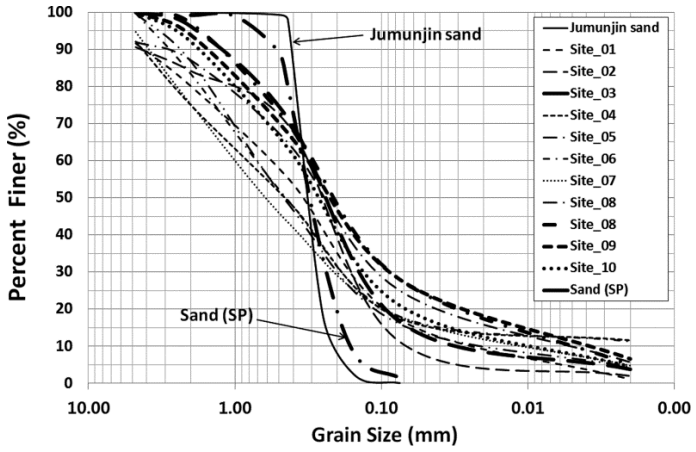

(b) In-situ sand (SM) vs. Jumunjin sand (SP)

Figure 3.19 Grain size distribution curves

Table 3.3 Properties of Jumunjin sand

USCS	G_s	Max. dry density (kN/m^3)	Min. dry density (kN/m^3)	e_{max}	e_{min}
SP-SM	2.65	16.18	13.63	0.908	0.527

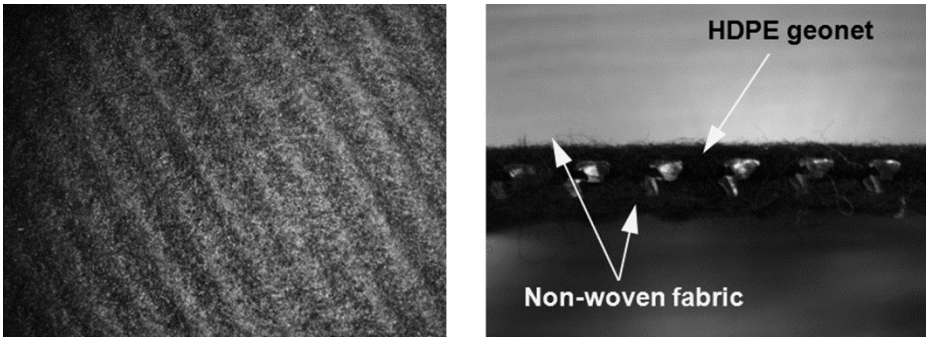

(a) surface (b) section

Figure 3.20 Geosynthetic materials

The specifications of the geocomposite are shown in Table 3.4. Nonwoven fabric is laminated on both sides of a geonet by thermal bonding. The main ingredient of the geonet is HDPE and the filament of the nonwoven fabric is made of Polyethylene and Polypropylene.

Table 3.4 Specifications of geocomposite

Type	Geocomposite (geonet + nonwoven fabric)
Manufacturer	GOLDENPOW, Korea
Ingredients	Geonet (HDPE), nonwoven fabric (PET+PP) Carbon black (2.2%), antioxidant
Thickness	7.0 mm (ASTM D 5199-12)
Tensile strength (kN/m)	18.1 (longitudinal) / 7.6 (transversal)
Unit weight (kN/m^3)	4.62
Density (kN/m^3)	9.29

3.3.2 Chemical conditions

This study is based on the idea that the chemical aggressor in the leachate generated from the decomposition process of the waste landfill shall affect the shear behavior of the geosynthetic-soil interface under the dynamic loading condition. As the antioxidant such as carbon black is added to the manufacturing process for HDPE, it is postulated that the soil decay shall be the main reason of shear strength degradation of the geosynthetic-soil interface. The researches on the shear strength degradation of geosynthetic-soil interface under the dynamic loading condition have been conducted limited (Desai et. al., 1997; Park et. al., 2000), or on the decay of raw materials from the chemical conditions only have been also performed (Masada et. al., 1994; Stessel and Hodge, 1995). However, this study

considered both the chemical effect on the geosynthetic-soil interface and the dynamic loading condition occurring at the same time.

Previous studies showed that the *p*H value changes dramatically due to the complicated biological and chemical reactions in the leachate (see Chapter 2.3.2). Therefore, in this study, the chemical conditions of leachate were incorporated by the buffer solutions showing different *p*H values, as demonstrated in Figure 3.22. The soil conditions under which the various substances are rendered soluble and removed through leaching or combination with other substances appear to depend mainly on the *p*H of the surround liquid (Gidigasu, 1976). For example, metal dissolution is enhanced at low *p*H which is one of the characteristics of young landfill leachate. Solid wastes contain soils and organic matter that have significant sorptive capacity especially at high *p*H values. Furthermore, the *p*H in the leachate is considered to be the most significant parameter affecting leachate concentration (Rafizul and Alamgir, 2012), as mentioned before. Therefore, *p*H values of the solutions are one of the mainly governing factors to manifest the characteristics of the leachate and can represent the chemical conditions in this study.

Both geosynthetic and soil specimen were submerged in the basic, neutral and acid solutions for 30 days and 850 days to consider the short and long-term response of the interface, respectively. The specific chemical conditions are displayed in Table 3.5. Note that this study concerns the geosynthetic-soil interface under severe chemical conditions.

Figure 3.21 Buffer solutions

Table 3.5 Specific chemical conditions

Chemical conditions	Basic	Neutral	Acid
*p*H	10.0	7.0	4.0
Submersion period, days	30 / 850	30 / 850	30 / 850
Main chemical substance	Sodium Bicarbonate ($NaHCO_3$)	Potassium Hydrogen Phthalate ($C_8H_5O_4K$), Phosphate (Na_2HPO_4)	Potassium Hydrogen Phthalate ($C_8H_5O_4K$)

3.3.3 Dynamic conditions

The predominant frequency range of the earthquake load is known to be between 0.1 to 15 Hz, based on the previous studies (Shibuya et al., 1995; Araei et al., 2009; Silva et al., 1988). Soil behavior is often assumed to be

independent of the frequency of seismic loading between 0.1 and 10 Hz. Additionally, ASTM D3999 recommends the frequency of 0.5 or 1.0 Hz in case of applying uniform sinusoidal loading. Based on those researches and recommendation, 0.5 Hz of sinusoidal loading was chosen to perform the cyclic simple shear test.

The effects of the amplitude of shear strain were reviewed in Chapter 2.4.4. A series of strain-controlled tests are required to investigate the tendency of cyclic shear behavior even close to the failure continuously. In this study, some preliminary tests were performed to decide appropriate amplitude of shear strain. The amplitude more than 5 %, the specimen failed too early, that means difficulties to obtain sufficient amount of data to analyze the shear stress-strain behavior. In case of the shear strain less than 1.5 %, shear stress-strain curves showed too steep and congested to examine. Much more cycles were required to reach failure, or the specimen did not even show the failure. Therefore, 3.0 % of shear strain is applied in this study.

3.3.4 Boundary conditions

As described in Chapter 2.4.4, there are three typical boundary conditions generally used in the laboratory test. In this study, the constant volume condition was considered in the apparatus to simulate the abrupt loading condition such as the earthquake loading practically. The advantages and disadvantages were already reviewed in Chapter 2.4.4.

3.3.5 Test schedule

Short and long-term shear behaviors of the geosynthetic-soil interface were considered in the laboratory tests. Each test was performed under the different normal stress conditions. It is reported that the average unit weight of waste landfill shows 15.9 to 17.3 kN/m^3 (Oweis and Khera, 1998) and the cross-sectional area of the specimen is 78.5 cm^2, then the normal stress which represents the height of the waste landfill can be calculated. In this study, the height of 20 m and 40 m were considered as the typical height of waste landfill site, as shown in Table 3.6. The cyclic simple shear test was conducted 6 times at the same chemical condition; therefore, 72 sets of test were accomplished. Table 3.7 summarized the entire experimental schedule.

Table 3.6 Equivalent heights corresponding to the normal stresses

Applied normal load (N)	2,350	5,000
Calculated normal stress (MPa)	0.3	0.6
Calculated height of landfill (m)	20	40

Table 3.7 Test schedule

Submerging period (days)	Normal stress (MPa)	Chemical condition
30	0.3	Acid
		Neutral
		Basic
	0.6	Acid
		Neutral
		Basic
850	0.3	Acid
		Neutral
		Basic
	0.6	Acid
		Neutral
		Basic

*2×2×3×6 = 72 sets

Apart from this test schedule, additional prototype tests considering the elevated temperature were performed and the results were also demonstrated. Temperatures of 20 and 60 ℃ which represent normal and high temperatures of the waste landfills were applied to verify the effect of thermal degradation which is combined with chemical conditions.

3.4 Test results

Totally 72 sets of cyclic simple shear tests were performed in order to investigate the chemical effects on the cyclic shear behavior of the geosynthetic-soil interface. Based on shear stress-strain hysteretic loop at each cycle, the disturbance and plastic shear strain trajectory were obtained. Accordingly, the disturbance function parameters A and Z were also estimated using linear regression technique.

3.4.1 Shear stress-strain behavior

Apart from the cyclic test results, static response of the geosynthetic-soil interface was displayed in Figure 3.22. Composite types of geosynthetics were submerged in acid, neutral, and basic solutions, respectively for 850 day. 0.3 MPa of normal stress was applied in the static simple shear test using M-PIA. In Figure 3.22, the maximum shear strength was 264.6 kPa under neutral condition and the minimum was 230.1 kPa under basic condition. However, shear stresses reached the peak values 14 % earlier in shear displacement under acid and basic conditions than neutral. The initial shear modulus was estimated as 3.9 MPa at all chemical conditions, which means the very initial static shear response of the interface is not susceptible to the chemical conditions. Additionally, a large shear displacement was observed due to slip between soil and geosynthetics.

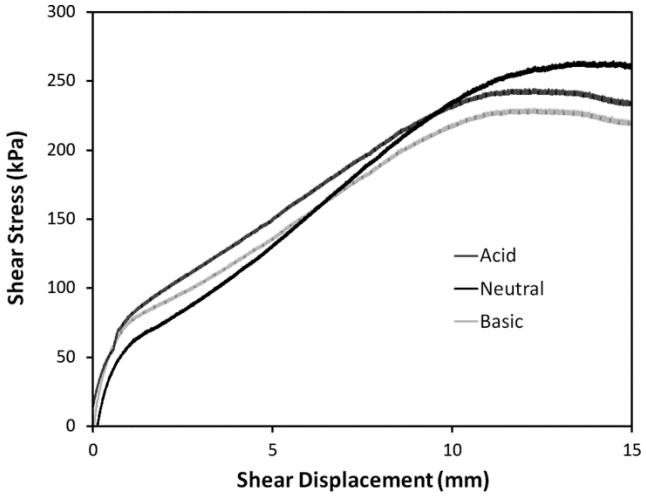

Figure 3.22 Simple shear test results (850 days, 0.3 MPa)

Shear stress-strain curves were obtained by cyclic simple shear test using the modified M-PIA. Figure 3.23 and 3.24 display the representative test results of shear stress-strain relationship under 30 and 850 days of submerging period, respectively. The results were compared in parallel according to the normal stresses. The normal displacement was set to be fixed throughout cycling to maintain constant volume condition.

Obvious shear stress degradation with an increasing number of cycles was observed in all cases. The total number of cycles was 200 and 100 for the specimen submerged for 30 and 850 days respectively because significantly rapid shear degradation occurred in case of 850 days of submerging period. The rate of shear degradation tended to decrease with the increasing number of cycles, but it was not able to be estimated the rate directly, yet. In all cases, shear stresses convergence appeared after 50 cycles, then, it is considered as a threshold of FA state. The maximum shear strain at each cycle showed almost identical value (3 %), therefore, the performance of apparatus seems to be

acceptable.

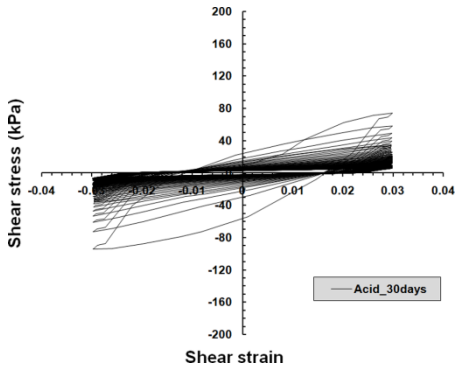

(a) Acid, 30 days, $\sigma_n = 0.3$ MPa

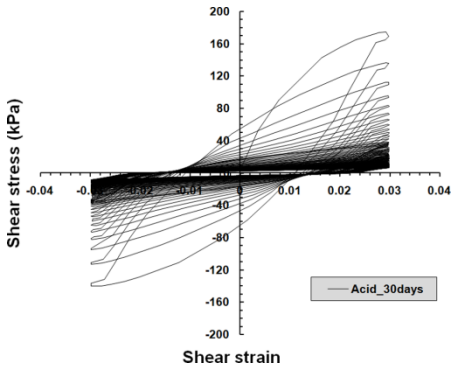

(b) Acid, 30 days, $\sigma_n = 0.6$ MPa

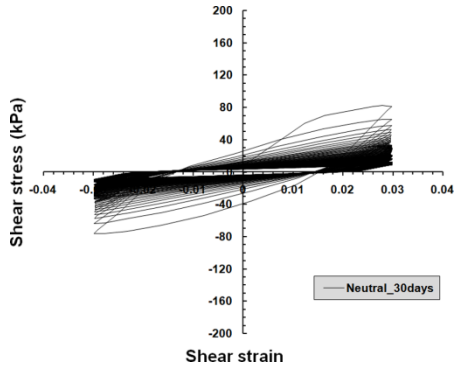

(c) Neutral, 30 days, $\sigma_n = 0.3$ MPa

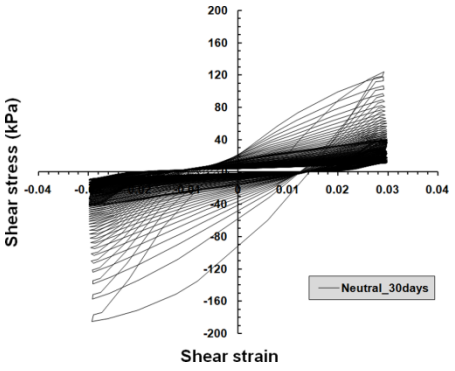

(d) Neutral, 30 days, $\sigma_n = 0.6$ MPa

Figure 3.23 Typical shear stress-strain relationships of 30 days

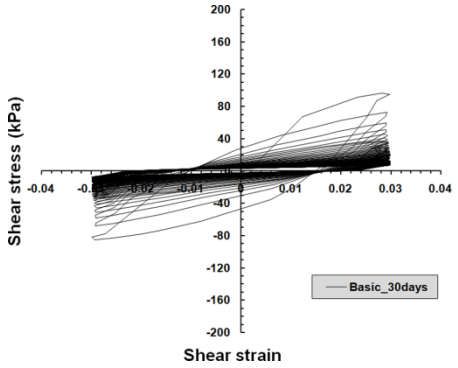

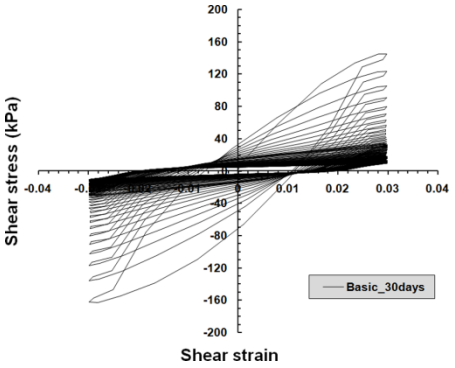

(e) Basic, 30 days, $\sigma_n = 0.3$ MPa (f) Basic, 30 days, $\sigma_n = 0.6$ MPa

Figure 3.23 Typical shear stress-strain relationships of 30 days (continued)

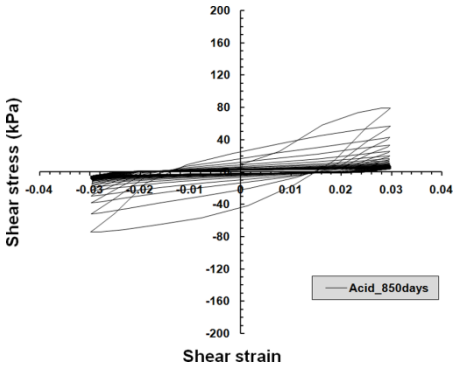

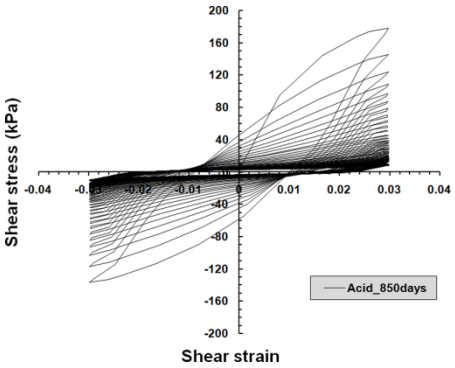

(a) Acid, 850 days, $\sigma_n = 0.3$ MPa (b) Acid, 850 days, $\sigma_n = 0.6$ MPa

Figure 3.24 Typical shear stress-strain relationships of 850 days

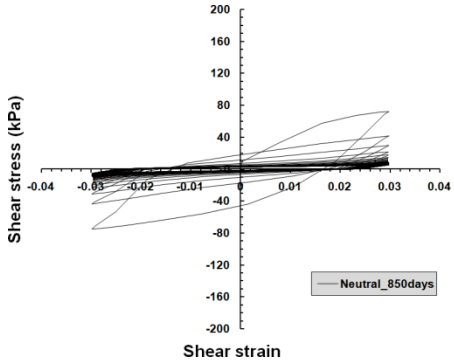

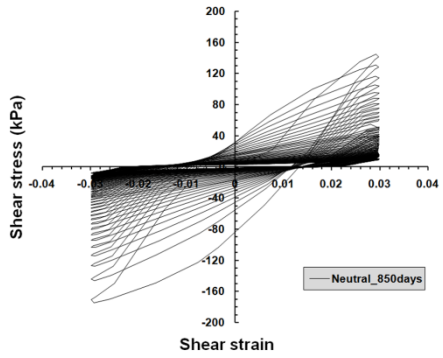

(c) Neutral, 850 days, $\sigma_n = 0.3$ MPa (d) Neutral, 850 days, $\sigma_n = 0.6$ MPa

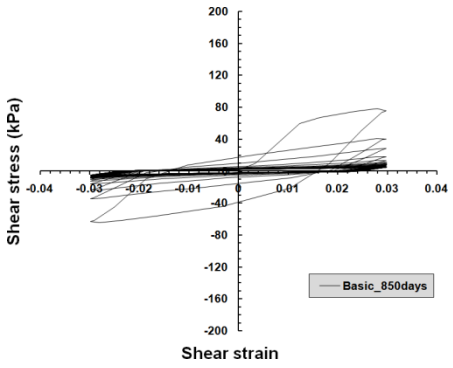

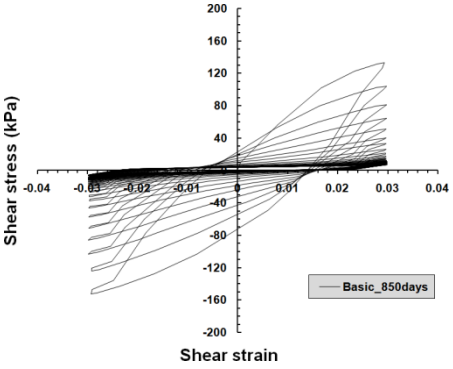

(e) Basic, 850 days, $\sigma_n = 0.3$ MPa (f) Basic, 850 days, $\sigma_n = 0.6$ MPa

Figure 3.24 Typical shear stress-strain relationships of 850 days (continued)

Cyclic simple shear loading was applied after the stabilization of the normal stress of the specimen; therefore, the initial normal stress at the beginning of the shearing should indicate almost identical values at each test, since all the tests are under constant volume condition. Figure 3.25 displays a typical result of the initial normal forces subject to the test conditions, just before shearing. The deviation of initial normal forces showed from 0.04 to 0.91 %, which is considerably acceptable.

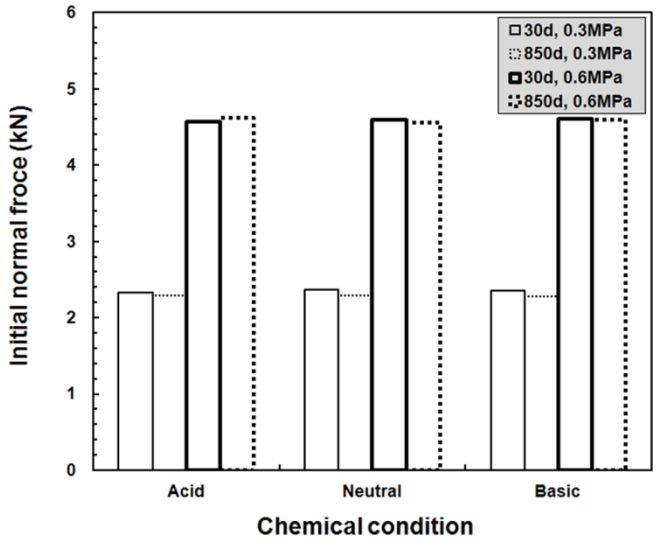

Figure 3.25 Initial normal forces

The plots of normal stress versus time were illustrated in Figure 3.26. The normal stress declined with cycling, showing different rate of decrease. It was observed that the maximum normal stress reached a peak at the first cycle, then, rapidly dropped and stabilized after 35 and 30 cycles in case of 0.3 and 0.6 MPa of normal stress conditions, respectively. The rate of the normal

stress decrease was fastest under the basic condition, especially in the specimen of 850 days of submergence. The variation of the normal stress according to the chemical condition displayed more distinguished in long-term submerged specimen, which means the geosynthetic-soil interface is more vulnerable to the submerging period and *p*H divergence.

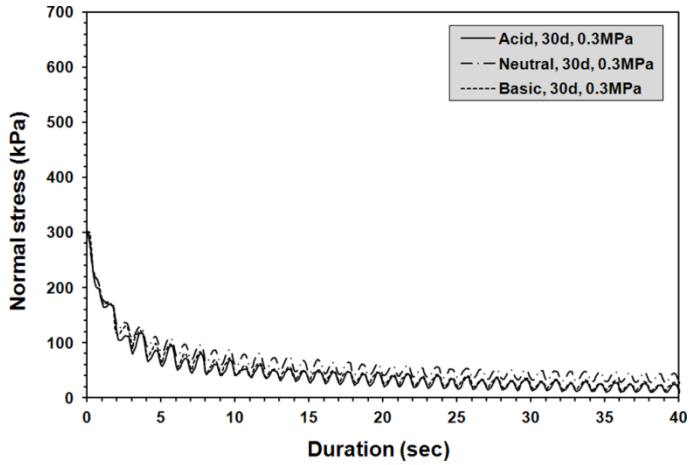

(a) 30 days, $\sigma_n = 0.3$ MPa

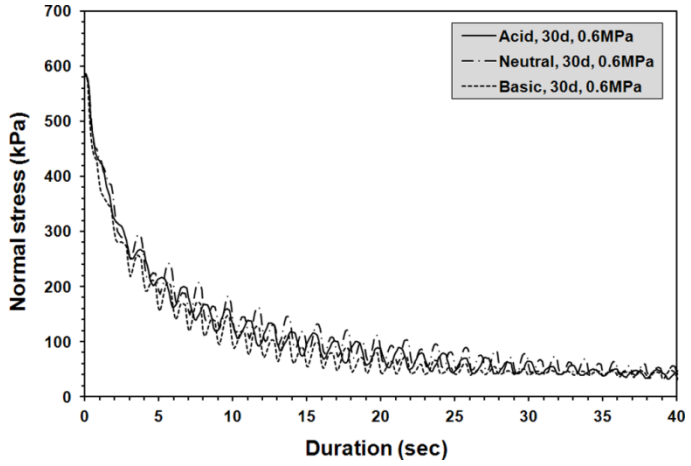

(b) 30 days, $\sigma_n = 0.6$ MPa

Figure 3.26 Typical normal stress behavior

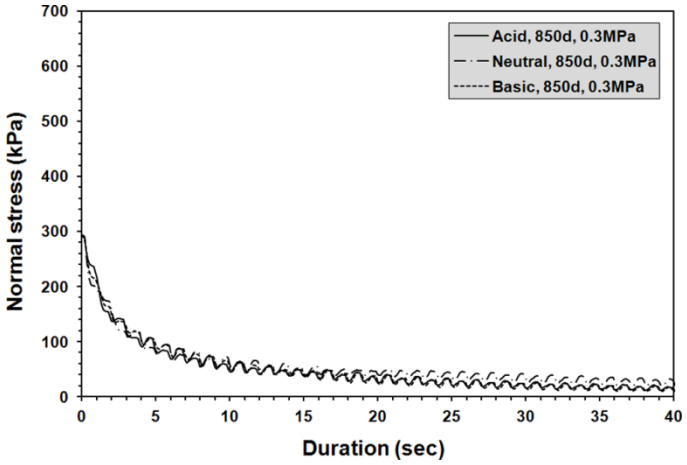

(c) 850 days, $\sigma_n = 0.3$ MPa

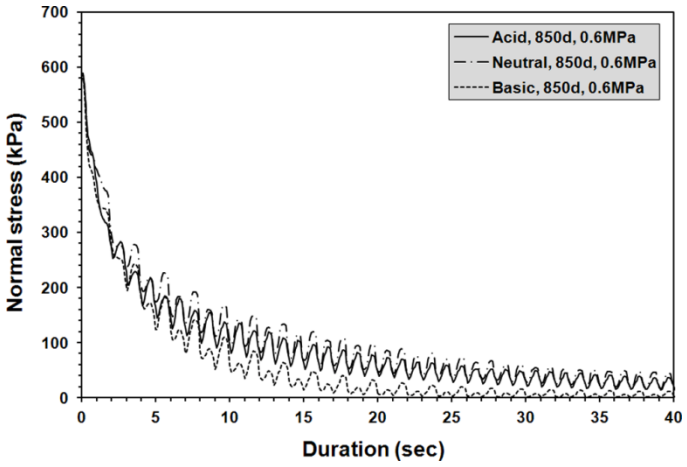

(d) 850 days, $\sigma_n = 0.6$ MPa

Figure 3.26 Typical normal stress behavior (continued)

The stress path, illustrated in Figure 3.27, demonstrated a gradual decrease in both the shear stress and normal stress with the load cycles. The envelopes of the peak strength were also plotted. Table 3.8 and 3.9 summarized the estimated gradient of peak envelopes with respect to the submerging periods and normal stresses.

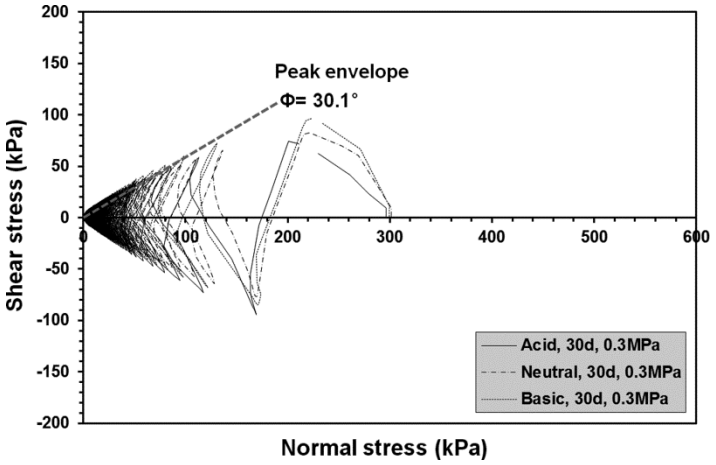

(a) 30 days, $\sigma_n = 0.3$ MPa

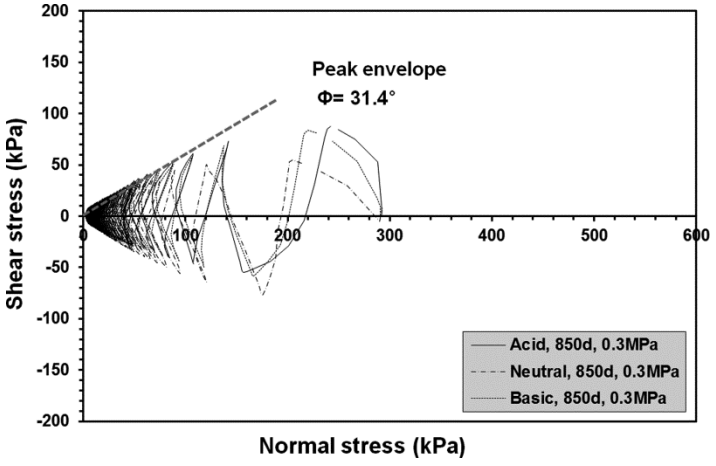

(b) 850 days, $\sigma_n = 0.3$ MPa

Figure 3.27 Typical stress paths with peak envelope

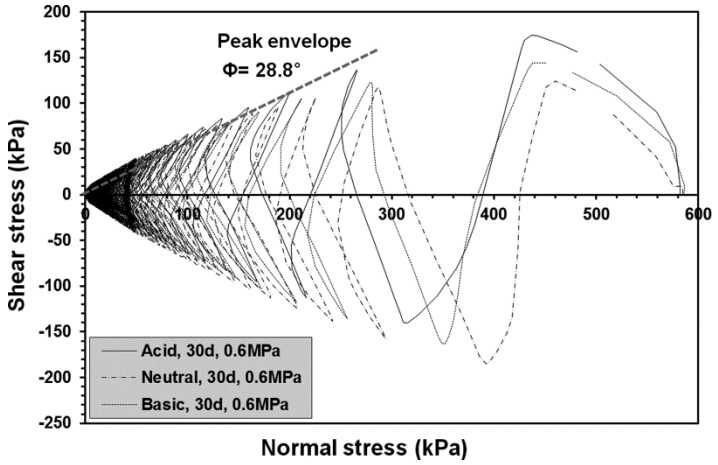

(c) 30 days, $\sigma_n = 0.6$ MPa

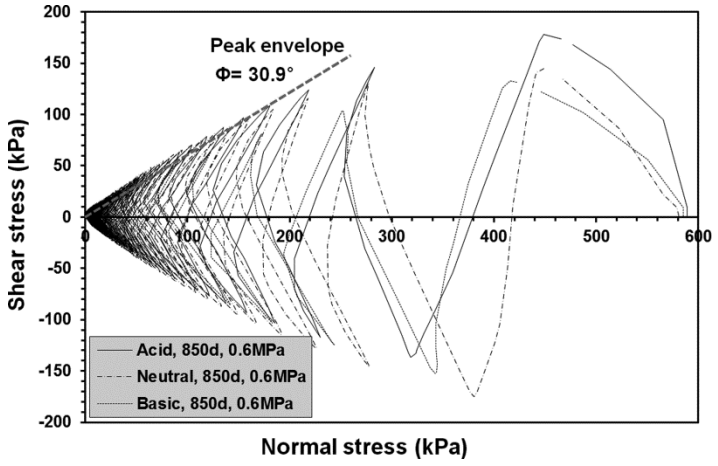

(d) 850 days, $\sigma_n = 0.6$ MPa

Figure 3.27 Typical stress paths with peak envelope (continued)

At failure, the stress path touched the failure envelope and subsequently stabilized with asymptotic normal stress toward the residual strength. For the specimens submerged for 850 and 30 days, the secant angle of peak envelope decreased about 1.6 % and 4.4 %, respectively, according to the increase of

the normal stress. The friction angle of granular soil under the constant volume condition decreases as the normal stress increases, and it is consistent result with the previous theories on the friction angle (Terzaghi et al., 1996), however, note that the variation of friction angle may show some uncertainty and inconsistent tendency under dynamic loading condition.

For the normal stresses of 0.3 and 0.6 MPa, each secant angle of peak envelope increased 4.3 % and 7.3 %, respectively, according to the increase of the submerging period.

Table 3.8 Secant angle of peak envelope with respect to submergence

Submerging period (days)	Gradient of peak envelope	
	$\sigma_n = 0.3$ MPa	$\sigma_n = 0.6$ MPa
850	31.4	30.9
30	30.1	28.8

Table 3.9 Secant angle of peak envelope with respect to normal stress

Normal stress (MPa)	Gradient of peak envelope	
	850 days of submergence	30 days of submergence
0.3	31.4	30.1
0.6	30.9	28.8

The plots of normal stress versus time (Figure 3.28) described that the peak strength was reached at the first cycle, same as shown in Figure 3.26.

The rapid changes in the shear stress continued up to the residual state, similar to the trend of the normal stress. Though the specific differences among the peak shear stresses showed some poor legibility, however, the overall trend could be recognized more clearly in the shear stress curves.

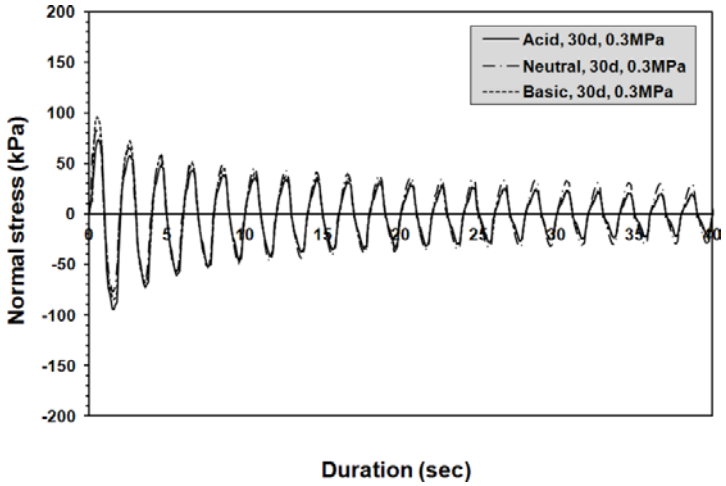

(a) 30 days, $\sigma_n = 0.3$ MPa

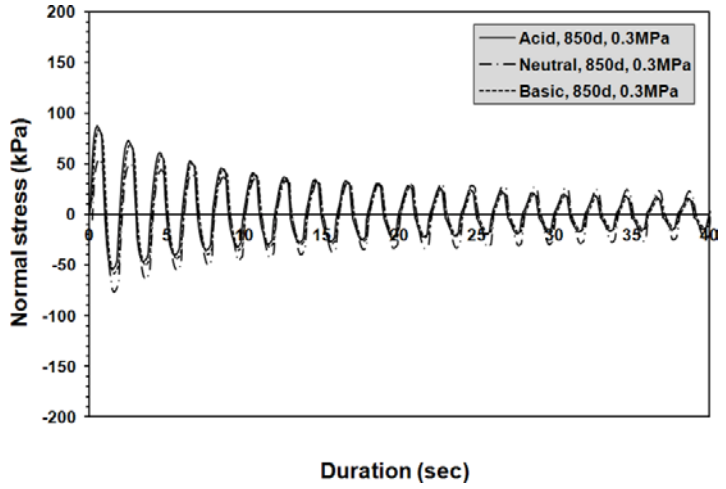

(b) 850 days, $\sigma_n = 0.3$ MPa

Figure 3.28 Typical normal stress behavior

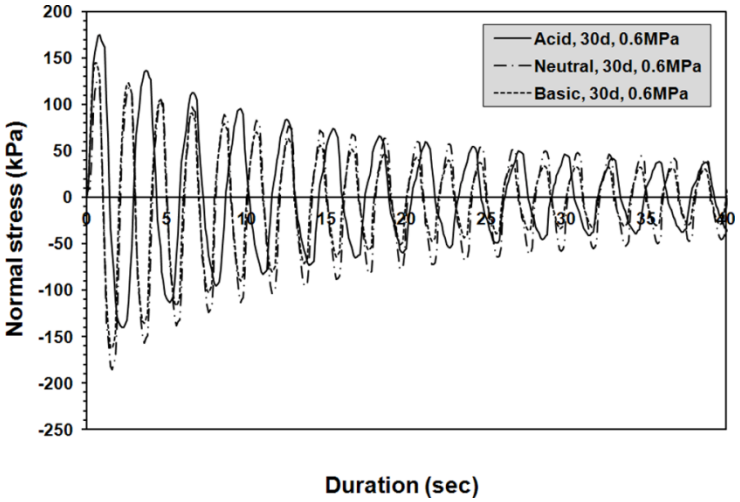

(c) 30 days, $\sigma_n = 0.6$ MPa

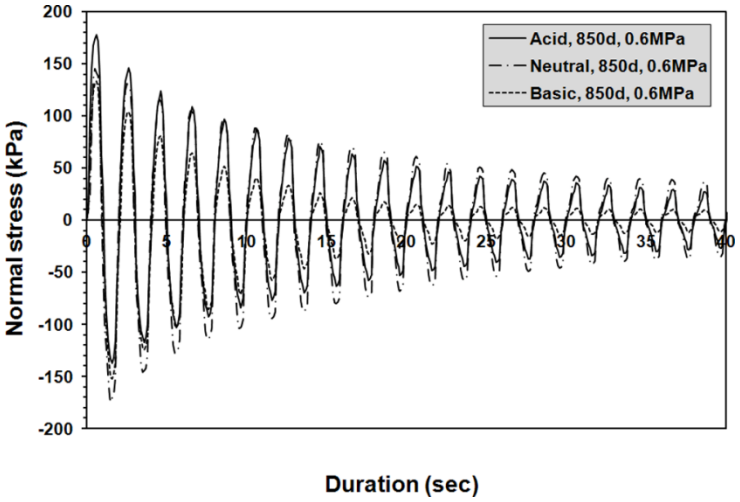

(b) 850 days, $\sigma_n = 0.6$ MPa

Figure 3.28 Typical normal stress behavior (continued)

3.4.2 Evaluation of disturbance function and parameters

The cyclic simple shear test results were analyzed from the conventional viewpoint. The overall trend of shear stress degradation and other dynamic characteristics under the test conditions were able to obtain, however, it is still ambiguous to quantify the degree of damage of geosynthetic-soil interface mathematically. This is mainly caused from the limitations of the conventional approach, therefore, the Disturbance State Concept (DSC) and the disturbance function have been employed to define the cyclic shear stress degradation mathematically and provide the basis of numerical formulation, which will be examined in Chapter 5. Aforementioned literatures verified the effectiveness and reliability of the DSC to investigate the cyclic shear behavior of various interfaces (refer to Chapter 2.5).

Disturbance function curves

Based on the experimental results in Chapter 3.4.1, shear stress-strain curves were obtained by cyclic simple shear test using M-PIA. The disturbance, D was able to be calculated by using shear stress-strain curves and Equation 2.9, and the deviatoric plastic strain trajectory, ξ_D, was able to be estimated by Figure 2.28 and Equation 2.10 and 2.11. The physical meaning of the disturbance function curve was already explained in Chapter 2.5.2. The relationships between D and ξ_D, i.e., the disturbance function curves, were evaluated for all cases and displayed in Figure 3.29-3.32. The shapes of the disturbance function curves were shown to be parabolic in all

conditions.

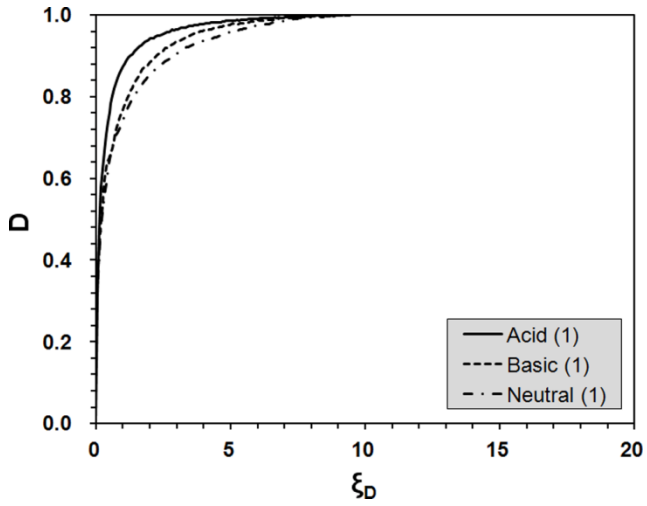

(a) test-1

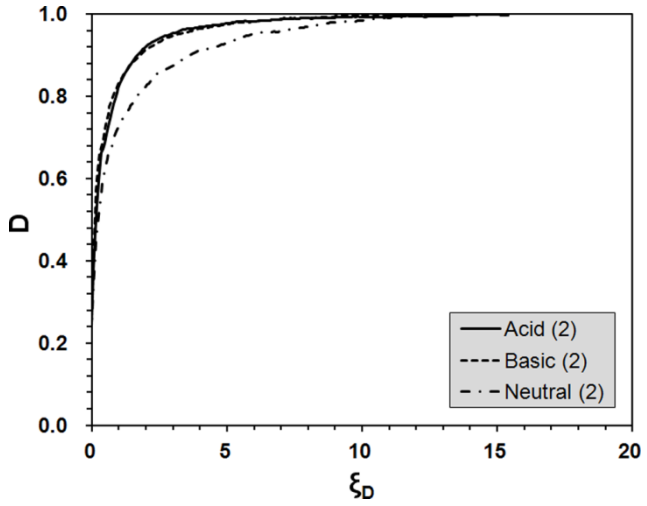

(b) test-2

Figure 3.29 Disturbance function curves (30 days, $\sigma_n = 0.3$ MPa)

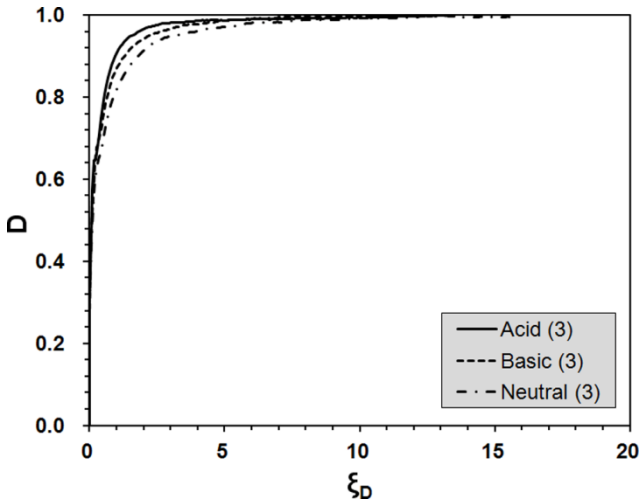

(c) test-3

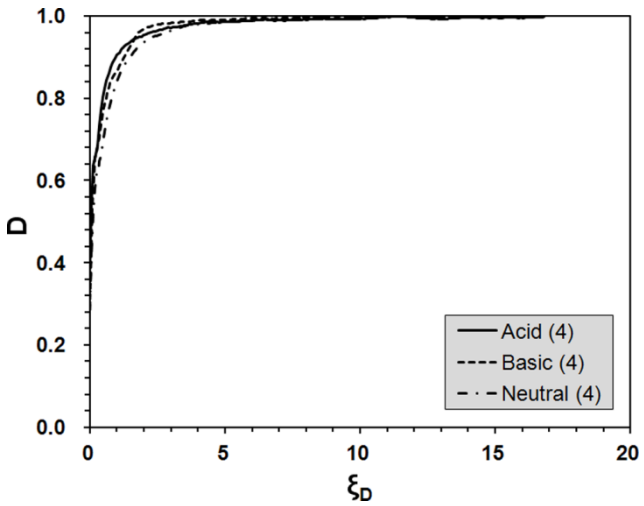

(d) test-4

Figure 3.29 Disturbance function curves (30 days, $\sigma_n = 0.3$ MPa) (continued)

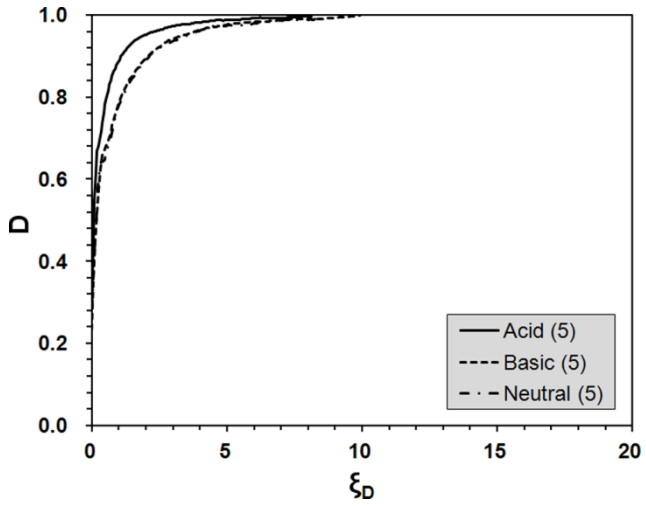

(e) test-5

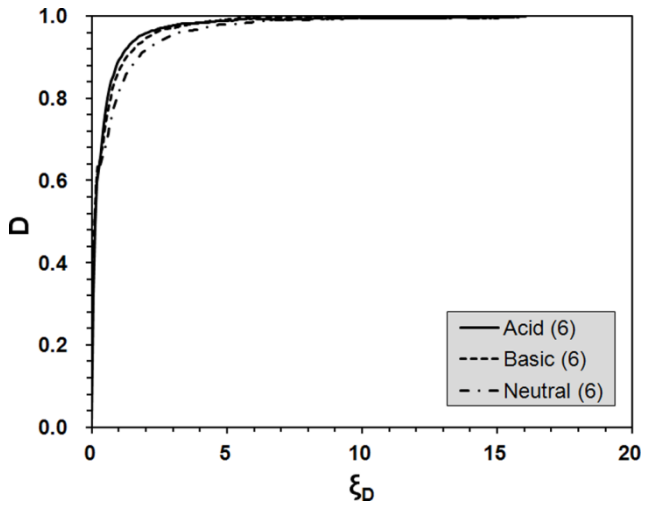

(f) test-6

Figure 3.29 Disturbance function curves (30 days, $\sigma_n = 0.3$ MPa) (continued)

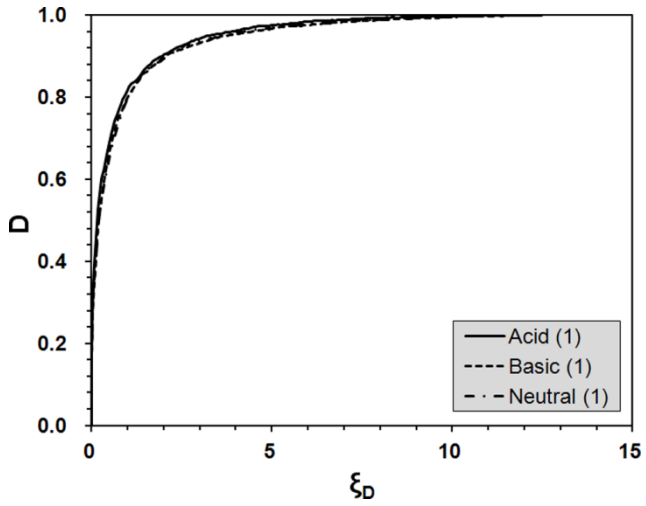

(a) test-1

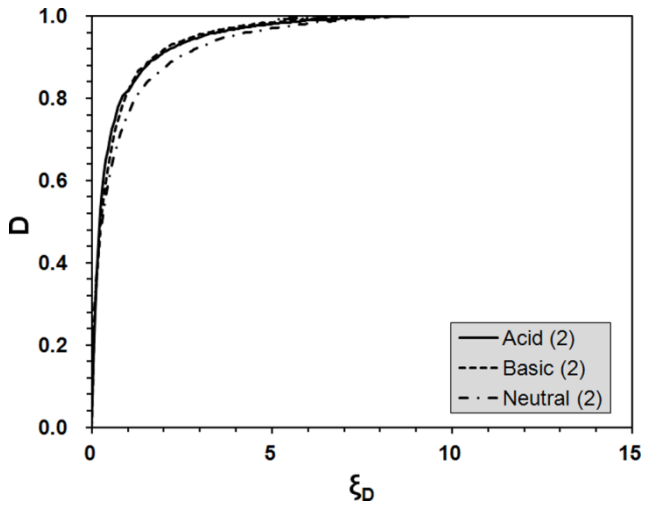

(b) test-2

Figure 3.30 Disturbance function curves (30 days, $\sigma_n = 0.6$ MPa)

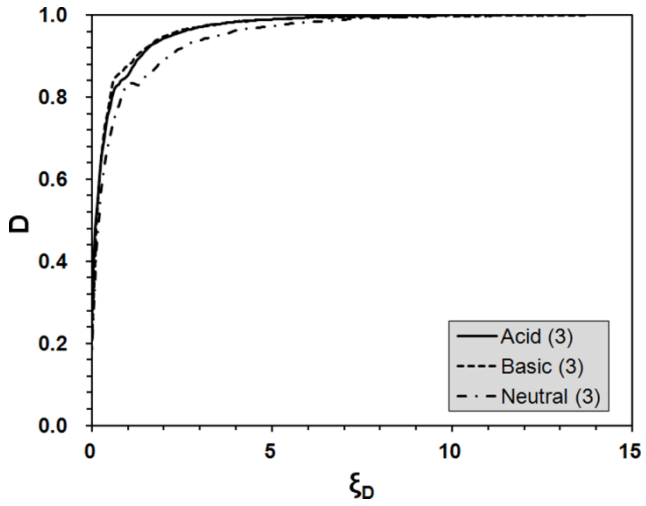

(c) test-3

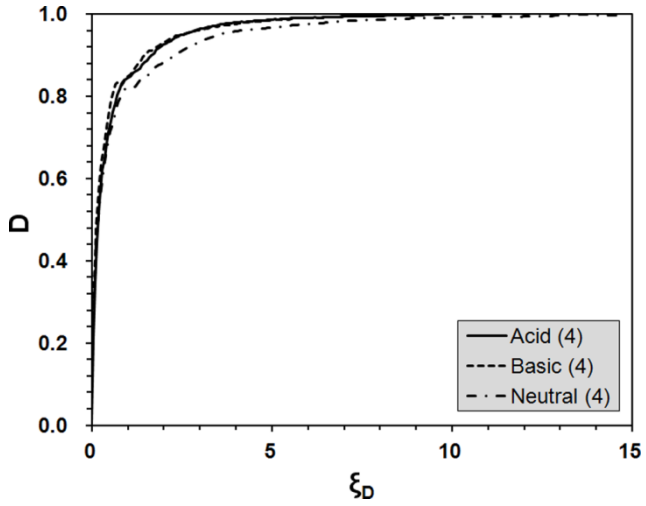

(d) test-4

Figure 3.30 Disturbance function curves (30 days, $\sigma_n = 0.6$ MPa) (continued)

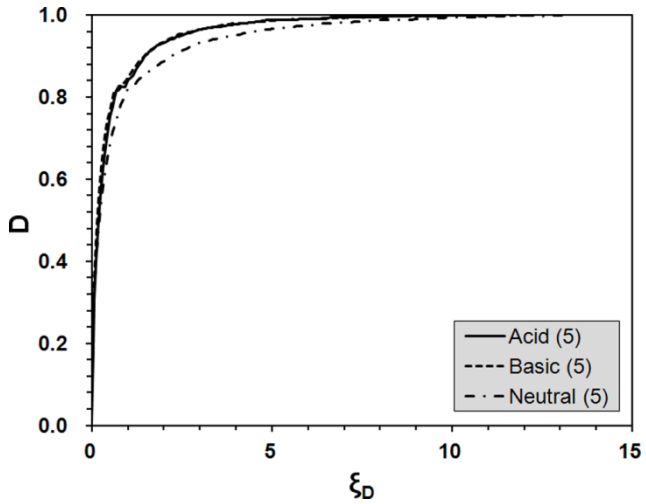

(e) test-5

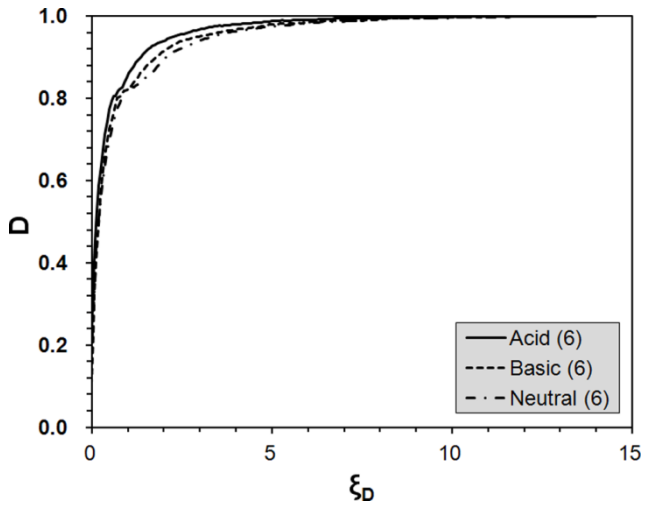

(f) test-6

Figure 3.30 Disturbance function curves (30 days, $\sigma_n = 0.6$ MPa) (continued)

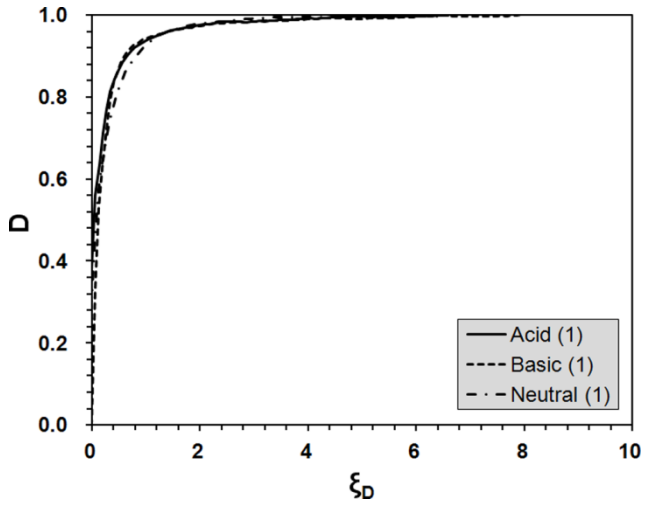

(a) test-1

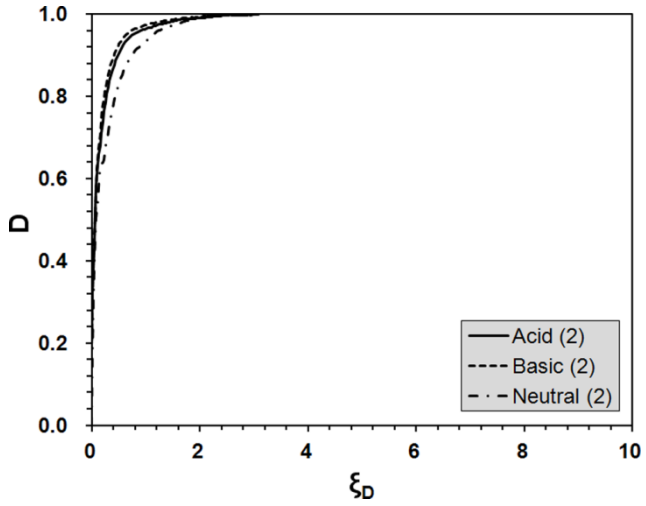

(b) test-2

Figure 3.31 Disturbance function curves (850 days, $\sigma_n = 0.3$ MPa)

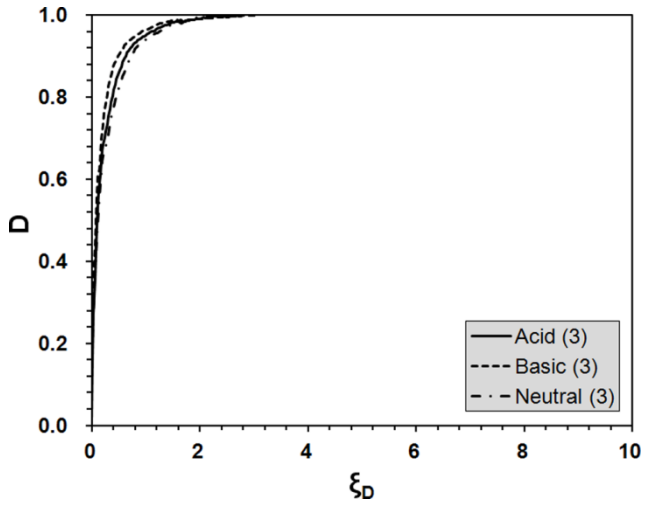

(c) test-3

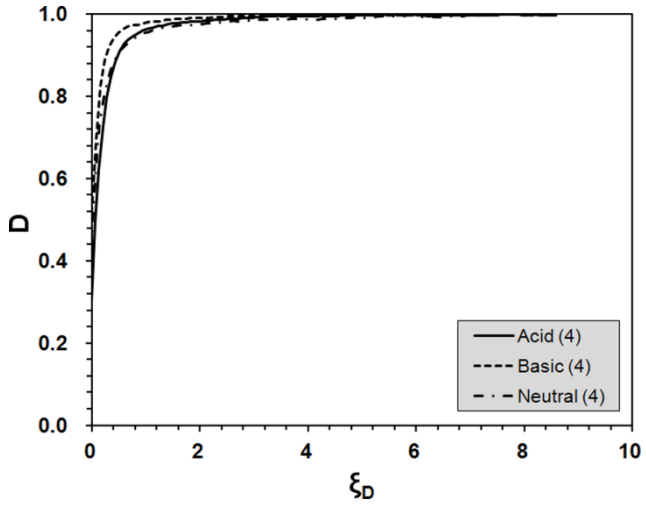

(d) test-4

Figure 3.31 Disturbance function curves (850 days, $\sigma_n = 0.3$ MPa) (continued)

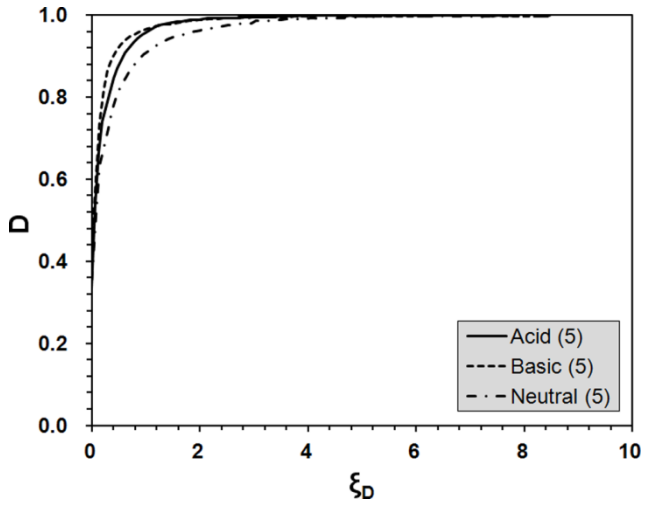

(e) test-5

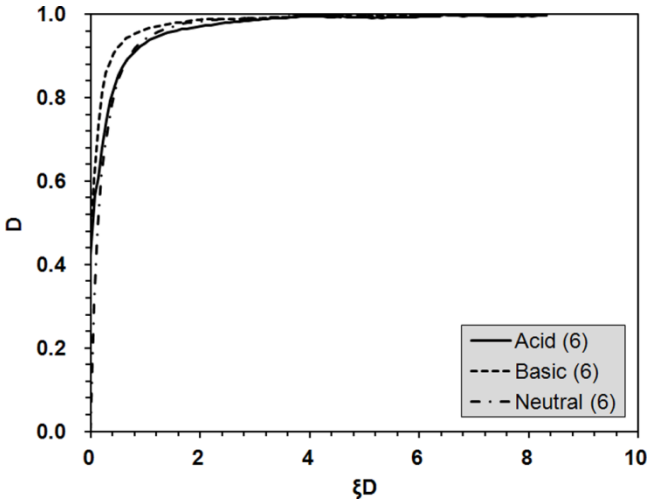

(f) test-6

Figure 3.31 Disturbance function curves (850 days, $\sigma_n = 0.3$ MPa) (continued)

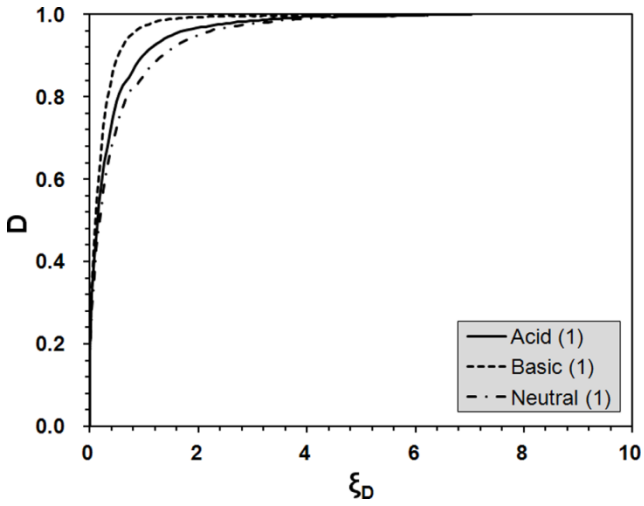

(a) test-1

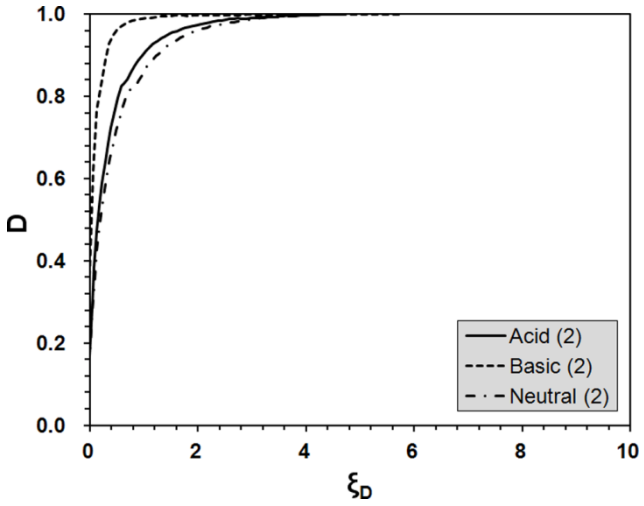

(b) test-2

Figure 3.32 Disturbance function curve (850 days, $\sigma_n = 0.6$ MPa)

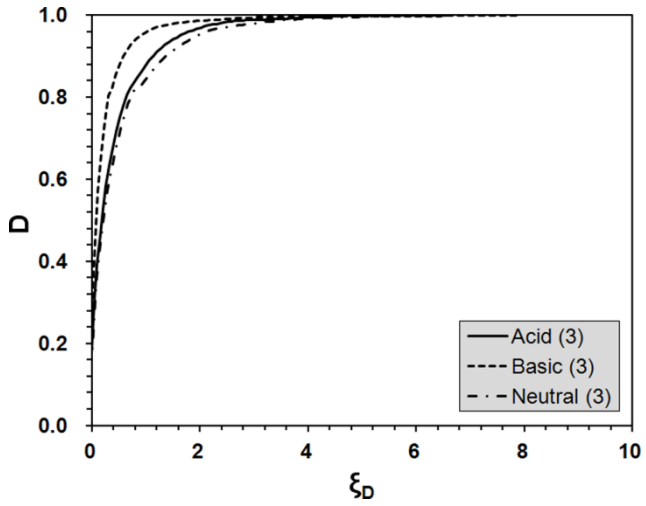

(c) test-3

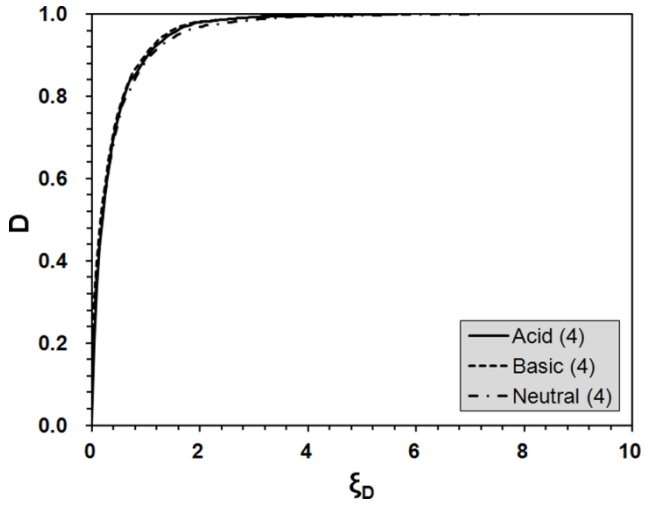

(d) test-4

Figure 3.32 Disturbance function curve (850 days, $\sigma_n = 0.6$ MPa) (continued)

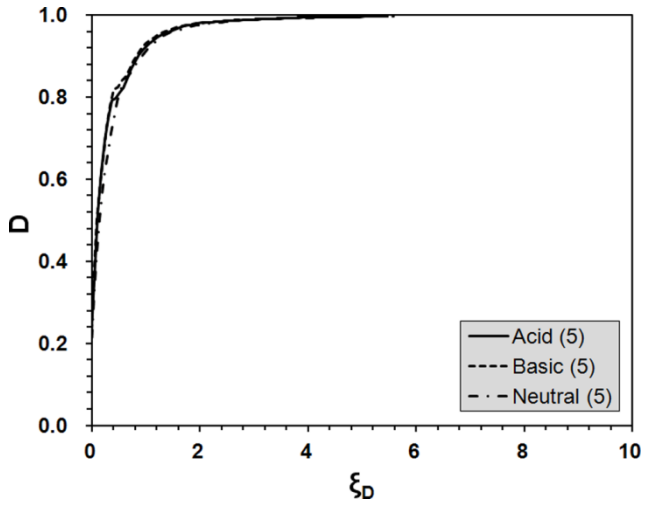

(e) test-5

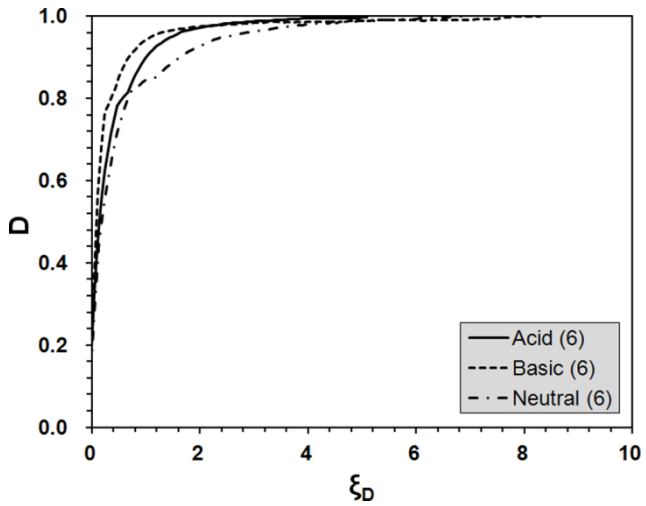

(f) test-6

Figure 3.32 Disturbance function curve (850 days, $\sigma_n = 0.6$ MPa) (continued)

The increase of disturbance, D represents the increase of the degree of damage in the geosynthetic-soil interface. In experiment results, the shape of disturbance function varied in accordance with chemical conditions. In most cases, the largest interface disturbance appeared under the basic condition.

Figure 3.33 and 3.34 illustrate the results of the comparison between disturbance function curves according to the normal stress under acid and basic conditions, for 30 and 850 days of submergence, respectively. For the relatively short-term behavior from the specimen submerged for 30 days was shown: (1) under the acid condition, the shear degradation of geosynthetic-soil interface was more severe under the 0.3 MPa of normal stress condition than 0.6 MPa. (2) under the basic condition, though the disturbance function curves were slightly dispersed, however, they still showed similar trend to the result of acid condition. For the relatively long-term behavior from the specimen submerged for 850 days was discovered that the trends of shear degradation of geosynthetic-soil interface were corresponded to the results of the short-term condition as shown in Figure 3.33. However, the difference in the shape of the disturbance function curves according to the normal stress was evident and concentrated in long-term behavior.

Figure 3.35 and 3.36 demonstrate the comparison results of the disturbance function curves according to the submerging period under acid and basic conditions, for different normal stresses, respectively. In all cases, more rigorous disturbance was observed in long-term (850 days) behavior. The difference of disturbance subjected to the submerging period was more apparent in the basic condition and low normal stress conditions.

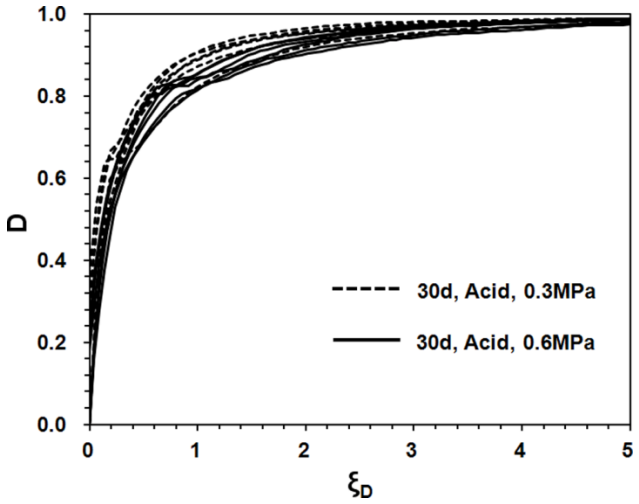

(a) acid condition

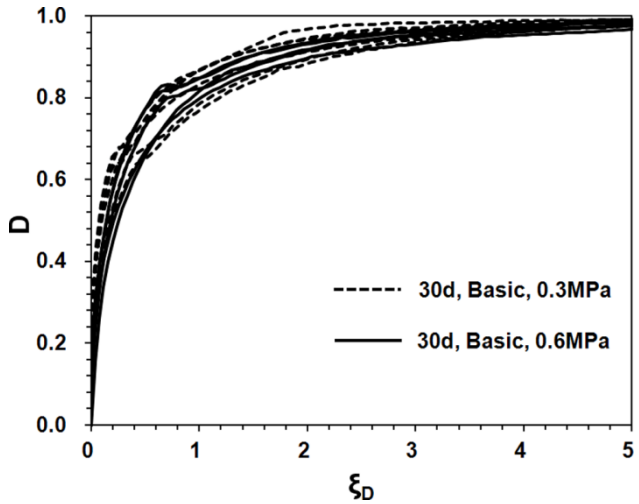

(b) basic condition

Figure 3.33 Comparisons with normal stress (30 days)

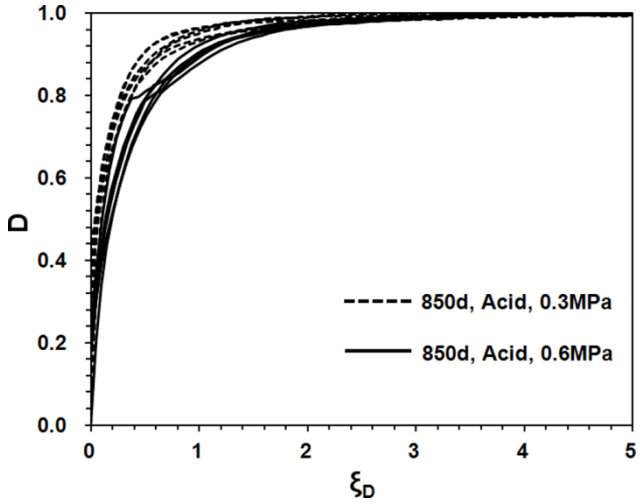

(a) acid condition

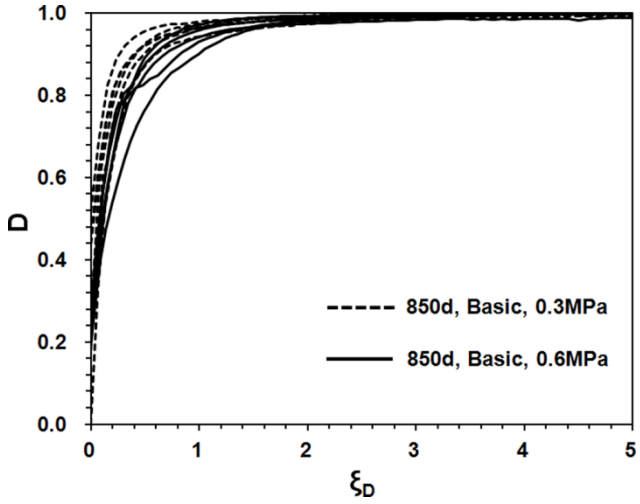

(b) basic condition

Figure 3.34 Comparisons with normal stress (850 days)

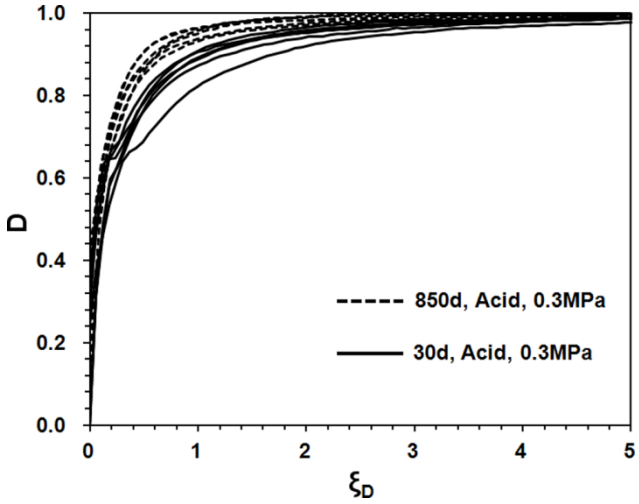

(a) acid condition

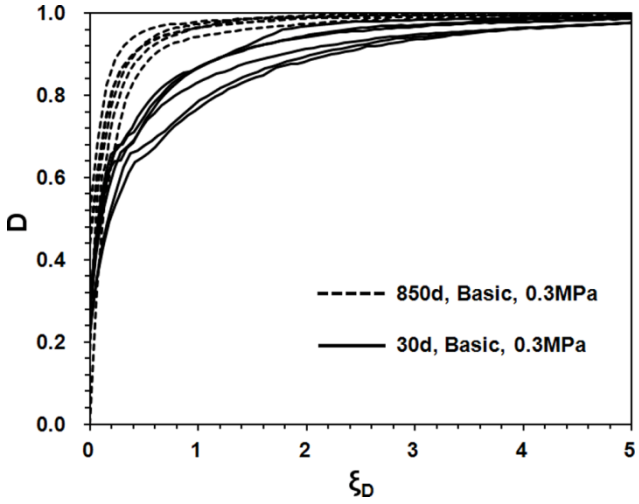

(b) basic condition

Figure 3.35 Comparisons with submerging period (0.3 MPa)

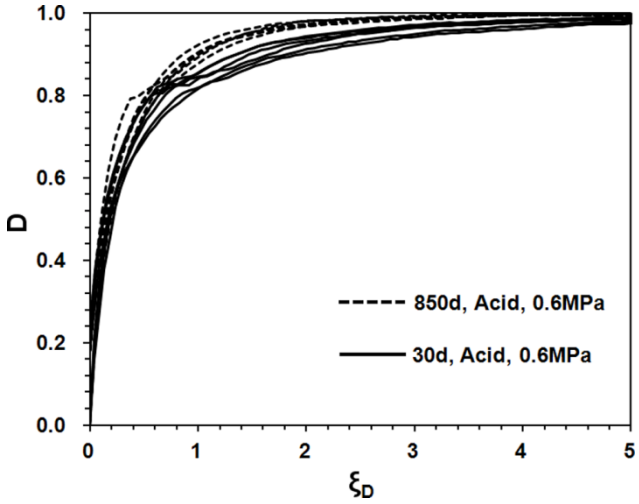

(a) acid condition

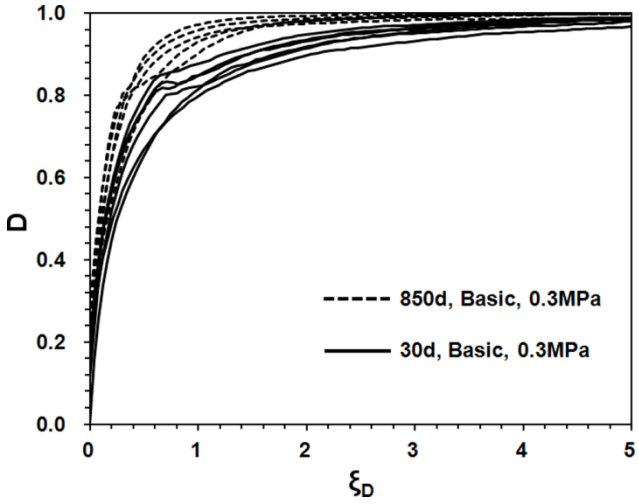

(b) basic condition

Figure 3.36 Comparisons with submerging period (0.6 MPa)

Critical Disturbance, D_c

In DSC theory, the material under load can be considered a mixture involving continuous interaction between its components. Depending on the mechanical and environmental loading such as thermal, fluid, chemical, etc., the material mixture can undergo degradation in its strength and stiffness, which leads to the decay or damage (Desai, 2001). The degree of damage can be numerically expressed by the disturbance function and curves. Desai et al. (1996) introduced the concept of the critical disturbance, D_c.

Figure 3.37 displays a typical disturbance function curve and there is a specific location where significant change occurs in the rate of change in disturbance. This change of disturbance is related to the transformation of the RI state into FA state. Physically, the critical disturbance is the beginning point of phase change in the interface. FA parts in the interface increase steeply, and then begin to turn in the failure state. During deformation, there can be significant change in the rate of disturbance, which is considered as "threshold transitions" in the microstructure (Desai et al., 1996). It also indicates the initiation of shear failure without volume change under external load, mechanically. Such a point when the behavior transforms into the FA state, begins to approach the ultimate, and the disturbance trends becomes to stabilize is called the critical disturbance, D_c.

D_c can be obtained mathematically by finding the minimum radius of curvature from the functional form of the disturbance. The radius of curvature equation is defined as:

$$R = \left| \frac{(D'^2+1)^{3/2}}{D''} \right| \tag{3.1}$$

where, D is the disturbance function defined as Equation (2.8). The first and second derivative D with respect to ξ_D are expressed as:

$$\frac{dD}{d\xi_D} = 0.99\, A\, Z\, {\xi_D}^{Z-1}\, e^{-A{\xi_D}^Z} \tag{3.2}$$

$$\frac{d^2D}{d{\xi_D}^2} = A\, Z\, {\xi_D}^{Z-2} e^{-A{\xi_D}^Z} \left\{ Z\left(0.99 - 0.99\, A\, {\xi_D}^Z\right) - 0.99 \right\} \tag{3.3}$$

Substituting Equation (3.2) and (3.3) into (3.1) yields the radius of curvature at each ξ_D as demonstrated in Figure 3.38.

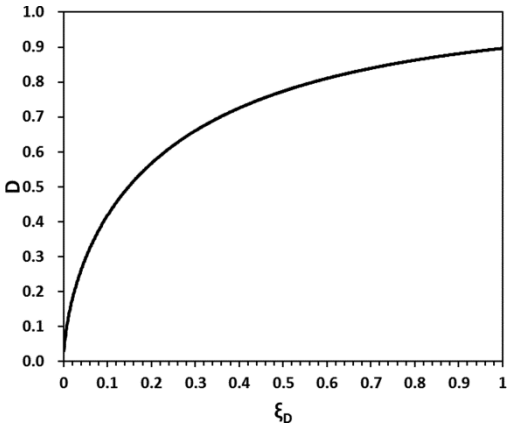

Figure 3.37 Typical disturbance function curve (850 days, 0.6 MPa, Acid)

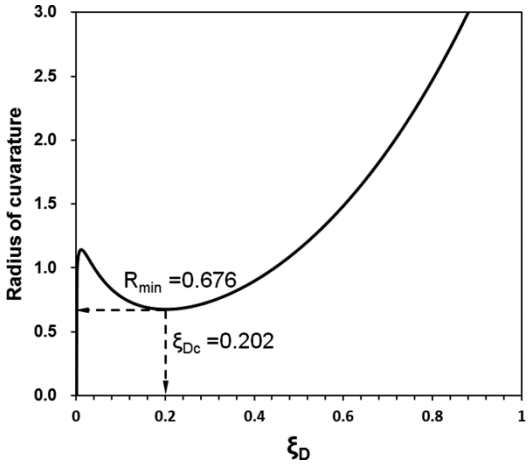

Figure 3.38 Radius of curvature (850 days, 0.6 MPa, Acid)

From Figure 3.38, ξ_D at the minimum radius of curvature can be obtained; therefore, the critical disturbance, D_c is also evaluated as shown in Figure 3.39.

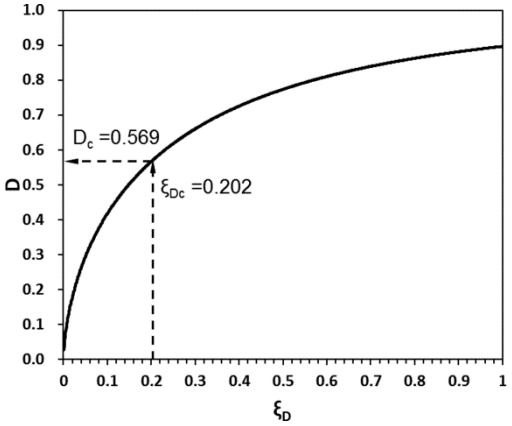

Figure 3.39 Evaluating D_c (850 days, 0.6 MPa, Acid)

It was mentioned that the critical disturbance is the beginning point which the behavior of the interface turns to be FA state. The shear strain at the

critical disturbance can be calculated by finding the minimum radius of curvature; therefore, the critical disturbance is able to be a guideline of the limitation of strain level for the structure or material under specific conditions. It also can be applied to evaluate the dynamic stability on the viewpoint of strain for a waste landfill site considering chemical effects, in the further study.

Disturbance function parameters

The characteristics of the interface shear behavior can be expressed by the disturbance function curves as described in Figure 3.28-3.31. Conversely, the disturbance function curve is able to be reproduced by mathematical combination with the functional form of the curve and disturbance parameters, A and Z. The parameters represent the intrinsic material characteristics and determined by linear regression of the curves from the laboratory test results. The specific procedure and technique were described in Chapter 2.5.2 and previous studies (Kwak et al., 2013[b]).

Figure 3.40 to 3.42 demonstrate the representative plots of the linear regression and the comparison result between test and calculated values.

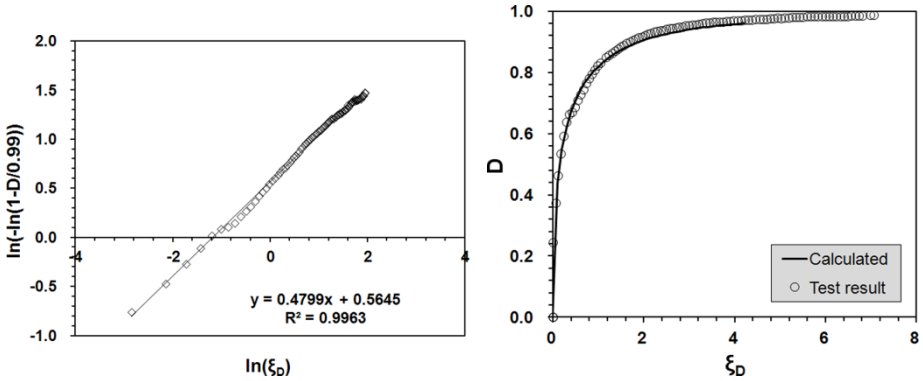

(a) linear regression (b) verification

Figure 3.40 Linear regression and verification (Acid, 30 days)

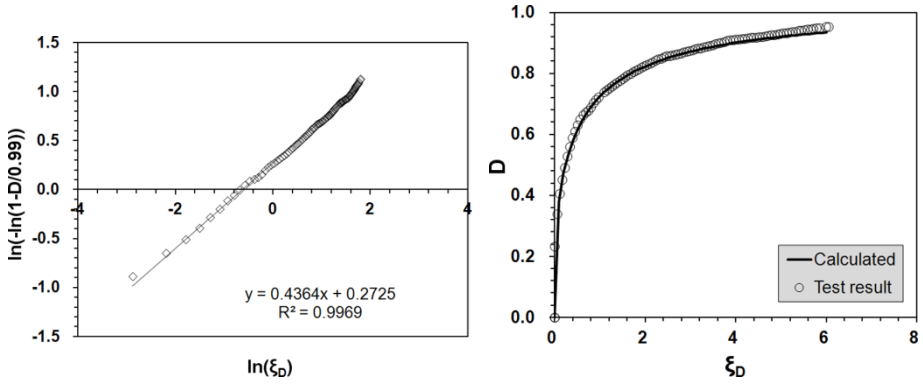

(a) linear regression (b) verification

Figure 3.41 Linear regression and verification (Neutral, 30 days)

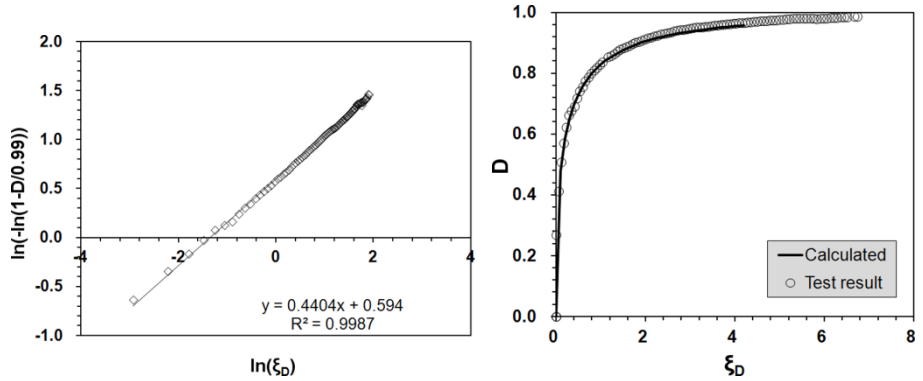

(a) linear regression (b) verification

Figure 3.42 Linear regression and verification (Basic, 30 days)

The cyclic simple shear test was conducted six times for the same condition to minimize the deviation among the test results; therefore, 72 sets of test results were obtained in total.

All of A and Z parameters calculated via the linear regression were suggested and the average values including the standard deviations (SD) were also estimated in Table 3.10. The lower (LL) and upper (UP) limits which are

the boundary values away from 1.0 SD from the average value were also suggested.

Table 3.10 A and Z parameters

Submerging period (days)	Normal stress (MPa)	Chemical condition	Para-meters	Avg.	LL	UP	SD
30	0.3	Acid	A	1.9269	1.4850	2.3688	0.4419
			Z	0.4536	0.4284	0.4788	0.0252
		Neutral	A	1.7287	1.6018	1.8556	0.1269
			Z	0.4859	0.4557	0.5161	0.0302
		Basic	A	1.9723	1.7276	2.2170	0.2447
			Z	0.4768	0.4477	0.5059	0.0291
	0.6	Acid	A	1.8193	1.6497	1.9889	0.1696
			Z	0.5260	0.4894	0.5626	0.0366
		Neutral	A	1.5810	1.5035	1.6585	0.0775
			Z	0.4972	0.4685	0.5259	0.0287
		Basic	A	1.7989	1.5969	2.0009	0.2020
			Z	0.5179	0.4719	0.5639	0.0460
850	0.3	Acid	A	2.9476	2.6730	3.2222	0.2746
			Z	0.4852	0.3858	0.5846	0.0994
		Neutral	A	2.7061	2.4916	2.9206	0.2145
			Z	0.5286	0.4171	0.6401	0.1115
		Basic	A	3.2338	2.8210	3.6466	0.4128
			Z	0.4329	0.3231	0.5427	0.1098
	0.6	Acid	A	2.3057	2.1891	2.4223	0.1166
			Z	0.6040	0.5445	0.6635	0.0595
		Neutral	A	2.0655	1.8778	2.2532	0.1877
			Z	0.6179	0.5758	0.6600	0.0421
		Basic	A	2.9057	2.3215	3.4899	0.5842
			Z	0.4885	0.3879	0.5891	0.1006

According to Figure 2.32, A and Z parameters determine the shape of the disturbance function curve. The shape of the disturbance function curve enables to predict the degree of damage corresponding to the plastic shear strain level. The variation of A and Z values was described in Figure 3.43 and 3.44, respectively.

The parameter A increased with the increase of submersing period under the same chemical and normal stress conditions, which denotes the shape of the disturbance curve tends to move left, hence, the geosynthetic-soil interface undergoes more damage at small plastic strain level, namely the interface approaches the failure in spite of small plastic strain according to the increase of submerging period. On the contrary, A decreased with the increase of the normal stress under the same chemical and submergence conditions, which demonstrates the shape of the disturbance curve tends to move right, hence, the geosynthetic-soil interface manifest more resistance against the damage at small plastic strain level. It is an identical trend with the characteristics of shear stress degradation analyzed previously.

The parameter Z increased with the increase of submersing period and the normal stress, under the same chemical condition. It denotes the slope of curve tends to increase, which means the rapid increase of the material damage, namely, the damage significantly grows with small increment of plastic strain. The variation from the average value of A and Z was relatively small in case of neutral condition compared to the acid and basic conditions.

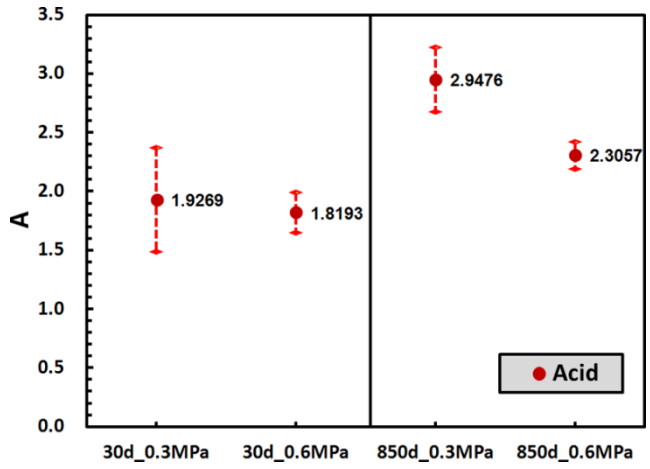

(a) acid condition

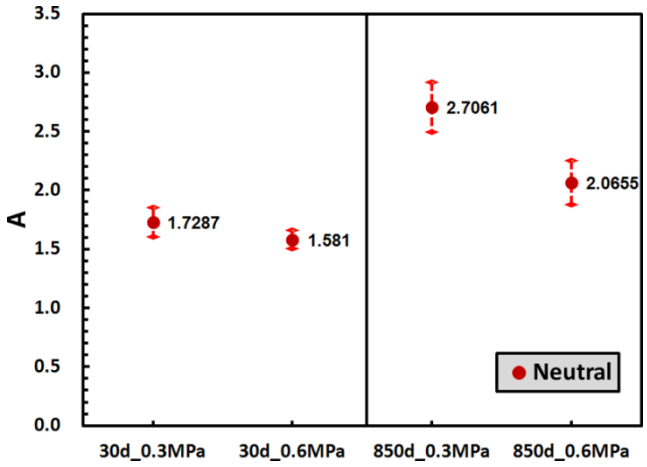

(b) neutral condition

Figure 3.43 Variation of A values

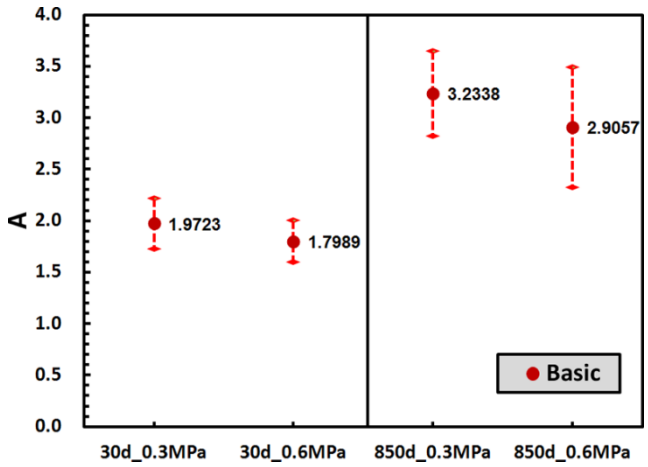

(c) basic condition

Figure 3.43 Variation of A values (continued)

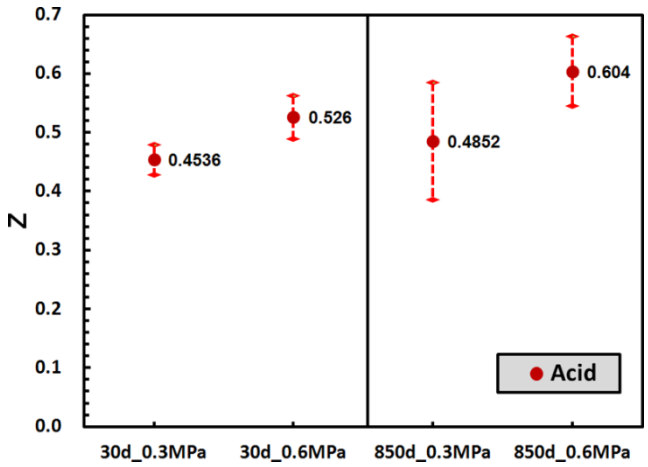

(a) acid condition

Figure 3.44 Variation of Z values

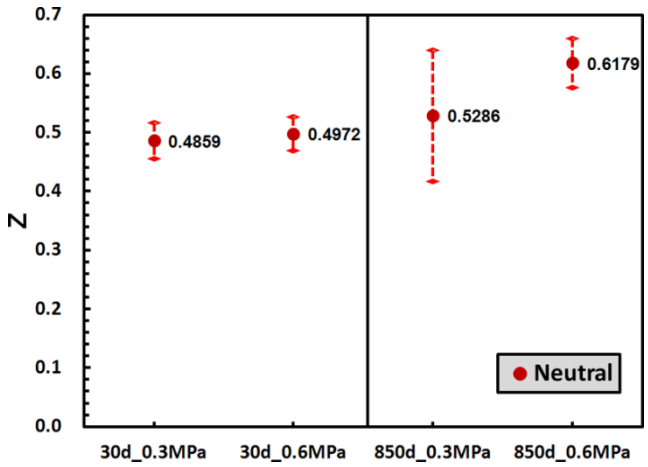

(b) basic condition

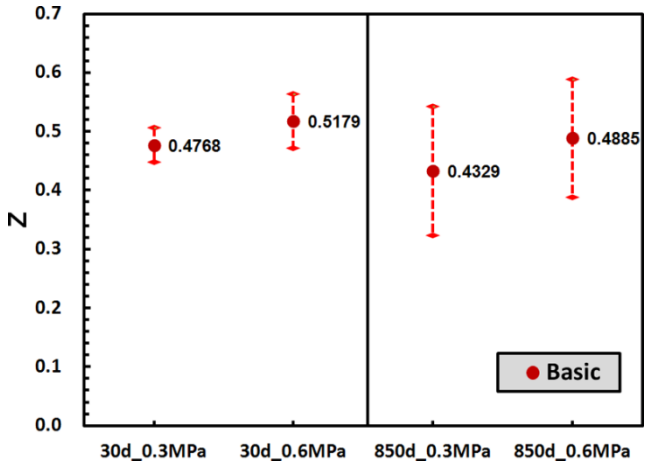

(c) neutral condition

Figure 3.44 Variation of Z values (continued)

3.4.3 Suggestion of new disturbance function curves

Based on a series of cyclic simple shear test and new disturbance function parameters suggested in Table 3.10, accordingly, new disturbance function curves corresponding to the chemical and normal stress conditions were evaluated. Figure 3.45 illustrates the new disturbance function curves. Each curve represents the comprehensive test result. In the short-term (30 days of submergence) behavior, acid and basic conditions were more vulnerable as shown in Figure 3.45 (a) and (b). The disturbance function curves of acid and basic conditions showed almost identical shape under short-term condition. For long-term behavior, the differences of the disturbance function values at a certain deviatoric plastic strain trajectory, ξ_D, showed more distinct than the values under short-term conditions. The differences between the disturbance curves at a certain strain level can be intuitionally observed by the comparison of curves on the same domains.

In all cases, it was discovered that the basic condition was the most vulnerable. It is deduced that the damage of the filament of nonwoven fabric due to the vulnerability for the basic condition can cause the most significant damage of the geosynthetic-soil interface.

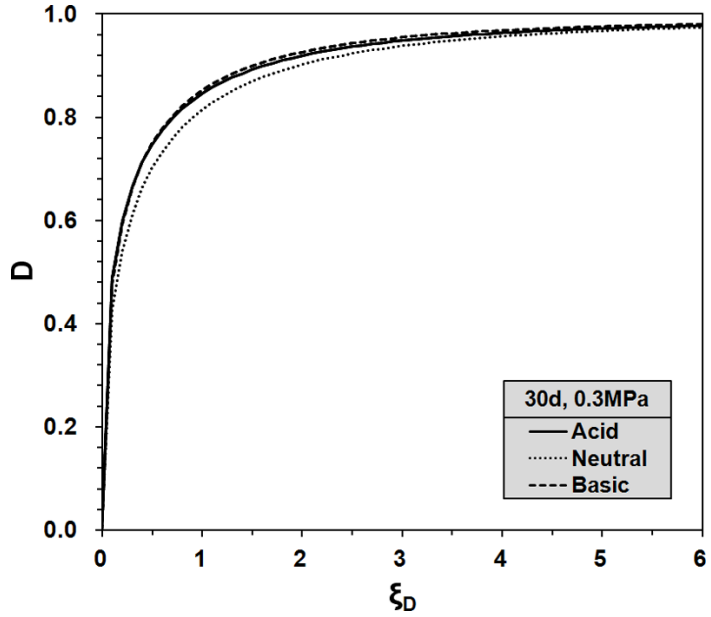

(a) 30 days, 0.3 MPa

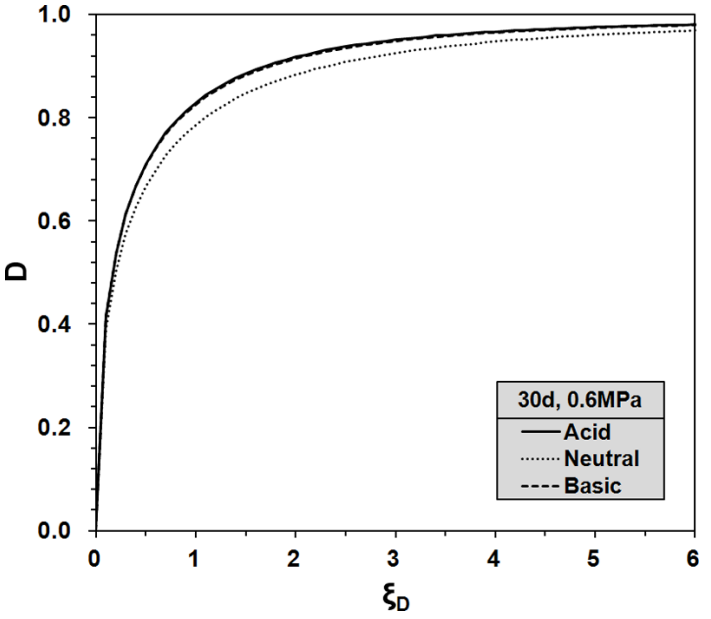

(b) 30 days, 0.6 MPa

Figure 3.45 New disturbance function curves

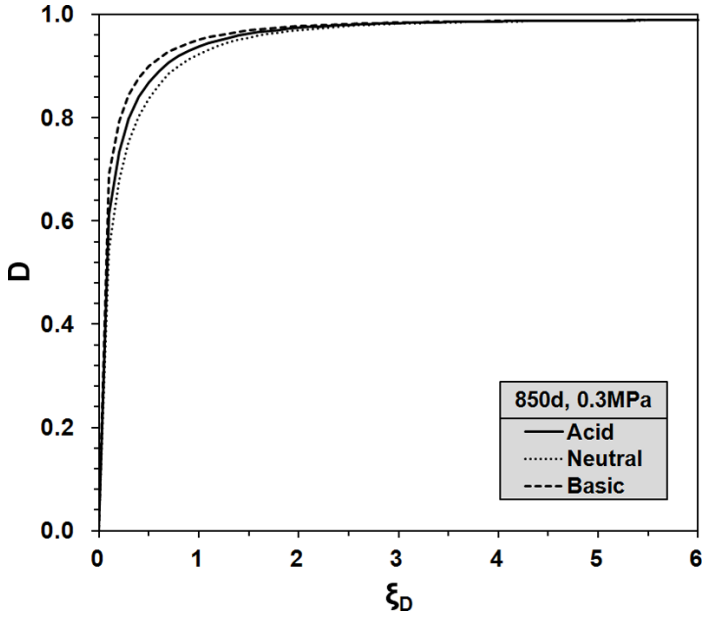

(c) 850 days, 0.3 MPa

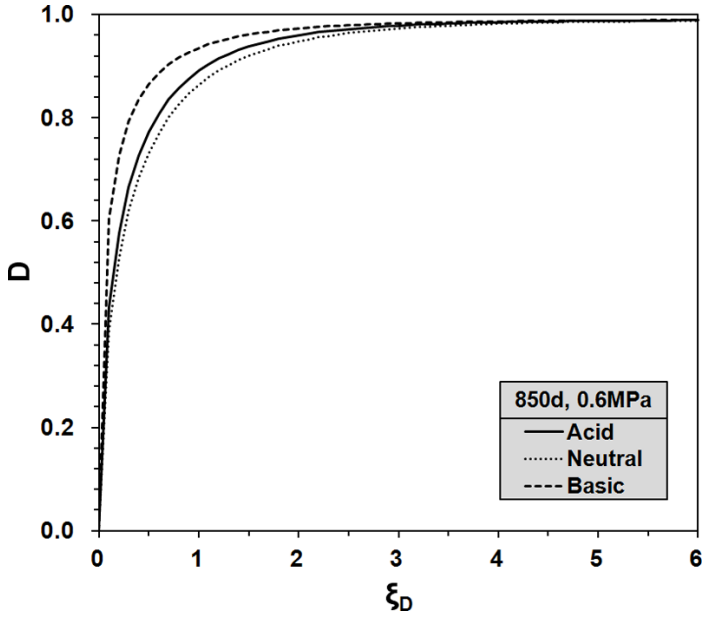

(d) 850 days, 0.6 MPa

Figure 3.45 New disturbance function curves (continued)

3.4.4 Parallel analysis of the result

A parallel study on the suggested disturbance function curves was conducted. The effects of the submerging period and normal stress were analyzed by comparison of the curves. The disturbance function curves by parallel analysis were plotted in Figure 3.46-3.48.

Generally, the disturbance intensified in case of the long-term submergence condition in all cases, however, the differences of the disturbance decreased in case of higher normal stress condition because confining effect may resist the abrupt progress of damage in the geosynthetic-soil interface. The variation between the disturbance curves under each submerging period was significant and the largest variation was observed in basic condition under applying 0.3 MPa of the normal stress. Table 3.11 summarized the maximum decreases of the disturbance between the results under 30 and 850 days of the submerging periods and Figure 3.47 and 3.48 displayed the maximum variation of the disturbance curves according to the submerging period.

Table 3.11 Maximum variations of the disturbance curves (submerging period)

Chemical conditions	Max. decreases of disturbance (ΔD_{max}) (between the results of 30 and 850 days)		
	Basic	Neutral	Acid
0.3 MPa of normal stress	31 %	23 %	22 %
0.6 MPa of normal stress	26 %	10 %	8 %

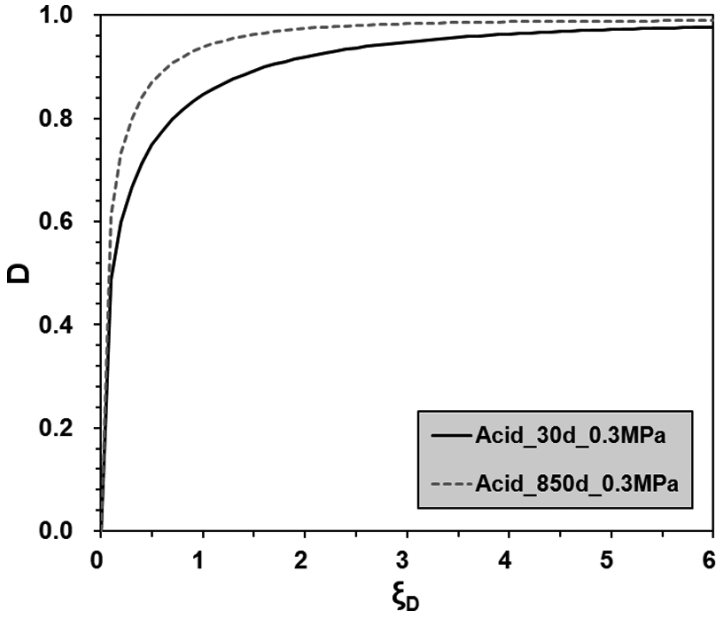

(a) acid, 0.3 MPa

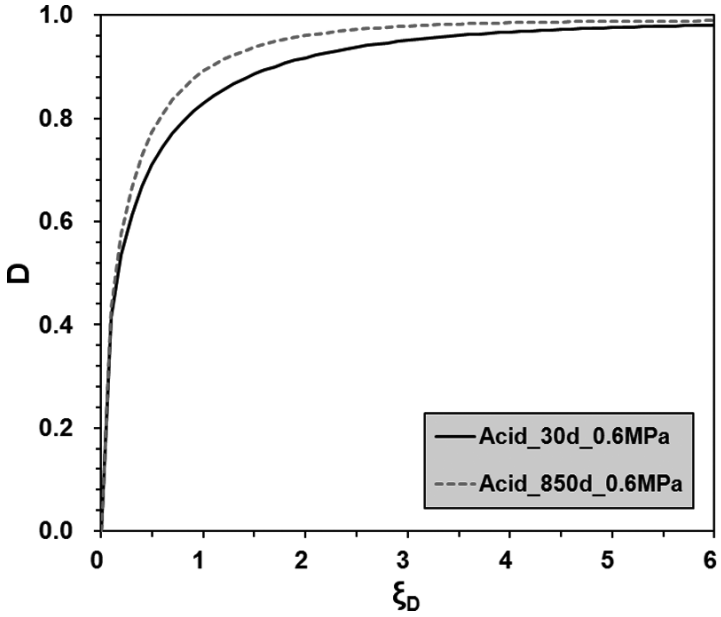

(b) acid, 0.6 MPa

Figure 3.46 Effects of submerging period

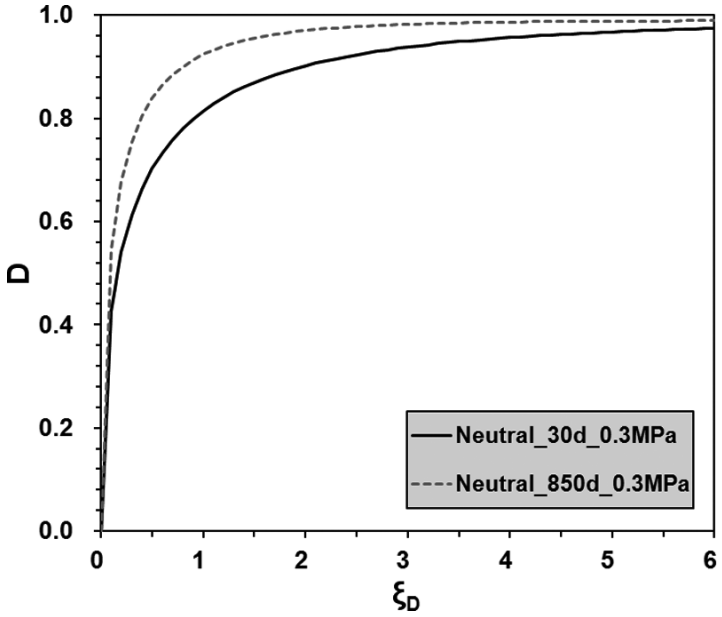

(c) neutral, 0.3 MPa

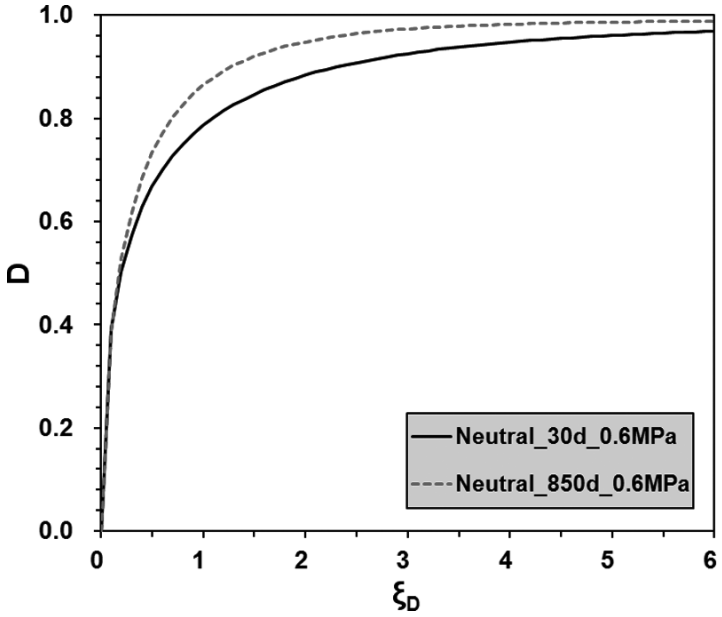

(d) neutral, 0.6 MPa

Figure 3.46 Effects of submerging period (continued)

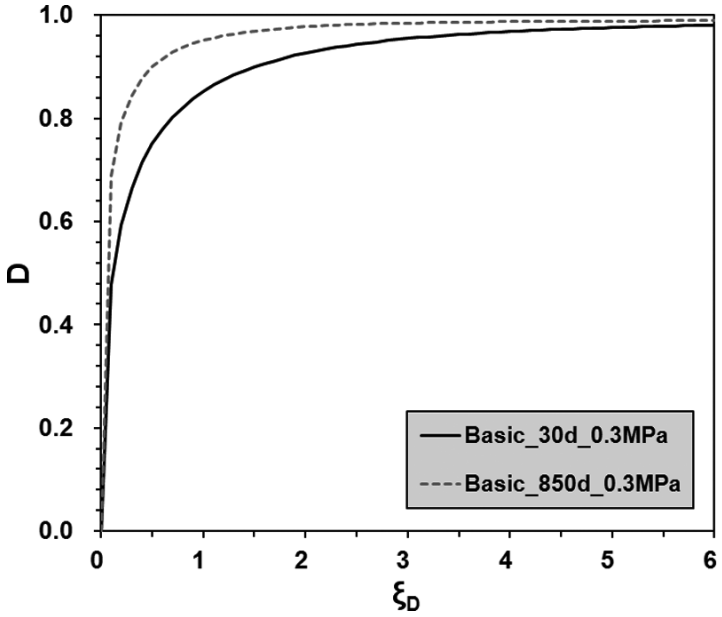

(e) basic, 0.3 MPa

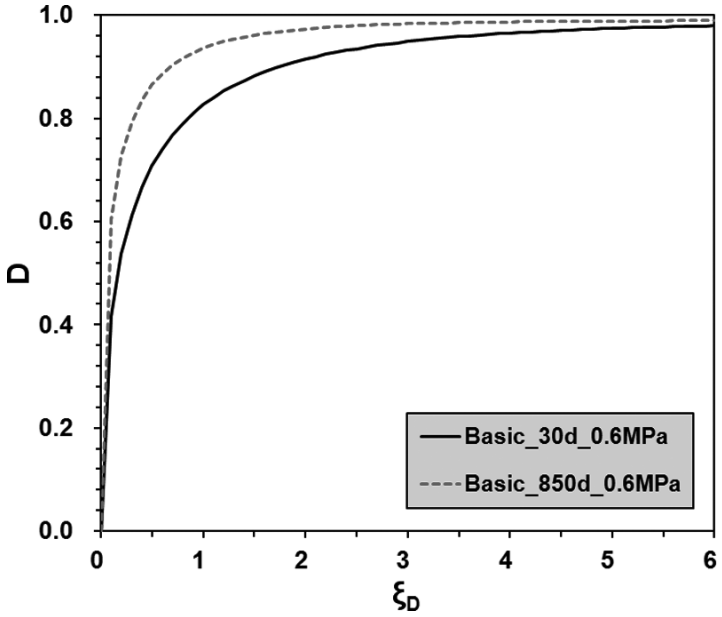

(f) basic, 0.6 MPa

Figure 3.46 Effects of submerging period (continued)

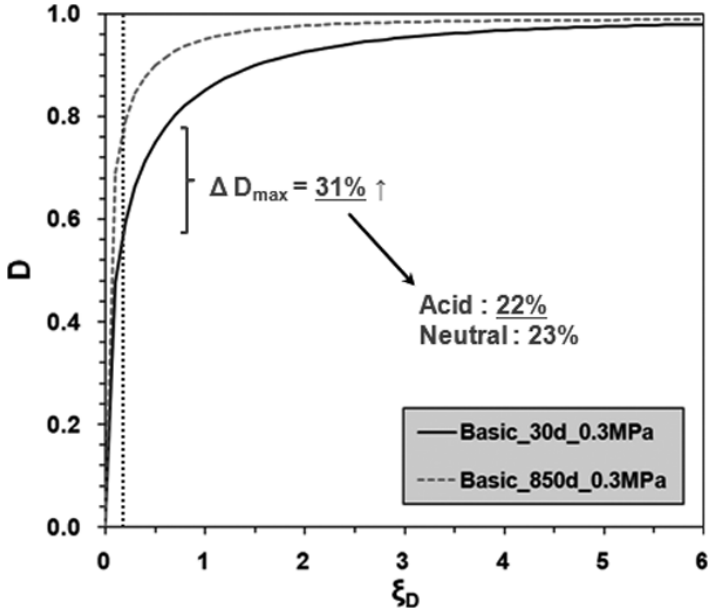

Figure 3.47 Max. decreases of disturbance (ΔD_{max}) under 0.3 MPa

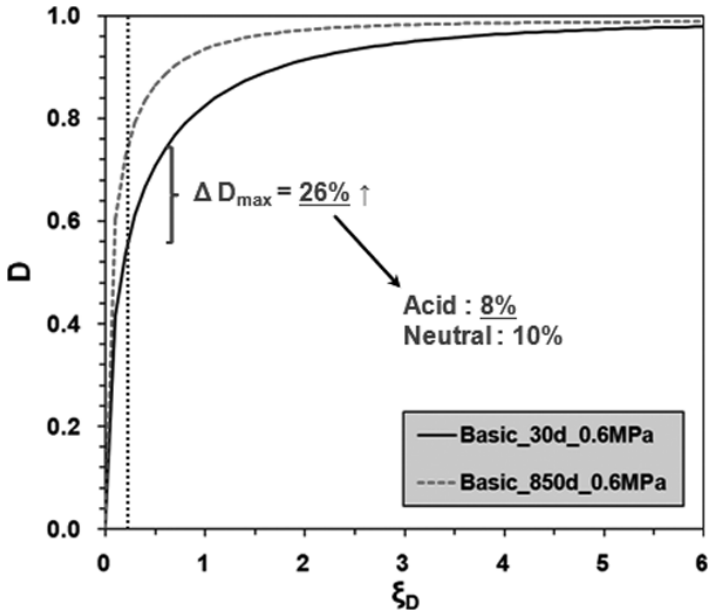

Figure 3.48 Max. decreases of disturbance (ΔD_{max}) under 0.6 MPa

The variation between the disturbance curves under each normal stress condition was also remarkable and the largest variation was observed in acid condition under 850 days of the submerging period. Table 3.12 summarized the maximum decreases of the disturbance between the results under 0.3 and 0.6 MPa of the normal stress conditions and Figure 3.49 and 3.50 displayed the maximum variation of the disturbance curves according to the normal stress conditions.

As a result of the parallel study based on the newly suggested disturbance function curves, it has been proved that the submerging period and the normal stress conditions are both important factors affect the cyclic shear stress degradation of the geosynthetic-soil interface.

Table 3.12 Maximum variations of the disturbance curves (normal stress)

Chemical conditions	Max. decreases of disturbance (ΔD_{max}) (between the results under 0.3 and 0.6 MPa)		
	Basic	Neutral	Acid
30 days of submerging period	15 %	7 %	18 %
850 days of submerging period	41 %	40 %	14 %

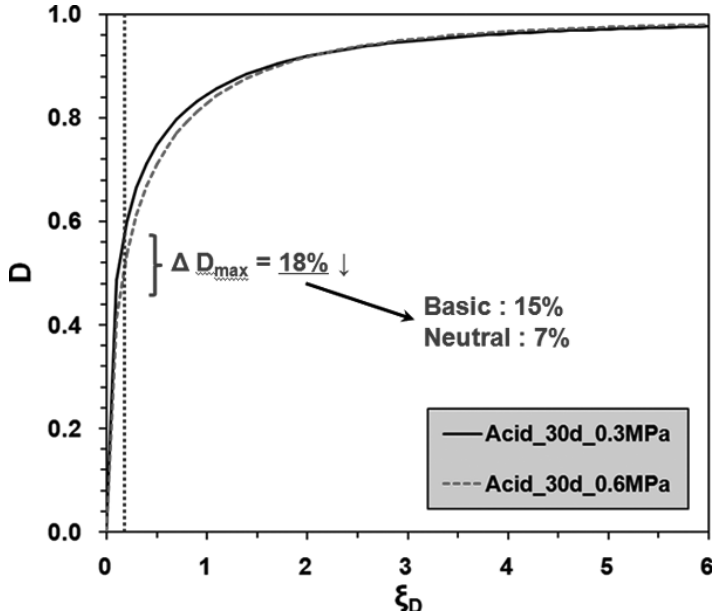

Figure 3.49 Max. decreases of disturbance (ΔD_{max}) for 30 days

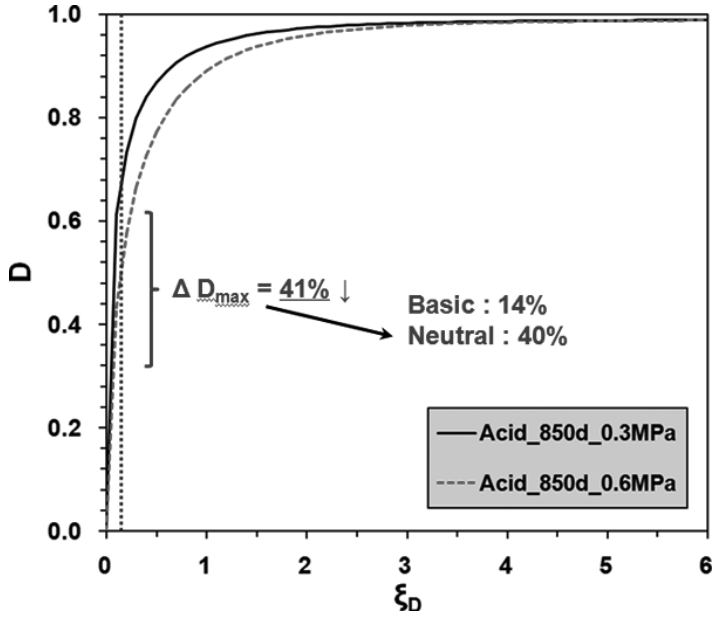

Figure 3.50 Max. decreases of disturbance (ΔD_{max}) for 850 days

3.4.5 Prototype test results considering temperature elevation

A set of cyclic simple shear tests was performed in order to investigate the chemical and thermal effects on the cyclic shear behavior of the geosynthetic-soil interface. Submerging period of the soil and geosynthetics was 180 days. Based on shear stress-strain hysteretic loop at each cycle, the disturbance function curves were obtained to represent the degree of damage in the interface quantitatively. Figure 3.51 and 3.52 display shear stress-strain curves according to the cyclic loadings. Obvious shear stress degradation with an increasing number of cycles was observed in all cases. The rate of shear degradation tended to decrease with the increasing number of cycles.

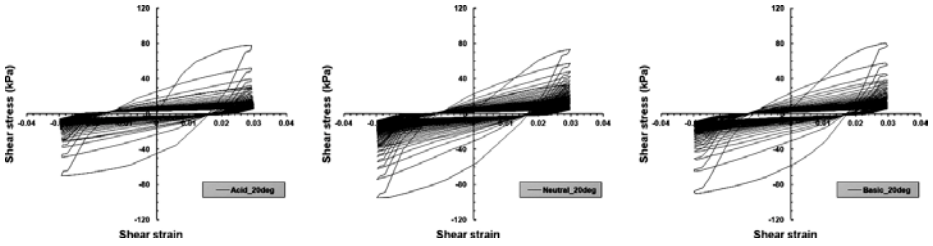

Figure 3.51 Shear stress-strain curves at 20℃

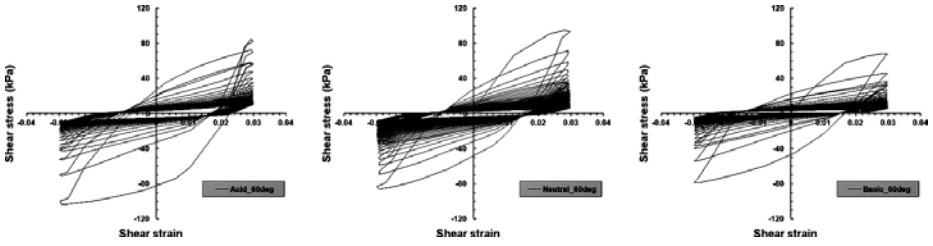

Figure 3.52 Shear stress-strain curves at 60℃

Based on the experimental results, the disturbance function curves which are decided by the disturbance, D and the deviatoric plastic strain trajectory, ξ_D, were able to be calculated with respect to chemical conditions as shown in Figure 3.53.

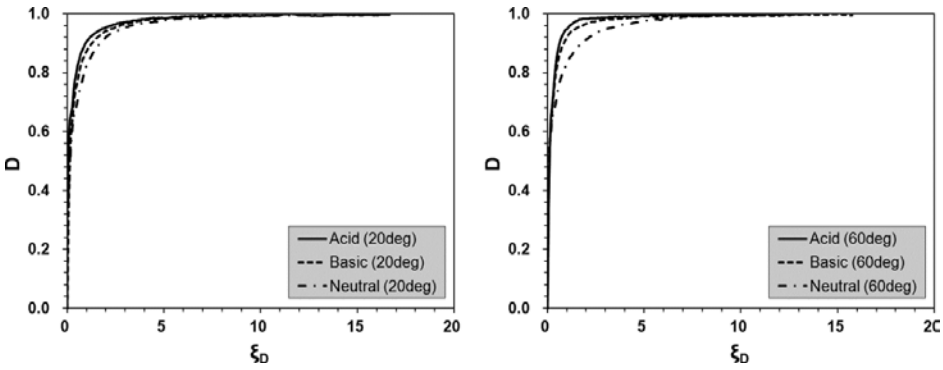

Figure 3.53 Disturbance function curves

In figure 3.53, the increase of disturbance D, represents the increase of the degree of damage in the geosynthetic-soil interface, and the shape of disturbance function curve varies in accordance with chemical and thermal conditions. In all cases, the largest interface disturbance appeared under the acid condition. The small difference of D between acid and basic condition was observed both 20 and 60℃, while the remarkable difference of D between chemical and neutral condition was discovered under 60℃. More rapid increase of D was observed in small plastic strain level under acid and basic condition of 60℃.

Figure 3.54 displays the results of comparison of disturbance, D with the chemical condition and temperature, respectively. Under the same chemical condition, more disturbances were observed under high temperature

(60℃) and the difference of D was larger under acid condition as shown in Table 3.13. However, the disturbance under neutral condition showed almost identical, which means the effect of elevated temperature is limited under neutral condition, in relatively short-term interface behavior. It is deduced that the elevated temperature can degenerate the shear resistance of the geosynthetic-soil interface under severe acid and basic conditions.

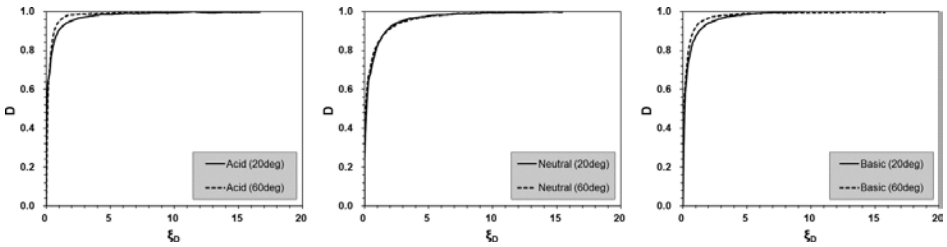

Figure 3.54 Comparison of disturbance function curves

Table 3.13 Difference of the maximum disturbance

Chemical condition	Acid		Basic	
Temperature (℃)	20	60	20	60
Max. D	0.92	0.969	0.888	0.932
ξ_D	1.27		1.05	
Max. difference (%)	5.33		4.95	

Note that the results are from the prototype tests to consider the effect of the temperature elevation. More tests under various temperature conditions are required to evaluate DSC parameters and tendency in the future.

3.5 Concluding remarks

It is known that the cyclic shear behaviors of the geosynthetic-soil interface are one of the most important responses of the waste landfill systems under dynamic (earthquake) condition. Chemical aggressors in the leachate may also affect the cyclic shear behavior of the interface; however, it has not been investigated yet in detail. Therefore, it was required to develop an appropriate testing device and perform an experimental study considering the chemical effects on the interface to overcome some limitations in theoretical approach.

A new apparatus, named M-PIA (multi-purpose interface apparatus) to investigate the chemical effects on the geosynthetic-soil interface under cyclic loading was manufactured in 2010, initially. Afterward, one minor and another major revision for the apparatus were performed successfully to overcome structural and material shortcomings

72 sets of cyclic simple shear tests were conducted by using the modified M-PIA. The overall trend of shear stress degradation and other dynamic characteristics under the test conditions were able to obtain, however, it was still ambiguous to understand the degree of damage of geosynthetic-soil interface quantitatively. This may be the limitations of the conventional approach, therefore, the Disturbance State Concept (DSC) and the disturbance function have been employed to evaluate the cyclic shear stress degradation mathematically and provide the basis of numerical formulation. Furthermore, the critical disturbance is able to be a guideline of the limitation of strain level for the structure or material under specific conditions.

Based on the results of the experimental study, all disturbance function curves and parameters, A and Z were estimated. In the short-term (30 days of submergence) behavior, acid and basic conditions were more vulnerable and the disturbance function curves showed almost identical shape. For long-term behavior, the similar trend were observed, however, the differences of the disturbance function values at a certain deviatoric plastic strain trajectory, ξ_D, showed more distinct than the values under short-term conditions. In all cases, it was discovered that the basic condition was the most vulnerable.

Additionally, a parallel study on the suggested disturbance function curves was conducted. The effects of the submerging period and normal stress were analyzed by comparison of the curves. Generally, the disturbance intensified in case of the long-term submergence condition in all cases, however, the differences of the disturbance decreased in case of higher normal stress condition because confining effect may resist the abrupt progress of damage in the geosynthetic-soil interface. The variation between the disturbance curves under each submerging period was significant and the largest variation was observed in basic condition under applying 0.3 MPa of the normal stress. The variation between the disturbance curves under each normal stress condition was also remarkable and the largest variation was observed in acid condition under 850 days of the submerging period.

As a result of the parallel study based on the newly suggested disturbance function curves, it has been proved that the submerging period and the normal stress conditions are both important factors affect the cyclic shear stress degradation of the geosynthetic-soil interface.

Additionally, to present the recent achievement, the prototype test results

considering thermal effect were demonstrated and the shear stress degradation due to the temperature elevation was evaluated by the disturbance function curves. More tests under various temperature conditions are required to evaluate DSC parameters and tendency in the future.

Consequently, the cyclic shear behaviors of the geosynthetic-soil interface considering chemical effects were intensively examined and the degree of damage of the interface was evaluated by the new disturbance parameters and curves, quantitatively.

4. Microscopic Observation

4.1 Introduction

Cyclic simple shear test results demonstrated definite variations of the disturbance function parameters and shape of the disturbance function curves according to the chemical conditions. As the chemical stability of HDPE geonet has been verified in the previous studies (Koerner, 1988; Rowe and Sangam, 2002), therefore, the hypothesis is that the chemical decay of soil particles mostly causes the variation of the disturbance, and the decay of the nonwoven fabric filament may cause the minor effects on the damage, in this study. Therefore, a specific approach to verify this hypothesis is required.

Nowadays, the microstructural approach became considered as a useful means to investigate the characteristics of the material and interface behaviors. Raghavan and Ghosh (2005) developed a continuum damage mechanics (CDM) model for fiber reinforced composites with interfacial debonding based on micromechanical analysis using Finite Element Method. Menut et al. (2003) analyzed solid surface by Laser-induced Breakdown Spectroscopy (LIBS) and developed quantitative surface mapping of multiple elements. Schlegel et al. (2008) combined microscopic and spectroscopic techniques to decipher the chemical and mineralogical properties of a saturated Fe-clay interface, then, confirmed the presence of a corrosion layer and a clay transformation layer. Kim et al. (2012) reviewed the developments and processing of Focused Ion Beam (FIB).

The Focused Ion Beam (FIB) electronic microscopy can produce three dimensional images to observe surface structure of material. In this study, the FIB electron microscope in the National Instrumentation Center for Environmental Management (NICEM) of Seoul National University was utilized to verify the hypothesis that the chemical decay of soil particle mostly causes the variation of the disturbance. The reason of the different shapes of disturbance function curves was also investigated by the FIB observation results.

4.2 Focused Ion Beam (FIB)

The technology of scanning an infinitesimal particles and detecting the resulting signals to form a magnified images has been an essential part of material science for about 50 years, since the commercialization of the Scanning Electron Microscope (SEM) (Pease and Nixon, 1965). Afterwards, there have been a number of significant improvements in microscopic instruments. Different instruments also exist which are capable of forming a beam of ions for better spatial resolution. The Focused Ion Beam (FIB, hereafter), introduced more than a decade ago, was mainly developed during the late 1970s and the early 1980s with high brightness which came from the invention of the liquid metal ion sources (LIMS). FIB has advantages such as high current density, the capability of very fine focusing, choice of a wide variety of ion masses, large energy density, and shorter penetration depth in solid. Nano-scaled material element is able to be observed by FIB with a high

accuracy (Kim et al., 2012). Furthermore, the characterization of the material surface is capable by collecting the secondary electron through photomultiplier tube while scanning the ion beams over the material surface. In this study, the microscopic observation was performed to discover the reason of dissimilar manifestation of damage at the interface under each chemical condition. FIB facility in the NICEM (National Instrumentation Center for Environmental Management) was utilized as shown in Figure 4.1. The specifications of FIB facility are displayed in Table 4.1.

Figure 4.1 Focused Ion Beam facility

Table 4.1 Specifications of FIB (After Kwak et al., 2013[b])

Apparatus	Focused Ion Beam
Model name	AURIGA
Manufacturer	Carl Zeiss (Germany)
Main purpose	To observe the surface structures and conditions at the high-resolution, high-powered magnification.
Performance	- Resolution: up to 1.0 nm (at 15 kV) - Acceleration voltage: 0.1~30 kV - Magnification: × (12~100 million)

4.3 FIB observation results

The geocomposite and soil particles were observed by FIB according to the chemical conditions. The FIB images of the geocomposite and soil particles were demonstrated in Figure 4.2 and 4.3, respectively.

In Figure 4.2 (c), (f), (i), the damage of HDPE geonet was almost negligible at all chemical conditions, which is consistent with the previous researches (Jeon et al., 2006). It is induced that the antioxidant and other ingredients such as carbon black exhibited robust chemical resistance. On the other hands, the filament of the nonwoven fabric showed partial decay in the acid and basic conditions as shown in Figure 4.2 (a), (d), (g), and Figure 4.3. The breakage of a few filaments was also found mainly in the neutral

condition, however, the damage and breakage of the filament were not observed as a major factor of the degradation of the interface, based on the frequency and severity of the observed damage. Based on the FIB observation results and previous studies, it is recommended that fibers with a larger diameter would be applied to the waste landfill site where the basic condition dominates.

For the sand particle, diverse patterns of damage were detected, as illustrated in Figure 4.4. Severe surface exfoliation was widely observed under the acid condition and pitting on the soil surface was observed under the basic condition. Consequently, it is concluded that the different damage patterns at soil particle entailed the variation of the disturbance function curves and accordingly, different A and Z parameters were estimated.

In long-term behavior, basic condition exhibited more disturbance than acid. This phenomenon appeared consistently in the tests and it is deduced that the exfoliated fine soil particles under acid condition locate at void, and accordingly induce the densification effect during cyclic loading. Additionally, soil particle crushing was detected by FIB due to the weakened material structure by chemical aggressors, as shown in Figure 4.5. Sieve analysis with soil specimen after test was performed to verify the transformation of particle size distribution, as shown in Figure 4.6. Grain diameter between 0.2 and 0.9 mm displayed diverse distribution under acid and basic conditions. Consequently, the effect of chemical attack was clarified by FIB observation and sieve analysis.

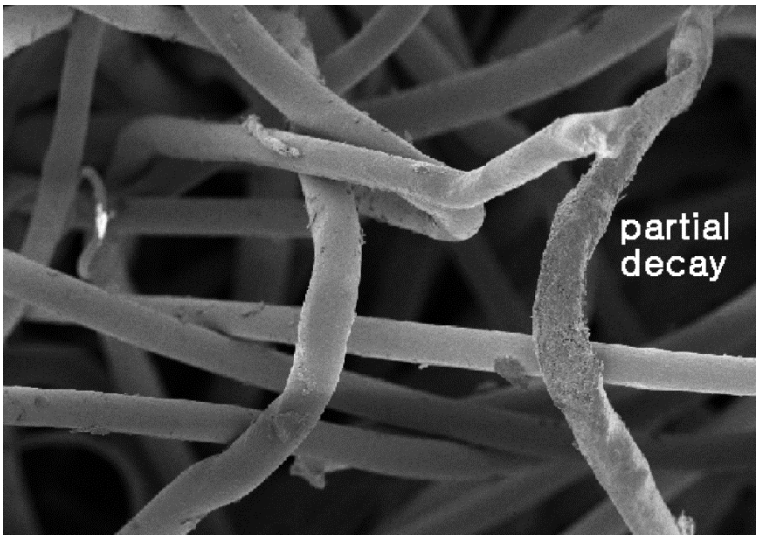

(a) geotextile filament under acid (×500)

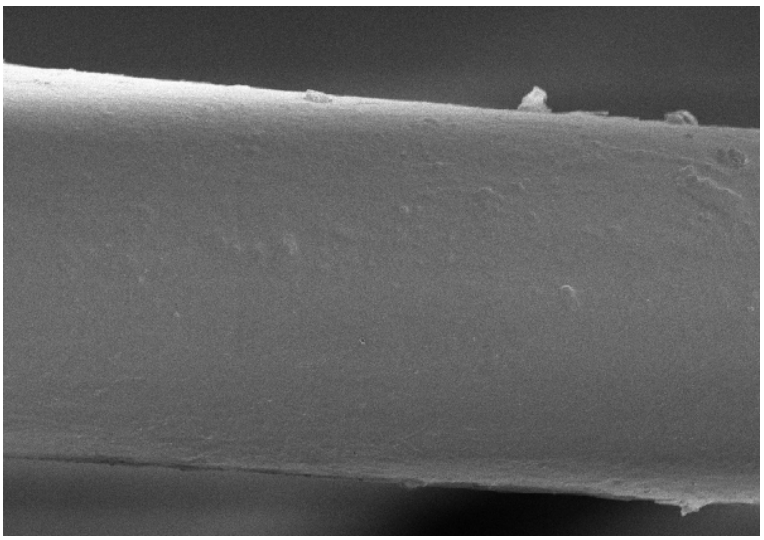

(b) geotextile filament under acid (×5,000)

Figure 4.2 FIB observation results on geocomposite (850 days)

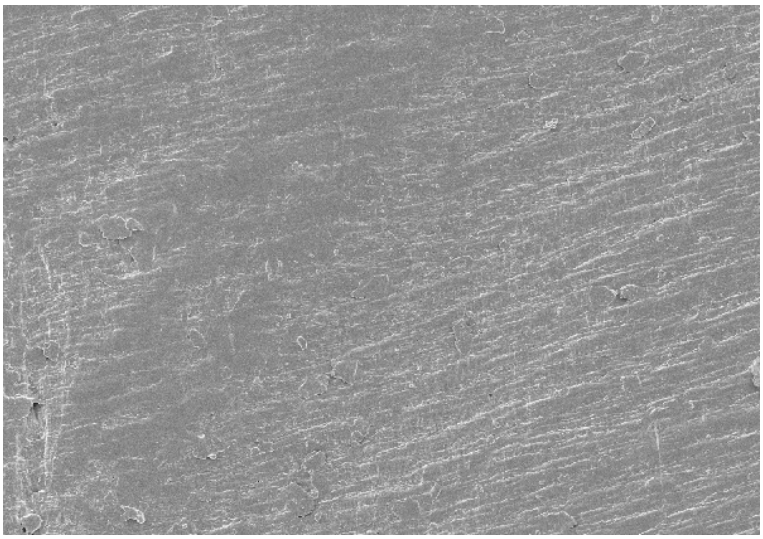

(c) HDPE surface under acid (×5,000)

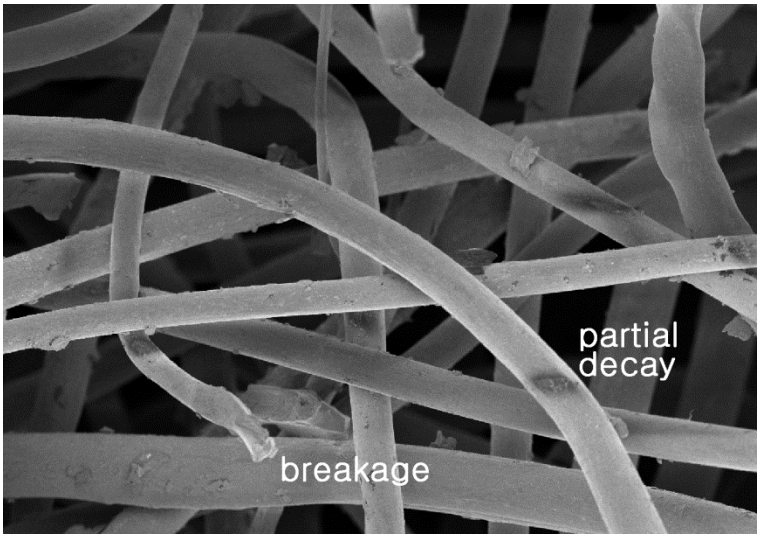

(d) geotextile filament under basic (×500)

Figure 4.2 FIB observation results on geocomposite (850 days) (continued)

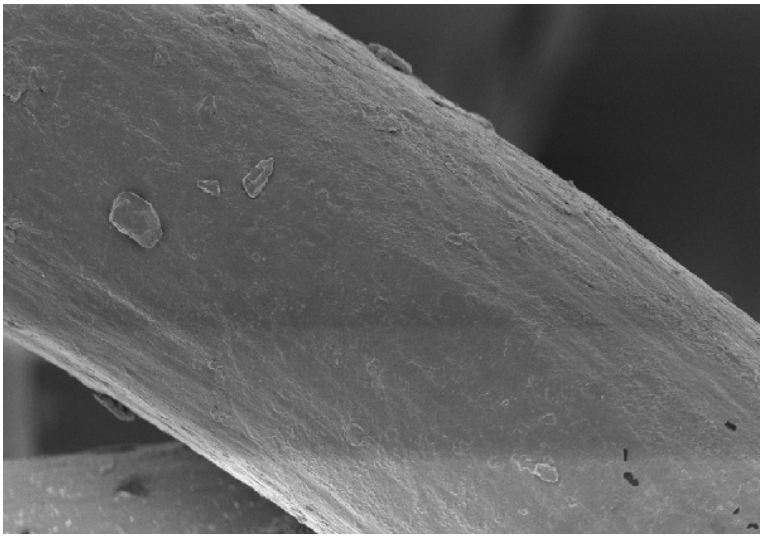

(e) geotextile filament under basic (×5,000)

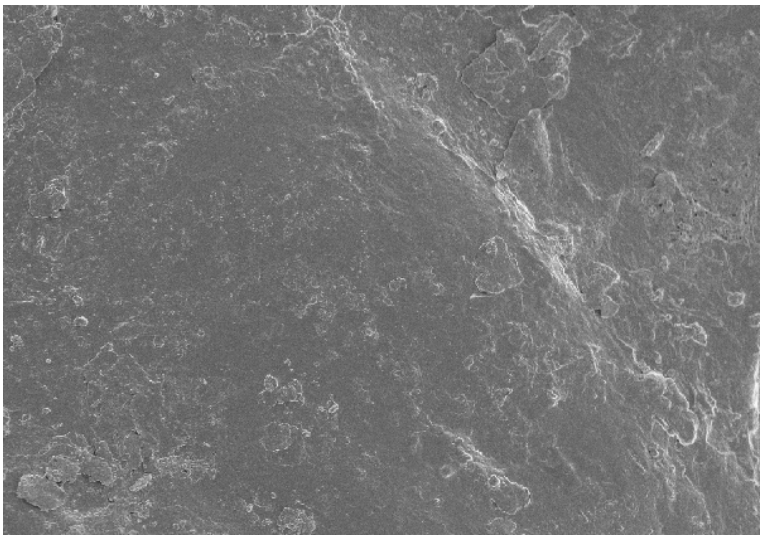

(f) HDPE surface under basic (×5,000)

Figure 4.2 FIB observation results on geocomposite (850 days) (continued)

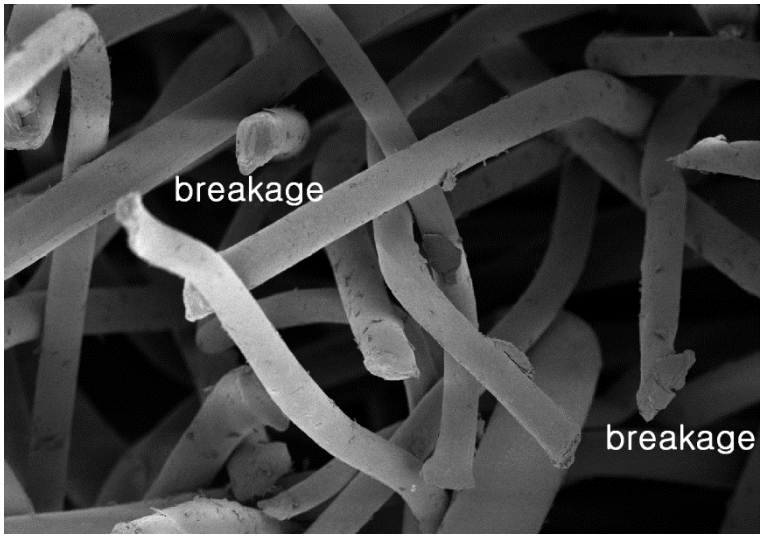

(g) geotextile filament under neutral (×500)

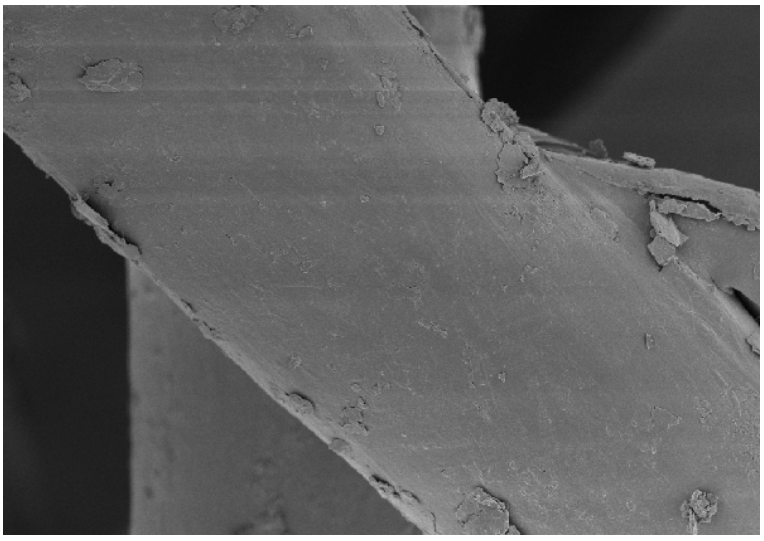

(h) geotextile filament under neutral (×5,000)

Figure 4.2 FIB observation results on geocomposite (850 days) (continued)

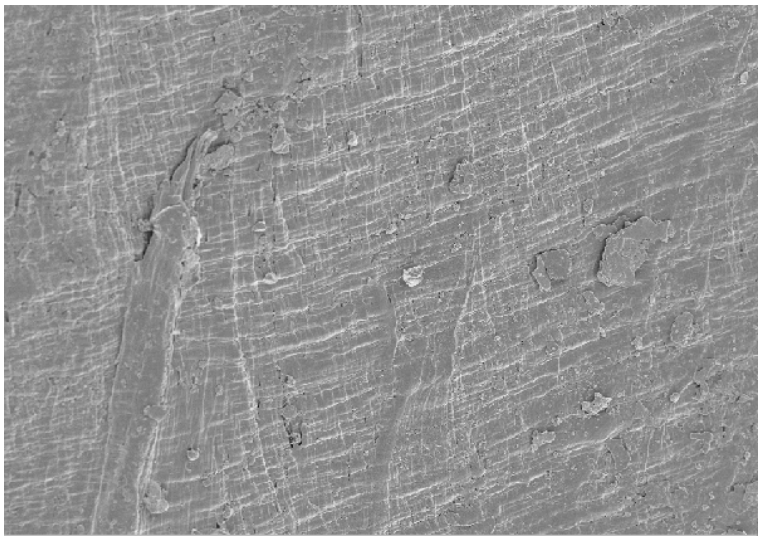

(i) HDPE surface under neutral (×5,000)

Figure 4.2 FIB observation results on geocomposite (850 days) (continued)

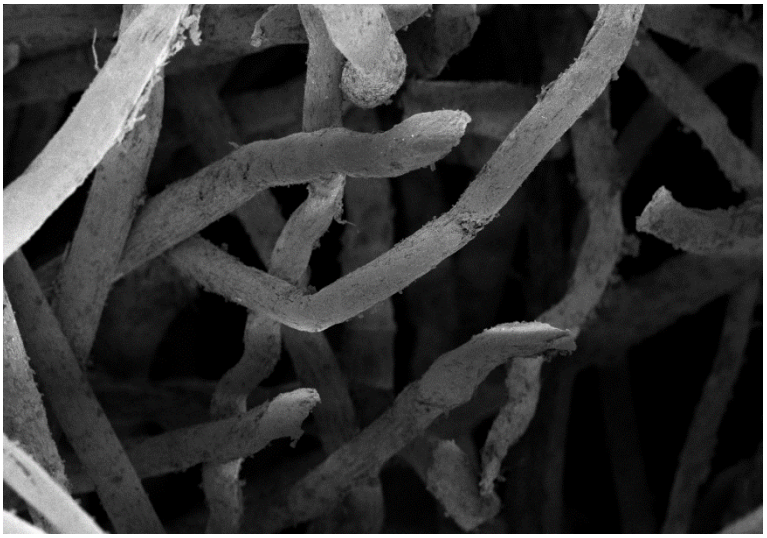

(a) basic (×500)

Figure 4.3 FIB observation results on fabric filament (850 days)

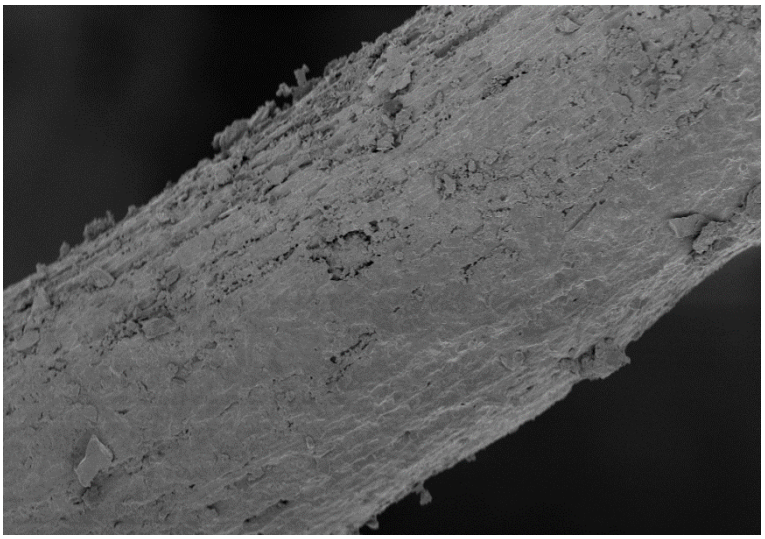

(b) basic (×5,000)

Figure 4.3 FIB observation results on fabric filament (850 days) (continued)

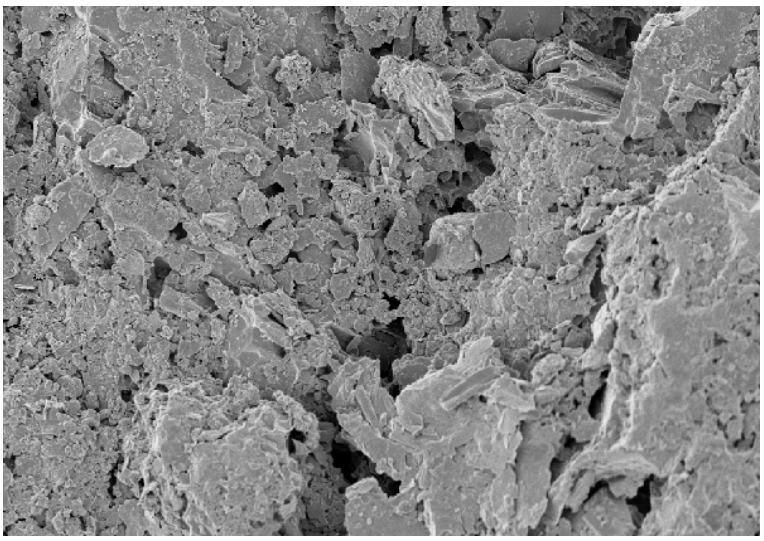

(a) acid (×10,000)

Figure 4.4 FIB observation results on soil particles (850 days)

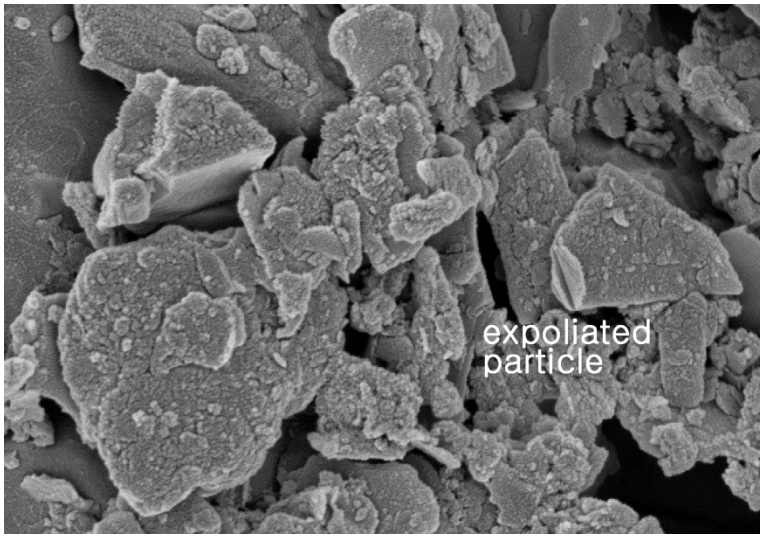

(b) acid (×100,000)

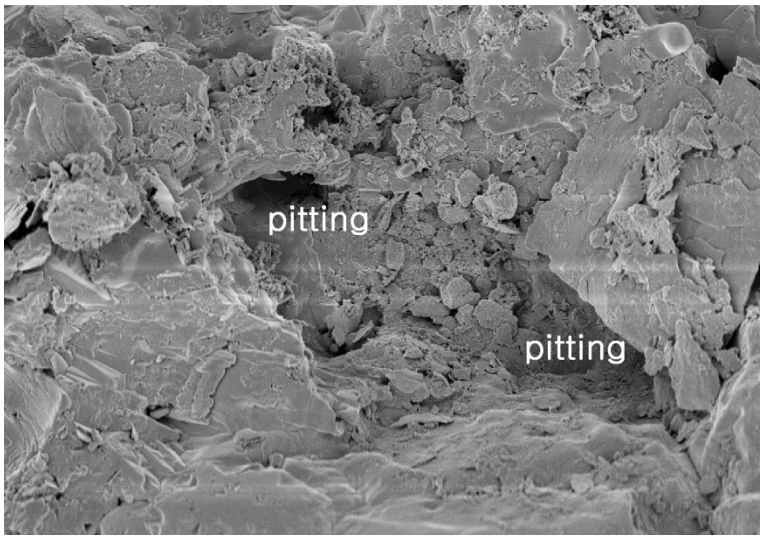

(c) basic (×10,000)

Figure 4.4 FIB observation results on soil particles (850 days) (continued)

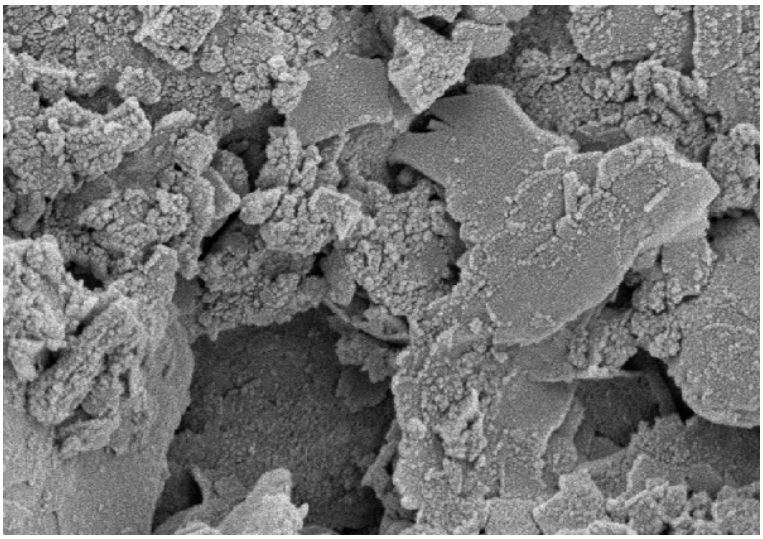

(d) basic (×100,000)

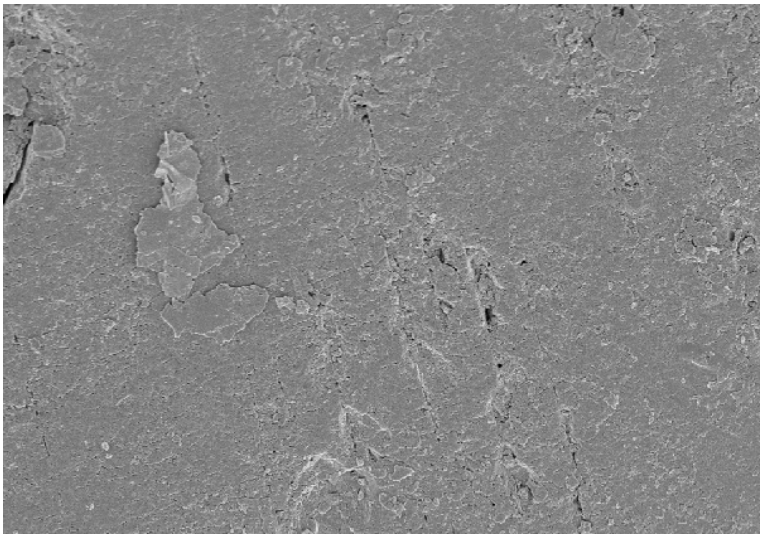

(e) neutral (×10,000)

Figure 4.4 FIB observation results on soil particles (850 days) (continued)

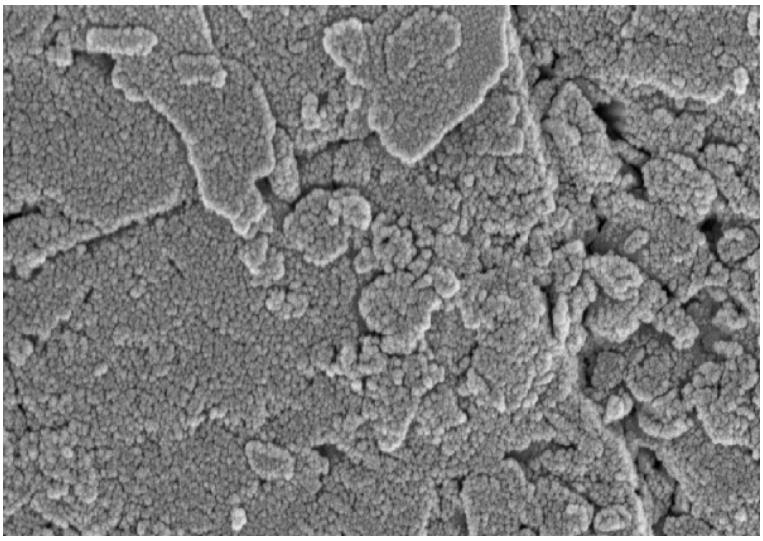

(f) neutral (×100,000)

Figure 4.4 FIB observation results on soil particles (850 days) (continued)

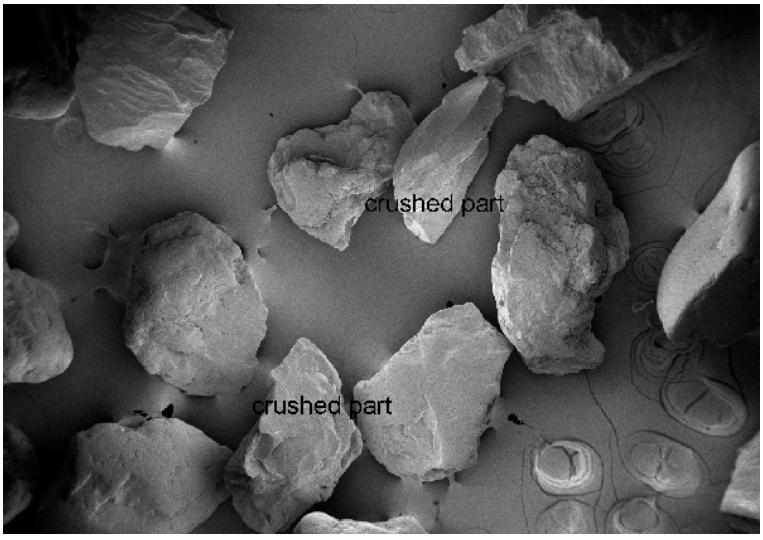

Figure 4.5 Crushed particles observed by FIB (acid, 850 days)

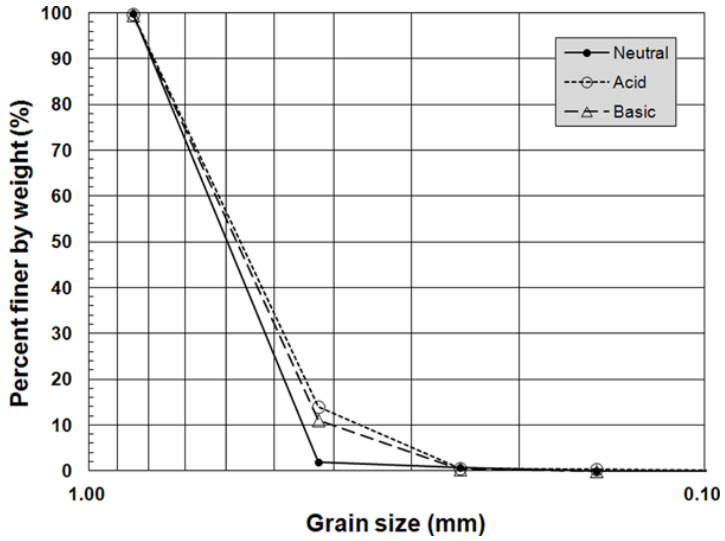

Figure 4.6 Sieve analysis result (850 days)

4.4 Concluding remarks

This chapter introduced the Focused Ion Beam (FIB) electronic microscopy and utilized it to clarify the reason of the different shapes of disturbance function curves. The chemical stability of the HDPE geonet was verified by a few previous researches; therefore, it was induced that the shear stress degradation of the geosynthetic-soil interface mainly originated by the different patterns of soil particles. Though the partial decay and breakage of nonwoven fabric filament were found, however, it might be the minor factor based on the frequency and severity of the observed damage. This hypothesis was verified by the FIB observation successfully. The antioxidant and other ingredients such as carbon black showed evident chemical resistance in HDPE geonet. On the contrary, severe surface exfoliation of soil particle was widely observed under the acid condition and pitting on the soil surface was observed under the basic condition. Consequently, it is concluded that the different damage patterns at soil particle mostly entailed the variation of the disturbance function curves and accordingly, different A and Z parameters were estimated.

In long-term behavior, basic condition exhibited more disturbance than acid. This phenomenon appeared consistently in the tests and it is deduced that the exfoliated fine soil particles under acid condition locate at void, and accordingly induce the densification effect during cyclic loading. Additionally, the crushed soil particles filled up the void with other debris from the chemical attack in the specimen, accordingly entailed a sort of densification effects. It was proved that the sieve analysis result supported this theory.

5. Back-prediction based on Parametric Study

5.1 Introduction

The behaviors of interface between geological and engineering materials subjected to the cyclic loading are complicated and induce various contact problems. However, most of the conventional theories and models only consider specific states during shear deformation such as the limit equilibrium or failure (Desai and Nagarj, 1988). Therefore, the Disturbed State Concept and the disturbance function were utilized to consider the degree of damage or healing of the interfaces. The DSC is based on the experimental approach; therefore, massive sets of laboratory tests were performed to characterize the cyclic shear behaviors of the geosynthetic-soil interface.

Though the laboratory test is one of the most elaborate means to understand the shear behaviors of the geosynthetic-soil interface, there are a few limitations practically. First of all, the test results are dependent on the skill and experience of the researchers; hence, the possibility of human errors is almost unavoidable. This usually causes problems on the reliability and reproducibility of the laboratory tests.

Secondly, the practical test requires considerable time and cost. The appropriate apparatus should be prepared or manufactured to achieve the objective of each test. Testing material and different peripheral devices are also required.

In this Chapter, the numerical back-prediction of the shear stress-strain

response based on the parametric study in Chapter 3.4.2 was performed and compared with the experimental results for verification of the DSC parameters, A and Z. Note that the numerical back-prediction of the cyclic stress-strain relationship are based on the test results; hence, the parameters A and Z should be determined by the laboratory test in the beginning of the numerical prediction. The main purpose of the numerical back-prediction is to verify the accuracy and applicability of the DSC parameters; then, reduce or minimize heft amount of laboratory tests and provide the basis of the numerical analysis of the entire waste landfill site considering the chemical effects on the geosynthetic-soil interface.

The verification of the obtained DSC parameters A and Z was conducted by the comparison of the test results with the numerical prediction results. The verified numerical back-prediction can be utilized to perform the numerical analysis by universal code with minimized laboratory works in the future.

5.2 Data used for back-prediction

In this study, the numerical back-prediction based on the experimental data obtained from the cyclic simple shear test was accomplished and verified. The cyclic shear stress-strain curves were numerically reproduced and compared with the test results. Each shear stress-strain curve at the cycle of 1^{st}, 5^{th}, 10^{th}, and 50^{th} for acid, basic and neutral conditions was considered as

shown in Figure 5.1, and the disturbance function parameters at each case were also displayed in Table 5.1.

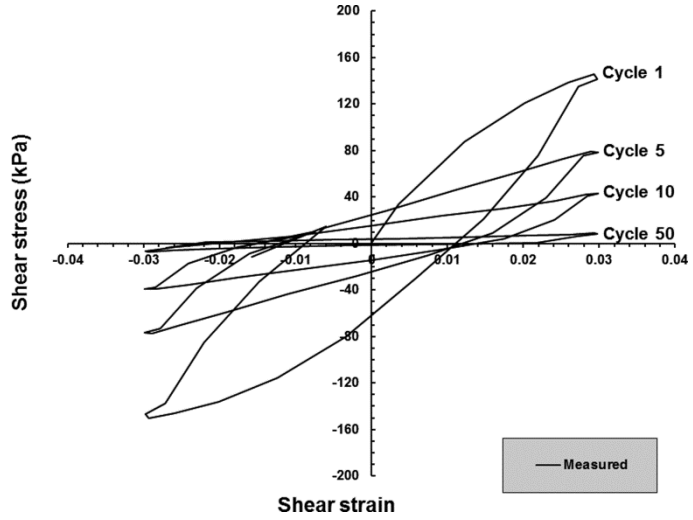

(a) acid condition (850 days, 0.6 MPa)

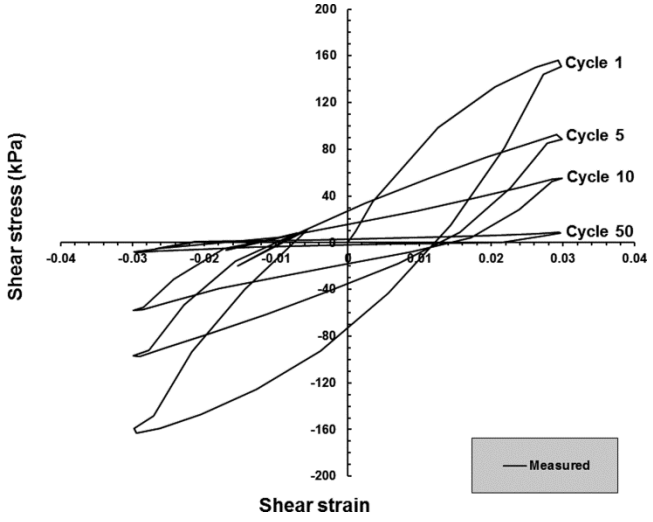

(b) neutral condition (850 days, 0.6 MPa)

Figure 5.1 Measured cyclic shear stress-strain curves

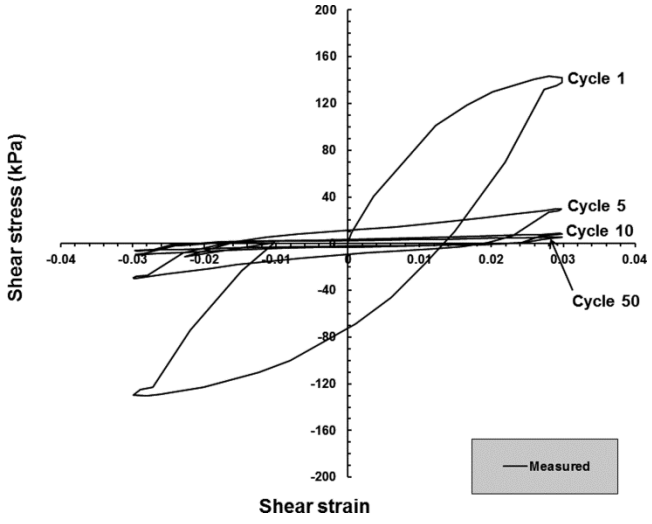

(c) basic condition (850 days, 0.6 MPa)

Figure 5.1 Measured cyclic shear stress-strain curves (continued)

Table 5.1 DSC parameters for back-prediction

Chemical conditions	DSC Parameters	
	A	Z
Acid	2.288	0.57
Neutral	2.132	0.633
Basic	3.975	0.399

5.3 Numerical back-prediction

5.3.1 Methodology

The numerical back-prediction is based on the laboratory cyclic simple shear test results in this study. The shear stress degradation is considered by means of the Disturbed State Concept and the disturbance function curves. From the shear stress-strain curves and Equation (2.9), the shear stresses at Relatively Intact (RI) condition, at Fully Adjusted (FA) condition, at the observed (present) condition can be obtained. As the observed shear stress, τ^i changes continuously at every cycle, the disturbance, D is also updated according to the load cycles.

In the functional form of the disturbance is expressed as Equation (2.8), and the disturbance parameters, A and Z are known by the laboratory test results or suggested values form the previous studies. Then, the practical form of the disturbance function is express as shown in Equation (5.1) below.

$$D = D_u \left[1 - e^{(-A\,\xi_D^Z)} \right] = 0.99 \left[1 - e^{(-A\,\xi_D^Z)} \right] \tag{5.1}$$

where, D_u is the ultimate disturbance and practically 0.99 is applicable based on the previous researches (Park, 1997).

The procedures for the numerical back-prediction are explained as follows.

(1) ***Obtain the DSC parameters and*** τ^i, τ^c**;** from the experimental test results.

(2) ***Define source curves;*** Cyclic shear stress-strain curves can be divided into 4 phases as described in Figure 5.2 (a). The target slope to define the each phase can be estimated as shown in Figure 5.2 (b).

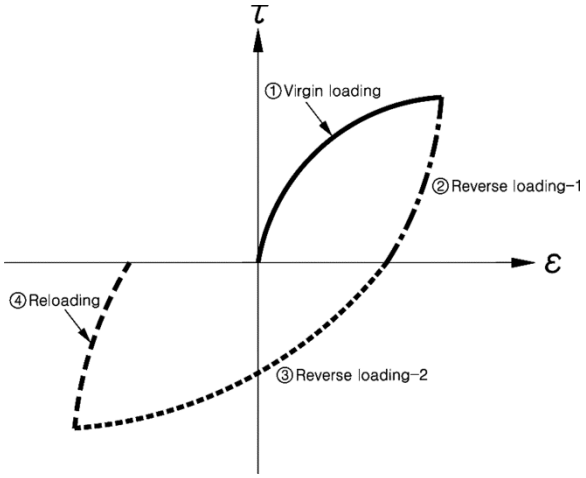

(a) 4 phases in a cyclic loading

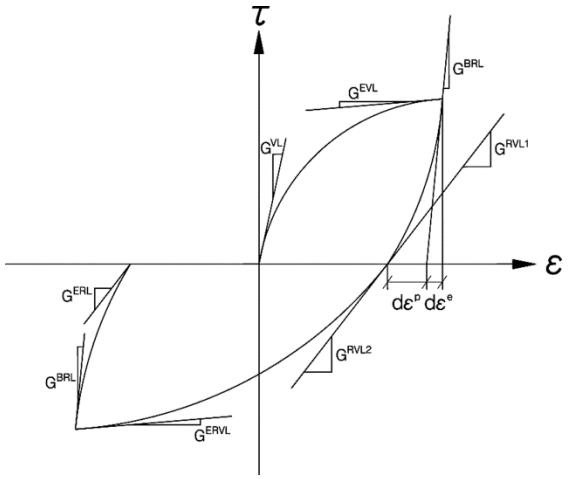

(b) target tangential slopes

Figure 5.2 Defining source curves

(3) ***Numerical interpolation*;** Equally dividing each curve by "n" segments, and obtain the average tangential slope by dividing the difference between the initial tangential slope (G_VL) and the final tangential slope (G_EVL), as demonstrated in Figure 5.3. Then, the linear equations at each dividing point (k/n, 2k/n, ⋯) can be calculated by the tangential slope at each dividing point as shown in Figure 5.3. The tangential slope at each dividing point is obtained by tangential slope increment between the initial and final tangential slopes.

Note that the total number of the linear equation is (n+1), and n=10 is applied in this study. Therefore, the equation of the initial tangential line can be expressed in Equation (5.2), and general equations are also expressed in Equation (5.3) to (5.5) in the virgin loading phase.

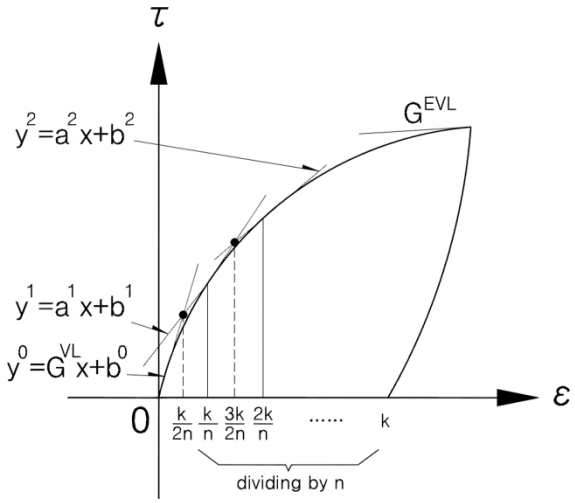

Figure 5.3 Numerical interpolation of hysteresis curve

$$y^0 = \tau^0 = G^{VL}\,x + b^0 = G^{VL}\,\varepsilon + b^0 \qquad (5.2)$$

$$y^1 = \tau^1 = \left[G^{VL} - \left\{\frac{G^{VL} - G^{EVL}}{n}\right\}\right] \varepsilon + b^1 \quad (5.3)$$

$$y^2 = \tau^2 = \left[G^{VL} - 2\left\{\frac{G^{VL} - G^{EVL}}{n}\right\}\right] \varepsilon + b^2 \quad (5.4)$$

The general form is expressed:

$$y^m = \tau^m = \left[G^{VL} - m\left\{\frac{G^{VL} - G^{EVL}}{n}\right\}\right] \varepsilon + b^m,\ 0 \le m \le n,\ \varepsilon = \frac{mk}{n} \quad (5.5)$$

It is assumed that the consecutive two linear equations intersect at the midpoint between the consecutive two dividing points. Every linear equation at the midpoints can be evaluated in sequence since all equations at the dividing points were known.

Practically, G_VL and G_BRL are almost identical. In the same manner, G_EVL and G_ERVL, G_ERL and G_RVL1, 2 are also regarded as the same values for the simplicity of the numerical interpolation, therefore; the back prediction becomes more convenient.

(4) ***Obtain*** $\boldsymbol{\tau^i}$**;** Combining the Equation (2.8) and (2.9) yields Equation (5.6) as follows. The updated shear stress at the each cycle, τ^i can be obtained by Equation (5.5).

$$\tau^a = \tau^i - (\tau^i - \tau^c)D = [\tau^i - (\tau^i - \tau^c)]\left[0.99\left\{1 - e^{(-A\,\xi_D^Z)}\right\}\right] \quad (5.6)$$

(5) ***Obtain the average strain increment;*** Based on the difference of shear strain between the RI (initial) and FA (failure) conditions, the average plastic strain incremental can be calculated. In this study, the number of cycle that begins to be FA state is considered as 50.

(6) ***Update*** $\boldsymbol{\tau^i}$**;** Based on the Equation (5.6) and average strain increment from the procedure (5), the cyclic shear stress at the target cycle can be calculated.

All the procedures are repeated, consequently, the cyclic shear stress-strain relationship is able to be reproduced. Figure 5.4 summarized the procedures of the numerical back-prediction methodology.

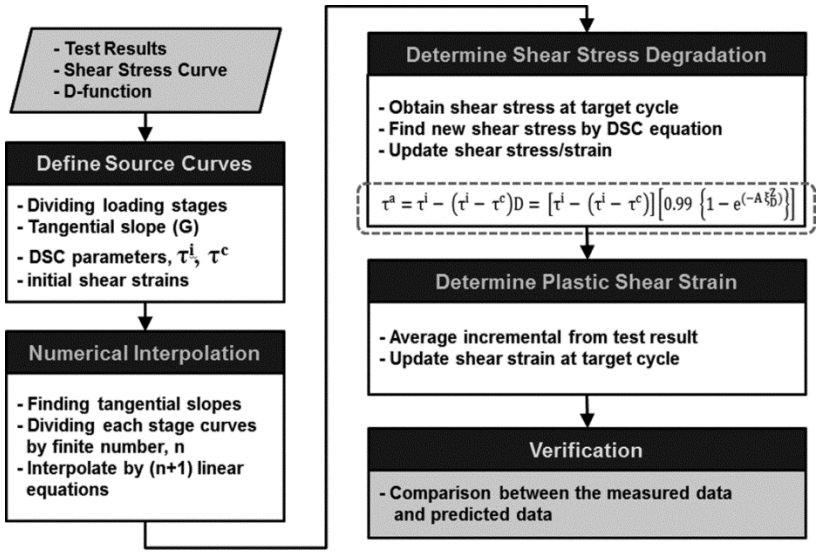

Figure 5.4 Procedures of numerical formulation

5.3.2 Back-prediction results

In DSC model, it is assumed that the external load generates the disturbances in a material and the disturbed area is expanded as the load exists or increases; therefore, the stress degradation occurs according to the accumulation of internal damage. The stress degradation can be described subjected to the type of the external load, as shown in Figure 5.5. RI state was considered as the first cycle and FA was considered as the 50th cycle in this study.

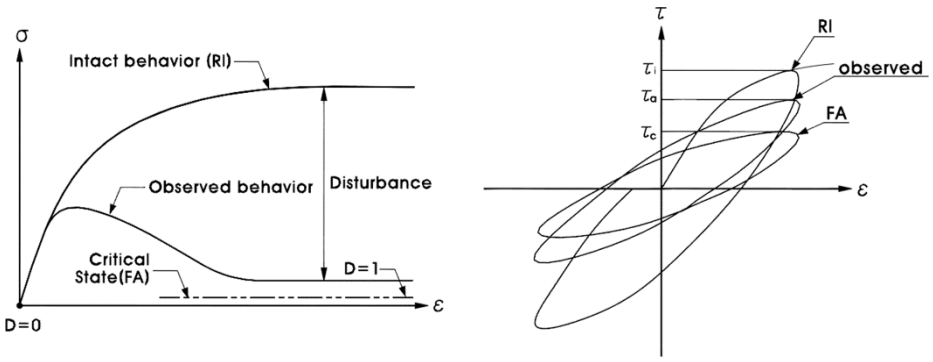

(a) static loading (b) cyclic loading

Figure 5.5 Schematic of stress degradation

The numerical back-prediction to reproduce the cyclic shear stress-strain relationship was developed by the numerical interpolation procedures previously mentioned. Once the cyclic shear stresses in RI (τ^i) and FA state (τ^c) are obtained with the strain, the cyclic shear degradation can be simulated based on the disturbance function parameters which can represent the effect of

chemical conditions. Table 5.1 already summarized the developed model parameters in this study and Figure 5.6 displayed the reproduced stress-strain curves based on the developed numerical modeling. The cyclic shear stress-strain curves are obtained at the cycle of 1^{st}, 5^{th}, 10^{th}, 50^{th}.

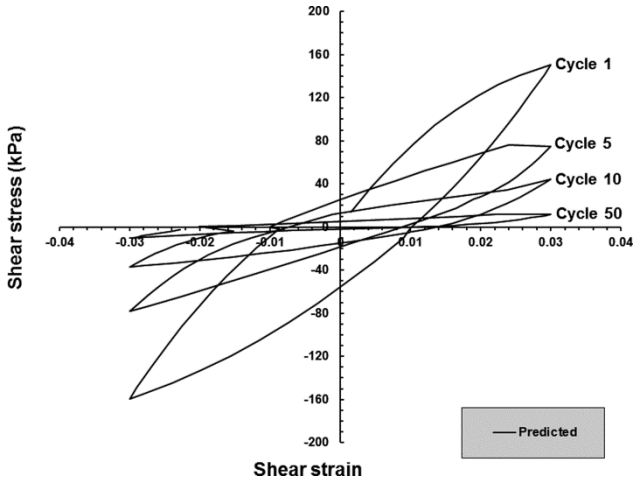

(a) acid condition (850 days, 0.6 MPa)

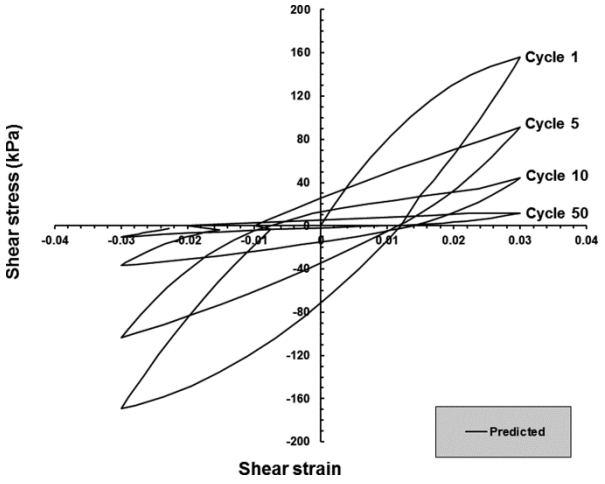

(b) neutral condition (850 days, 0.6 MPa)

Figure 5.6 Predicted result of cyclic shear stress-strain curves

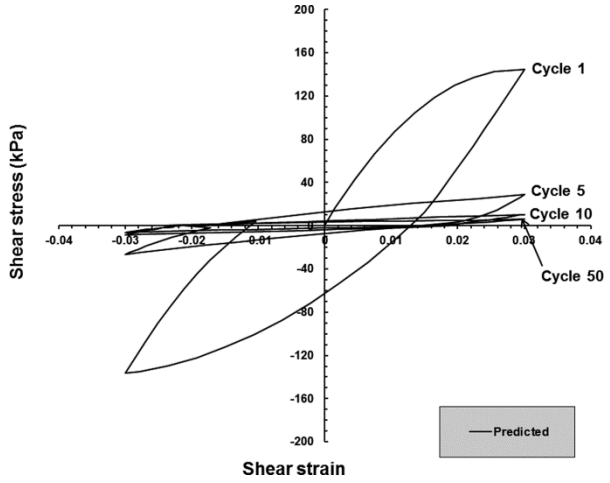

(c) basic condition (850 days, 0.6 MPa)

Figure 5.6 Predicted results of cyclic shear stress-strain curves (continued)

5.3.3 Comparisons between experimental and predicted results

The back-prediction results were verified through the comparison between numerical back-prediction results and the experimental data. The DSC parameters used in the back-prediction was listed in Table 5.1, previously. The experimental cyclic shear stress-strain curves at the cycle of 1^{st}, 5^{th}, 10^{th}, and 50^{th} were compared with the predicted results at the same cycles to verify the accuracy and compatibility. Figure 5.7 displays the comparison results between the measured and predicted results at each cycle. Note that, each load phase was divided into 10 segments then 40 points of predicted shear stress-strain values were obtained in this study. The smaller segment was applied, the more accurate result of the back-prediction is

expected. As the number of the measured points was 20; therefore, the 40 values are enough to be ensure the accuracy of the numerical back-prediction.

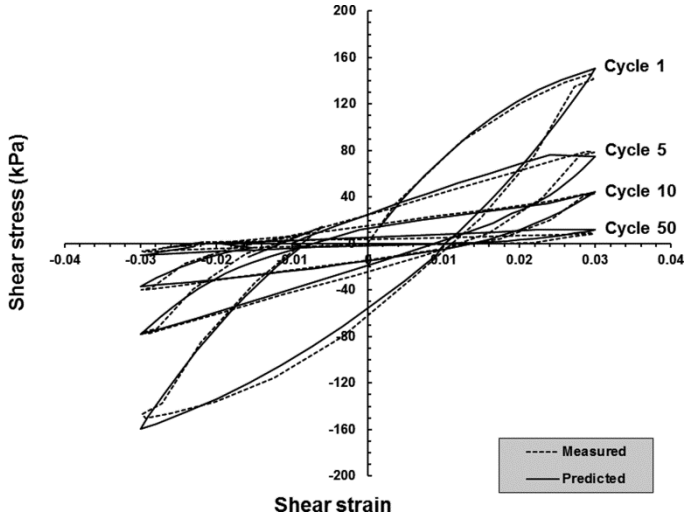

(a) acid condition (850 days, 0.6 MPa)

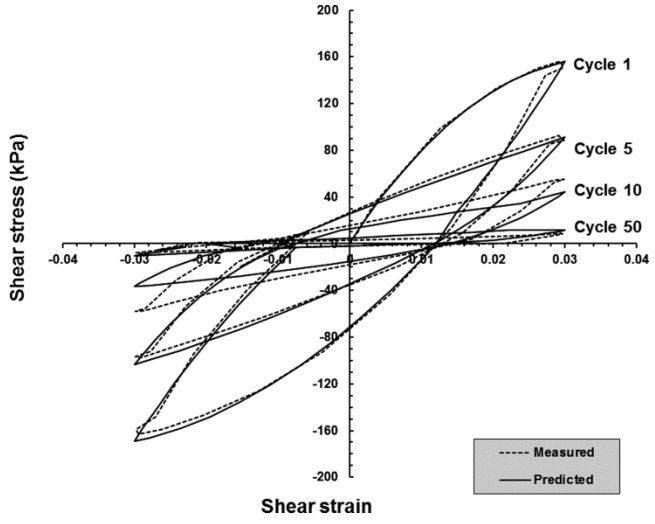

(b) neutral condition (850 days, 0.6 MPa)

Figure 5.7 Comparisons of measured and predicted results

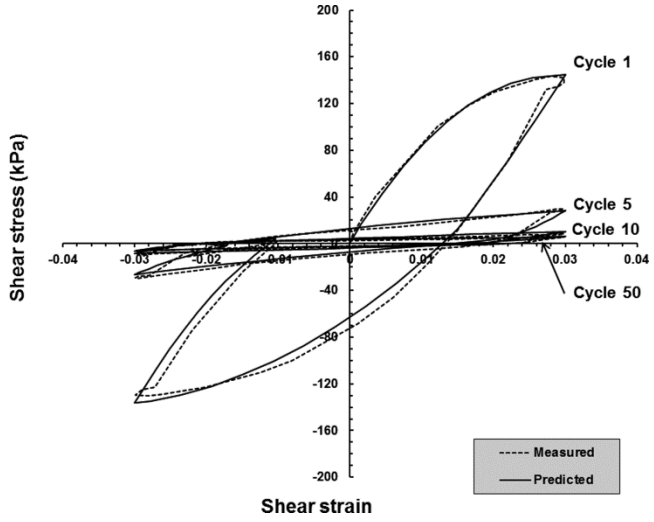

(c) basic condition (850 days, 0.6 MPa)

Figure 5.7 Comparisons of measured and predicted results (continued)

In Figure 5.7, though a few discrepant points were observed, however; the comparison result demonstrated good agreements, in general.

A few discrepancies were found at shear strain, which corresponds to the asymmetric stress response of the soil specimen due to its anisotropy, inhomogeneity, and reorientation of the particles due to stress reversal under cyclic loading (Thurairajah, 1974). This kind of error is unavoidable in a numerical simulation of the response under cyclic loading; however, the cyclic shear stress degradation was found to be in a good agreement, generally.

Apart from the comparison results in Figure 5.7, it is important to verify the predicted DSC parameters which are not obtained from the test result directly can simulate the shear stress-strain behavior. In order to compare the predicted shear stress-strain result with the experimental result, additional cyclic simple shear tests were conducted in accordance with the conditions as

displayed in Table 5.2.

Table 5.2 Additional test conditions for verification

Chemical conditions	DSC Parameters	Normal stress (MPa)		
		0.30	0.45	0.60
Basic	A	1.5529	1.7171 (predicted)	1.8814
	Z	0.5287	0.5804 (predicted)	0.6320

The submerging period is 12 months and the DSC parameters under 0.45 MPa of normal stress condition were predicted by linear interpolation. Therefore, predicted shear stress-strain behavior under 0.45 MPa of normal stress condition based on the predicted parameters, A and Z were compared with the test result. Figure 5.8 exhibits the shear stress-strain curves from the cyclic simple shear test.

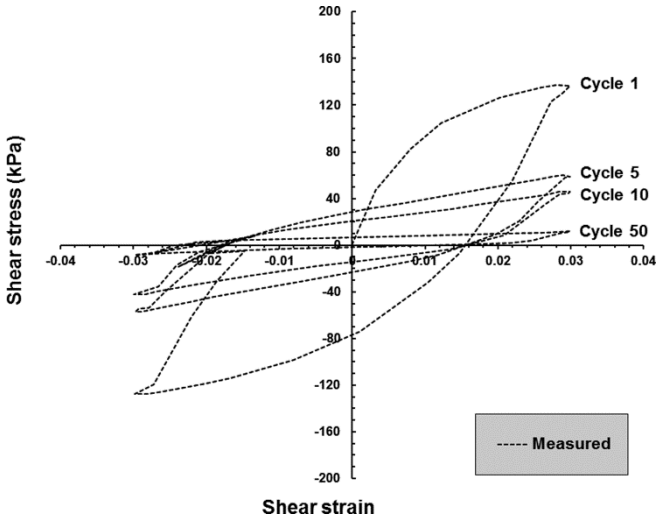

Figure 5.8 Additional test results (360 days, 0.45 MPa)

Based on the proposed methodology, the shear stress-strain response was predicted and compared with the test results at the cycle of 1st, 5th, 10th, and 50th as shown in Figure 5.9. The predicted result was able to simulate the shear stress-strain curve and shear stress degradation according to the loading cycles, in general. Little discrepancies were found at 50th cycle due to the shear reversal from the test results, as mentioned before, however; the comparison result displayed good agreements. Furthermore, such satisfactory results were attributed to the precise performance and convenience of the newly modified M-PIA.

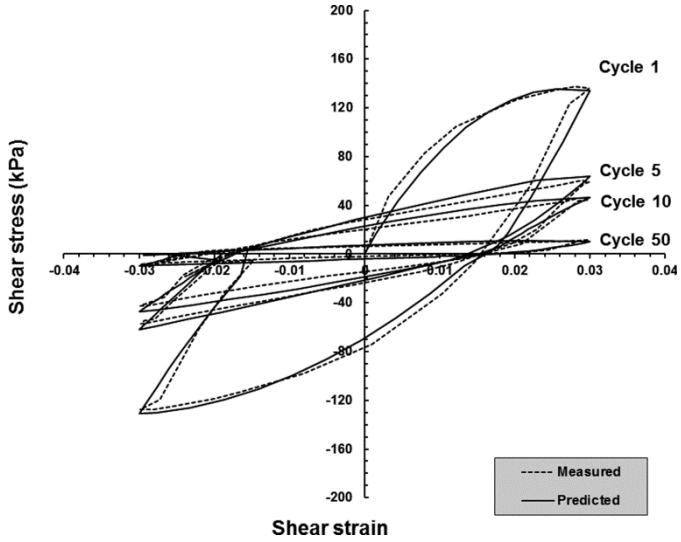

Figure 5.9 Verification of the predicted results (360 days, 0.45 MPa)

5.4 Concluding remarks

The numerical back-prediction of the cyclic shear stress-strain relationship was performed and verified based on the experimental results of the geosynthetic-soil interface considering chemical effects. Based on the experimental data obtained by cyclic simple shear tests and the DSC parameters were utilized to reproduce the cyclic shear stress according to the load cycle. The back-prediction was also verified to ensure the compatibility and accuracy of the DSC parameters, A and Z.

The methodology of numerical back-prediction is based on the idea that the hysteretic curve at a certain cycle can be divided into 4 phases and the each curve is equally divided into 10 segments again for numerical interpolation. The tangential slopes of the initial and final stress points in a curve can be calculated by linear tangential equations in sequence. Numerical interpolation enabled to obtain the cyclic shear stress-strain values at the midpoints in each segment and reproduce the cyclic shear stress-strain curves. Shear stress degradation was automatically calculated by the test results and the shear strain increment and updated at the target cycle. RI state was considered as the first cycle, and FA is considered as the condition after 50^{th} cycle of loading. Parameters related the model are; (1) tangential slope at the initial and end points at each phase, (2) shear strain at the initial and end points at each phase, which can be calculated by the average shear strain increment, (3) cyclic shear stress at the initial and end points at each phase, which estimated by the Equation (5.6).

The back-prediction results presented good agreements with the

experimental data obtained by the cyclic simple shear test in all chemical conditions. Though a few discrepancies were found at shear strain, which corresponds to the asymmetric stress response of the soil specimen under cyclic loading, the overall performance of the developed model was satisfactory.

The numerical back-prediction of the geosynthetic-soil interface considering chemical effects is expected to be a basis of building up a fully numerical analysis by universal codes in the future. Furthermore, this numerical back-prediction is also able to consider the shear stress degradation with sufficient accuracy and reduce hefty amount of laboratory tests.

6. Conclusions and Recommendations

6.1 Summary of research

The comprehensive objective of this dissertation is to investigate cyclic shear behaviors of geosynthetic-soil interface considering chemical effects.

For experimental research, a new test apparatus was built and modified for better performance. 72 sets of cyclic simple shear test were conducted and the shear stress degradation was estimated quantitatively by the Disturbed State Concept (DSC) and disturbance functions. As a result, new disturbance function parameters were suggested to characterize chemical conditions such as acid, basic and neutral.

Microscopic observation was performed to clarify the reason of variation of shear stress degradation at the interface subjected to the *p*H values by Focused Ion Beam (FIB). As a result, different patterns at soil particle surface were attributed to the variation of the disturbance function curves and parameters. The filament of nonwoven fabric showed partial decay and breakage; however, it was considered as a minor factor based on the frequency and severity of the observed damage.

Based on the experimental and microscopic approach, the numerical back-prediction of the cyclic shear stress-strain relationship was accomplished by numerical interpolation based on the experimental results. The back-prediction results were verified by the comparisons between the predicted and measured data, and demonstrated good agreements.

Consequently, a general methodology to estimate the cyclic shear stress degradation of geosynthetic-soil interface considering chemical effects was established and verified.

6.1.1 Multi-purpose interface apparatus (M-PIA)

Shear stress and deformation behaviors of waste landfill systems under dynamic (earthquake) loading are significantly influenced by the response of interfaces composed of geosynthetics and soil. Chemical aggressors in the leachate may affect the dynamic shear behavior of the interface; however, it has not been investigated yet in detail. Therefore, it is required to develop an appropriate testing device and perform an experimental study considering the chemical effects on the interface to overcome some limitations in theoretical approach. Though a few guidelines were suggested to test the geosynthetic-soil interfaces, it is still insufficient to test the cyclic shear behavior of the various kinds of interfaces under chemical and dynamic conditions, hence, the development of new apparatus and performing the cyclic simple shear test are the most important portion in the present study.

In this research, a new apparatus, named as M-PIA (multi-purpose interface apparatus) to investigate the chemical effects on the geosynthetic-soil interface under cyclic loading was manufactured in 2010. The geosynthetics and soil specimen is set in the circular shear box. Five independent shear rings that are 2 mm in thickness were Teflon-coated to avoid the frictional resistance between rings which may cause inaccuracy in

the test results.

In spite of some successful research results (Kwak et al., 2013[a]; Park et al., 2010) by using the M-PIA of 1st generation, there were two main items to be revised. One thing was the bending moment induced by the lateral force and the other was rough data acquisition system. Four major improvements such as the separation of loading system, Teflon shear rings, outer mold, and modified load control system to overcome the limitations of M-PIA were successfully applied.

6.1.2 Experimental study

A series of cyclic simple shear tests were conducted in accordance with the chemical conditions, submerging periods, and the normal stress applied to the specimen.

For the material, Jumunjin sand was chosen to represent the granular material and the geocomposite which is mostly applied in the waste landfill sites in Korea were utilized in the tests. Both geosynthetic and soil specimen were submerged in the basic, neutral and acid solutions for 30 days and 850 days to consider the short and long-term responses of the interface, respectively. For the dynamic condition, 0.5 Hz of sinusoidal loading was chosen to perform the cyclic simple shear test based on the results of the previous researches, and the 3 % of shear strain was applied to the specimen. Constant volume boundary condition was chosen to the apparatus to simulate the abrupt loading condition such as the earthquake loading.

Totally 72 sets of cyclic simple shear tests were performed in order to investigate the chemical effects on the cyclic shear behavior of the geosynthetic-soil interface. The conventional analysis seemed to be still applicable; however, it was difficult to estimate the degree of damage quantitatively. Therefore, the Disturbed State Concept (DSC) and the disturbance functions were utilized to estimate the shear stress degradation of the interface. Based on shear stress-strain hysteretic loop at each cycle, the disturbance and plastic shear strain trajectory were obtained. Accordingly, the disturbance function parameters, A and Z were also estimated using linear regression technique. A and Z parameters determine the shape of the disturbance function curve. The shape of the disturbance function curve enables to predict the degree of damage corresponding to the plastic shear strain level. Parameter A increased with the increase of submersing period under the same chemical and normal stress conditions. On the contrary, parameter A decreased with the increase of the normal stress under the same chemical and submergence conditions. Parameter Z increased with the increase of submersing period and the normal stress, under the same chemical condition.

Based on a series of cyclic simple shear test and new disturbance function parameters, accordingly, new disturbance function curves corresponding to the chemical conditions were evaluated. In the short-term (30 days of submergence) behavior, acid and basic conditions were more vulnerable. For long-term behavior, the differences of the disturbance function values at a certain deviatoric plastic strain trajectory, ξ_D, showed more distinct than the values under short-term conditions. The differences between

the disturbance curves at a certain strain level can be intuitionally observed by the comparison of curves on the same domains. In all cases, it was discovered that the basic condition was the most vulnerable.

Additionally, a parallel study on the suggested disturbance function curves was conducted. The effects of the submerging period and normal stress were analyzed by comparison of the curves. Generally, the disturbance intensified in case of the long-term submergence condition in all cases, however, the differences of the disturbance decreased in case of higher normal stress condition because confining effect may resist the abrupt progress of damage in the geosynthetic-soil interface. The variation between the disturbance curves under each submerging period was significant and the largest variation was observed in basic condition under applying 0.3 MPa of the normal stress. The variation between the disturbance curves under each normal stress condition was also remarkable and the largest variation was observed in acid condition under 850 days of the submerging period. Furthermore, it has been proved that the submerging period and the normal stress conditions are both important factors affect the cyclic shear stress degradation of the geosynthetic-soil interface.

To present the recent achievement, the prototype test results considering thermal effect were demonstrated and the shear stress degradation due to the temperature elevation was evaluated and analyzed by the disturbance function curves. Based on the test results, it is deduced that the elevated temperature can degenerate the shear resistance of the geosynthetic-soil interface under severe acid and basic conditions.

6.1.3 Microscopic observation

The Focused Ion Beam (FIB) electronic microscopy was introduced and utilized it to clarify the reason of the different shapes of disturbance function curves. The chemical stability of the HDPE geonet was verified by a few previous researches, therefore, it was deduced that the shear stress degradation of the geosynthetic-soil interface originated by the different patterns of soil particles. This hypothesis was verified by the FIB observation successfully. The antioxidant and other ingredients such as carbon black showed evident chemical resistance in HDPE geonet. On the contrary, the filament of nonwoven fabric showed partial decay and breakage; however, it was considered as a minor factor based on the frequency and severity of the observed damage. For soil particle, severe surface exfoliation was widely observed under the acid condition and pitting on the soil particle surface was observed under the basic condition. Consequently, it is concluded that the different damage patterns at soil particle mainly entailed the variation of the disturbance function curves and accordingly, different A and Z parameters were estimated. In long-term behavior, basic condition exhibited more disturbance than acid, then, it is deduced that the damage of the filament of nonwoven fabric due to the vulnerability for the basic condition can cause the most significant damage of the geosynthetic-soil interface as well as the surface damage of soil particle. Note that the hydrolytic reaction can cause the damage of the filament due to the reduction of the molecular weight via chain scission, as mentioned in Chapter 2.3.3. The hydrolytic reaction is a

topochemical reaction and is accelerated substantially by basic condition. Therefore, filament with a large diameter would be recommended to resist the severe basic condition. Additionally, the exfoliated fine soil particles under acid condition locate at void, and accordingly induce the densification effect during cyclic loading. The crushed soil particles filled up the void with other debris from the chemical attack in the specimen, accordingly entailed a sort of densification effects. It was discovered that the sieve analysis result supported this theory.

6.1.4 Back-prediction based on parametric study

The numerical back-prediction of the cyclic shear stress-strain relationship was performed and verified based on the experimental results of the geosynthetic-soil interface considering chemical effects. Based on the experimental data obtained by cyclic simple shear tests and the DSC parameters were utilized to reproduce the cyclic shear stress according to the load cycle. The back-prediction was also verified by comparison between the predicted and measured data and demonstrated good agreements, then, ensured the compatibility and accuracy of the DSC parameters, A and Z. The numerical back-prediction of the geosynthetic-soil interface considering chemical effects is expected to be a basis of building up a fully numerical analysis by universal codes in the future. Furthermore, this numerical back-prediction is also able to consider the shear stress degradation with sufficient accuracy and reduce hefty amount of laboratory tests.

Consequently, the academic achievement of the present study accomplished a general methodology including laboratory tests, the estimation of interface damage, microscopic observation, and numerical back-prediction to investigate the cyclic shear stress degradation of the geosynthetic-soil interface considering chemical effects, comprehensively.

6.2 Recommendations

I. A general and overall methodology has been suggested and verified by the experimental research. Test results were compared and dealt with statistically. Furthermore, cyclic simple shear test considering another various conditions such as moderate *p*H solutions, higher normal stress, etc. are worth to be studied. Based on the accumulated results of the experimental study, the construction of a database is recommended to characterize the effects of various conditions on the geosynthetic-soil interface.

II. The modified M-PIA is originally designed to be able to consider the thermal effects on the shear behaviors of the interface. In general, polymers are sensitive to the temperature; hence, the temperature may play an important role in the shear behavior of the interface. Additionally, the temperature affects the material characteristics of the geosynthetics instantly, in contrast with the chemical aggressor. A set of prototype test results considering thermal effect were presented to introduce the recent achievement in this study and it is deduced that

the elevated temperature can degenerate the shear resistance of the geosynthetic-soil interface under severe acid and basic conditions. However, more tests under various temperature conditions are required to evaluate DSC parameters and tendency in the future. Therefore, further study on the thermal impact on the geosynthetic-soil interface is recommended.

III. The suggested numerical back-prediction in the present study is mainly focused on the reproduction of the cyclic shear stress-strain relationship. Therefore, the modifications of the constitutive equations and the incremental functions of stress and strain are required to simulate the entire stress-strain behaviors for numerical analysis by universal codes. Dedicated research and investigation on the improvement of the constitutive equations in accordance with the test results will be a good theme to be explored.

References

Alanazy, A. S. (1996). “Testing and modeling of sand-steel interfaces under static and cyclic loading,” Ph.D Dissertation, Department of Civil Engineering and Engineering Mechanics, University of Arizona, Tuscon, Arizona

Araei, A. A., Razeghi, H. R., Tabatabaei, S. H. and Ghalandarzadeh, A. (2012), “Loading frequency effect on stiffness, damping and cyclic strength of modeled rockfill materials,” Soil Dynamics and Earthquake Engineering, Vol. 33. Pp. 1-18

Araei, A. A., Razeghi, H. R., Tabatabaei, S. H. and Ghalandarzadeh, A. (2009). “Evaluation of frequency content on properties of gravelly soils,” Research Project, No. 1-1775-2008, BHRC, Iran

Armaleh, S. H. and Desai, C. S. (1990). “Modeling include testing of cohesionless soils under disturbed state concept,” Report to the NSF, Department of Civil Engineering and Engineering Mechanics, University of Arizona, Tuscon, Arizona

Amer, M. I., Aggour, M. S. and Kovacs, W. D. (1986). “Testing using a large-scale cyclic simple shear device,” Geotechnical Testing Journal, Vol. 9, No. 3, pp. 140-146

ASTM D3999. (1996). “Standard Test Methods for the Determination of the Modulus and Damping Properties of Soils Using the Cyclic Triaxial Apparatus,” ASTM International, West Conshohocken, PA., Unite States.

ASTM D4439. (2002). “Standard terminology for geosynthetics,” ASTM International, West Conshohocken, PA., Unite States.

ASTM D5321. (2008). “Determining the coefficient of soil and geosynthetic or geosynthetic and geosynthetic friction by the direct shear method,” ASTM International, West Conshohocken, PA., Unite States.

ASTM D5322. (2009). “Standard practice for immersion procedures for evaluating the chemical resistance of geosynthetics to liquids,” ASTM International, West Conshohocken, PA., Unite States.

ASTM D5496. (1998). “Standard practice for in field immersion testing of geosynthetics,” ASTM International, West Conshohocken, PA., Unite States.

ASTM D5747. (1998). “Standard practice for tests to evaluate the chemical resistance of geomembranes to liquids,” ASTM International, West Conshohocken, PA., Unite States.

ASTM D6243. (2008). “Determining the internal and interface shear resistance of geosynthetic clay liner by the direct shear method,” ASTM International, West Conshohocken, PA., Unite States.

Bilgili, M. S., Demir, A., Ince, M. and Ozkaya, B. (2007). “Metal concentrations of simulated aerobic and anaerobic pilot scale landfill reactors,” Journal of Hazardous Materials, Vol. 145, pp.186-194

Bouazza, A., Zornberg, J. G. and Adam, D. (2002). “Geosynthetics in waste containment facilities: recent advances,” In Proceedings of 7th International Conference on Geosynthetics, Nice, Vol. 90, No. 5809, pp. 445-507

Cassidy, P. E., Mores, M., Kerwick, D. J. and Koeck, D. J. (1992). “Chemical resistance of geosynthetic materials,” Geotextiles and Geomembranes, Vol. 11, pp. 61-98

Christensen, T. H., and Kjeldsen, P. (1995). “Landfill emissions and environmental impact: An introduction in SARDINIA ‘95,” In Proceedings of 5th International Landfill Symposium, Vol. 3, CISA, Cagliari, Italy.

Chu, H. H. and Vucetic, M. (1992). “Settlement of compacted clay in a cyclic direct simple shear device,” Geotechnical Testing Journal, Vol. 15, No. 4, pp. 371-379

Das, B. M. (1993). “Principles of soil dynamics,” PWS-KENT Publishing Company, Boston, Massachusetts, U.S.A., pp. 111-116

De, A. and Zimmie, T. F. (1997). “Landfill stability: static and dynamic geosynthetic interface friction value,” Geosynthetic Asia’97, Bangalore, India, pp. 271-278

Desai, C. S. (1974). “A consistent finite element technique for work-softening behavior,” In Proceedings of International Conference on Computer Mechanics In Nonlinear Mechanics, University of Texas Press, Austin, Texas

Desai, C. S. (1981). “Behavior of interfaces between structural and geologic media,” In Proceedings of International Conference on Recent Advances in Geotechnical Earthquake Engineering and Soil Dynamics, St. Louis, MO.

Desai, C. S. (1995). “Chapter 8: Constitutive Modeling Using the Disturbed State as Microstructure Self-Adjustment Concept,” Continuum Models for Material with Microstructure, H.B. Muhlhaus, ed., John Wiley & Sons, U.K.

Desai, C. S. (2001). “Mechanics of materials and interfaces – The Disturbed State Concept,” CRC Press LLC, 2000, N.W., pp. 18-77, 422-468

Desai, C. S. and Ma, Y. (1992). “Modeling of joints and interfaces using the disturbed state concept,” International Journal for Numerical and Analytical Methods in Geomechanics, Vol. 16, No. 9, 623-653

Desai, C. S. and Nagaraj, B. K. (1988). “Modeling for cyclic normal and shear behavior of interfaces,” Journal of Engineering Mechanics, Vol. 114, No. 7, 1198-1217

Desai, C. S. and Rigby, D. B. (1997). “Cyclic interface and joint shear device including pore pressure effects,” Journal of Geotechnical and Geoenvironmental Engineering, Vol. 123, No. 6, pp. 568-579

Desai, C. S., Shao, C. and Rigby, D. B. (1996). “Discussion to Evaluation of Soil Liquefaction by energy principles,” by Figueroa et al., Journal of Geotechnical Engineering, ASCE Vol. 122, No. 3, pp. 241-242

Desai, C. S., Shashank, K. P. and Cohen, D. (2005). “Cyclic testing and constitutive modeling of saturated sand-concrete interfaces using the disturbed state concept,” International Journal of Geomechanics, Vol. 5, No. 4, pp. 286-294

Ehrig, H.J. (1988). “Water and element balances of landfills,” The Landfill, Baccini, P., Eds., Springer Verlag, Berlin, Germany, pp. 83-115

Eith, A. W. and Koerner, R. M. (1997). "Assessment of HDPE geomembrane performance in a municipal waste landfill double liner system after eight years of service," Geotextiles and Geomembranes Vol. 15, No. 4, pp. 277-287.

Fakharian, K. and Evgin, E. (1996). “An automated apparatus for three-dimensional monotonic and cyclic testing of interfaces,” Geotechnical Testing Journal, Vol. 19, No. 1, pp. 22-31

Fakharian, K. and Evgin, E. (1997). “Cyclic simple-shear behavior of sand-steel interfaces under constant normal stiffness condition,” Journal of Geotechnical and Geoenvironmental Engineering, Vol. 123, No. 12, pp. 1096-1105

Fishman, K. L. and Pal, S. (1994). “Further study of geomembrane/cohesive soil interface shear behavior,” Geotextiles and Geomembranes, Vol. 13, pp. 571-590

Finn, W. D. L., Pickering, D. J. and Bransby, P. L. (1971). "Sand liquefaction in triaxial and simple shear test," Journal of the Soil Mechanics and Foundations Division, In Proceedings the American Society of Civil Engineers, Vol. 97, No. SM4, April, pp. 639-659

Gere, J. M. and Timoshenko, S. P. (1991). “Mechanics of materials,” 3rd Eds., Chapman & Hall, Singapore, pp. 29-31

Gidigasu, M. D. (1976). “Laterite Soil Engineering: Pedogenesis and Engineering Principles,” Elsevier Scientific Publication Company, Amsterdam, pp. 35-36

Gilbert, R. B., Scranton, H. B. and Daniel, D. E. (1997). “Shear strength testing for geosynthetic clay liners,” Wells, L. W. Eds., Testing and Acceptance for Geosynthetic Clay Liners, SPT 1308, American Society for Testing and Materials, pp. 121-135

Hazirbaba, K. (2005). “Pore pressure generation characteristics of sands and silty sands: A strain approach,” Ph.D dissertation, The University of Texas, Austin

Hawkins, W. L. (1984). “Polymer degradation and stabilization, Polymers” Polymers – Properties and Applications Series, Vol. 8, Springer, Berlin/Heidelberg, Germany, pp. 119

Hsuan, Y. G. and Koerner, R. M. (1995). “The single point – Notched constant tension load test: A quality control test for assessing stress crack resistance,” Geosynthetics International, Vol. 2, No. 5, pp. 831-843

Hsuan, Y. G., Lord Jr., A. E. and Koerner, R. M. (1991). “Effects of outdoor exposure on high density polyethylene geomembrane,” In Proceedings of Geosynthetics ’91, Atlanta, IFIA, St. Paul, MN, USA, pp. 287-302

Ishihara, K. G. (1996). “Soil behavior in earthquake engineering,” Oxford, Clarendon Press.

Iverson, N. R., Mann, J. E. and Iverson, R. M. (2010). “Effects of soil aggregates on debris-flow mobilization: Results from ring-shear experiments,” Engineering Geology, Vol. 114, pp. 84-92

Jiang, Y., Xiao, J., Tanabashi, Y. and Mizokami, T. (2004). “Development of an automated servo-controlled direct shear apparatus applying a constant normal stiffness condition,” International Journal of Rock Mechanics and Mining Sciences, Vol. 41, pp. 275-286

Jeon, H. Y., Kim, S. H., Lyoo, W. S., Yoo, C., and Koerner, G. R. (2006). “Evaluation of the long-term performance of geosynthetic reinforcements from their reduction factors,” Polymer Testing, Vol. 25, pp. 289-295

Kjeldsen, P., Barlaz, M. A., Rooker, A. P., Baun, A., Ledin, A., and Christensen, T. H. (2002). “Present and long-term composition of MSW landfill leachate: A review,” Critical reviews in environmental science and technology, Vol. 32, No. 4, pp. 297-336.

Kjellman, W. (1951) "Testing the shear strength of clay in Sweden," Geotechnique, Vol. 2, No. 3, pp. 225-235

Koerner, R. M. (2005). “Designing with geosynthetics,” 6th Edition, Xlibris Corporation, pp. 2-15, 165-171

Koerner, R. M., Soong, T. Y. and Gontar, A. (1998). “Selected aspects of GCL shear strength testing,” In Proceedings of Geo-Beno 1998, Insatec Publications, France, pp. 97-110

Kwak, C. W., Park, I. J., and Park, J. B. (2013)[a]. “Evaluation of disturbance function for geosynthetic–soil interface considering chemical reactions based on cyclic direct shear tests,” Soils and Foundations, Vol. 53, No. 5, pp. 720-734

Kwak, C. W., Park, I. J., and Park, J. B. (2013)[b]. “Modified cyclic shear test for evaluating disturbance function and numerical formulation of geosynthetic–soil interface considering chemical effect,” Geotechnical Testing Journal, Vol. 36, No. 4, pp. 553-567

Kwak, C. W., Park, I. J., and Park, J. B. (2014). “Dynamic Shear Behavior of Concrete-soil Interface based on Cyclic Simple Shear Test,” KSCE Journal of Civil Engineering, Vol. 18, No. 3, pp. 1-7

Kim, C. S., Ahn, S. H., Jang, D. Y. (2012) “Review: developments in micro/nanoscale fabrication by Focused Ion Beams”, Vaccum, Vol. 86, pp. 1014-1035

Pease, R. F. W., Nixon, W. C. (1965) “High resolution scanning electron microscopy”, Journal of Scientific Instruments, Vol. 42, pp. 81-85

Lee, K. M. and V. R. Manjunath. (2000), “Experimental and numerical studies of geosynthetic-reinforced sand slopes loaded with a footing,” Canadian Geotechnical Journal Vol. 37, No. 4, pp. 828-842.

Leichnitz, W. (1985). “Mechanical properties of rock joints,” International Journal of Rock Mechanics and Mining Sciences, Vol. 22, No. 5, pp. 313-321

Ling, H. I., Burke, C., Mohri, Y. and Matsushima, K. (2002). “Shear strength parameters of soil-geosynthetic interfaces under low confining pressure using a tilting table,” Goesynthetics International, Vol. 9, No. 4, pp. 373-380

Liu, S. H., Sun, D. and Matsuoka, H. (2005). “On the interface friction in direct shear test,” Computers and Geotechnics, Vol. 32, pp. 317-325

Ma, Y. (1990). “Disturbed state concept for rock joints,” Ph.D Dissertation, Department of Civil Engineering and Engineering Mechanics, University of Arizona, Tuscon, Arizona

Masada, T., Mithell, G. F., Sargand, S. M. and Shashikumar, B. (1994). “Modified direct shear study of clay liner-geomembrane interfaces exposed to landfill leachate,” Geotextiles and Geomembranes, Vol. 13, pp. 165-179

Martin, J. P., Koerner, R. M. and Whitty, J. E. (1984). “Expeimental friction evaluation of slippage between geomembranes, geotextiles, and soils,” International Conference on Geomembranes, Denver, IFAI, St. Paul, Minnesota, pp. 191-196

Matasovic, N., Kavazanjian, E., and Anderson, R. L. (1998). “Performance of solid waste landfills in earthquakes,” Earthquake Spectra, Vol. 14, No. 2, pp. 319-334

Menut, D., Fichet, P., Lacour, J. L., Rivoallan, A. and Mauchien, P. (2003) “Micro-laser-induced breakdown spectroscopy technique: A powerful method for performing quantitative surface mapping on conductive and nonconductive samples”, Applied Optics, Vol. 42, No. 30, pp. 6063-6071

Mor, S., Ravindra, K., Dahiya, R. P. and Chandra, A. (2006). “Leachate characterization and assessment of groundwater pollution near municipal solid waste landfill site,” Environmental Monitoring and Assessment, Vol. 118, pp. 435-456

Mortezaie, A. R. and Vucetic, M. (2012). “Small-strain cyclic testing with standard NGI simple shear device,” Geotechnical Testing Journal, Vol. 35, No. 6, pp. 935-948

Navayogarajah, N. and Desai, C. S. (1992). “Hierarchical single-surface model for static and cyclic behavior of interfaces,” Journal of Engineering Mechanics, Vol. 118, No. 5, 990-1011

Oden, J. T. and Pires, T. B. (1983). “Nonlocal and nonlinear friction laws and variational principles for contact problems in elasticity,” Journal of Applied Mechanics, Vol. 50, pp. 67-75

Ooi, L. H. and Carter, J. P. (1987). “A constant normal stiffness direct shear device for static and cyclic loading,” Geotechnical Testing Journal, Vol. 10, No. 1, pp. 3-12

O’reilly, M. P., Brown, S. F. (1991). “Cyclic loading of soils: from theory to design,” New York, Blackie and Son.

Orloff, K. and Falk, H. (2003). “An international perspective on hazardous waste practices,” International Journal of Hygiene and Environmental Health, Vol. 206, pp. 291-302.

Oweis, I. S. and Khera, R. P. (1998). "Geotechnology of waste management," 2nd Edition, PWS Publishing Company, Boston, MA, pp. 1-24295-299

Pal, S. and Wathugala, G. W. (1999). “Disturbed state model for sand-geosynthetic interfaces and application to pull-out tests,” International Journal for Numerical and Analytical Methods in Geomechanics, Vol. 23, 1873-1892

Park, I. J. (1997). “Disturbed state modeling for dynamic and liquefaction analysis,” Ph.D Dissertation, Department of Civil Engineering and Engineering Mechanics, University of Arizona, Tuscon, Arizona

Park, I. J. and Desai, C. S. (2000). “Cyclic behavior and liquefaction of sand using disturbed state concept,” Journal of Geotechnical and Geoenvironmental Engineering, ASCE, Vol. 126, No. 9, 834-846

Park, I. J., Kwak, C. W. and Kim, J. K. (2010). “The characteristics of dynamic behaviors for geosynthetic-soil interface considering chemical influence factors,” Journal of Korean Geo-Environmental Society, Vol. 11, No. 11, pp. 47-54

Park, I. J., Yoo, J. H. and Kim, S. I. (2000). “Disturbed state modeling for dynamic analysis of soil-structure interface,” Journal of the KGS Vol. 16, No. 3, 5-13

Peacock, W. H. and Seed, H. B. (1968). "Sand liquefaction under cyclic loading simple shear conditions," Journal of the Soil Mechanics and Foundations Division, In Proceedings the American Society of Civil Engineers, Vol. 94, No. SM3, May, pp. 689-708

Pestana, J. M., Biscontin, G., Nadim, F. and Andersen, K. (2000), “Modeling cyclic behavior of lightly overconsolidated clays in simple shear,” Soil Dynamics and Earthquake Engineering, Vol. 19, pp. 501-519

Press release No. 13-164. (2013). Green Urban Environment Division, Infrastructure Bureau, Multifunctional Administrative City Construction Agency, August, 2013

Rafizul, I. M. and Alamgir, M. (2012). “Characterization and tropical seasonal variation of leachate: Results from landfill lysimeter studied,” Waste Management, Vol. 32, pp.2080-2095

Raghavan, P. and Ghosh, S. (2005) “A continuum damage mechanics model for unidirectional composites undergoing interfacial debonding”, Mechanics of Materials, Vol.37, pp. 955-979

Rigby, D. B. and Desai, C.S. (1995) “Testing, modeling, and application of saturated interfaces in dynamic soil-structure interaction,” Report to the NSF, Department of Civil Engineering and Engineering Mechanics, University of Arizona, Tuscon, Arizona

Roscoe, K. H. (1953). "An apparatus for the application of simple shear to soil samples," In Proceedings the Third International Conference on Soil Mechanics and Foundation Engineering, Zurich, Switzerland, pp. 186-191

Rowe, R. K. and Sangam, H. P. (2002). “Durability of HDPE Geomembranes,” Geotextiles and Geomembranes, No. 20, Elsevier Science Publishers, Ltd., England, pp. 77-95

Sassa, K., Fukuoka, H., Wang, G. and Ishikawa, N. (2004). “Undrained dynamic-loading ring-shear apparatus and its application to landslide dynamics,” Landslides, Vol. 1, pp. 7-19

Schlegel, M. L., Bataillon, C., Benhamida, K., Blanc, C., Menut, D. and Lacour, J. L. (2008) “Metal corrosion and argillite transformation at the water-saturated, high-temperature iron–clay interface: A microscopic-scale study”, Applied Geochemistry, Vol. 23, pp. 2619-2633

Schmidt, R. K., Young, C. and Hewitt, J. (1984). “Long term field performance of geomembranes – fifteen years’ experience,” In Proceedings of International Conference of Geomembrane, St. Paul, Minnesota, Vol. 2, pp. 307-310

Seed, H. B. and Peacock, W. H. (1971). "Test pocedures for masuring Soil liquefaction characteristics," Journal of the Soil Mechanics and Foundations Division, In Proceedings the American Society of Civil Engineers, Vol. 97 No. SM8, August, pp. 1099-1119

Seo, M. W., Park, I. J. and Park J. B. (2004). “Development of displacement-softening model for interface shear behavior between geosynthetics,” Soils and Foundations, Vol. 44, No. 6, pp. 27-38

Seo, M. W., Park, J. B. and Park I. J. (2007). “Evaluation of interface shear strength between geosynthetics under wet condition,” Soils and Foundations, Vol. 47, No. 5, pp. 845-856

Shibuya, S. Mitachi, T., Fukuda, F. and Degoshi, T. (1995). “Strain-rate effects on shear modulus and damping of normally consolidated clay,” Geotechnical Testing Journal, Vol. 18, No. 3, pp. 365-375

Silva, W. J., Turcotte, T. and Moriwaki, Y. (1988). “Soil response to earthquake ground motion,” EERI Report NP-5747, Electric Power Research Institute, Palo Alto, CA

Song, B. W., Yasuhara, K. and Murakami, S. (2004). “Direct simple shear testing for post-cyclic degradation in stiffness of nonplastic silt,” Geotechnical Testing Journal, Vol. 27, No. 6, pp. 607-613

Stark, T. D. and Poeppel, A. R. (1994). “Landfill liner interface strengths from torsional-ring-shear tests." Journal of Geotechnical Engineering Vol. 120, No. 3, pp. 597-615.

Stark, T. D., Williamson, T. A. and Eid, H. T. (1996). “HDPE geomembrane/geotextile interface shear strength,” Journal of Geotechnical Engineering, Vol. 122, No. 3, pp. 197-203

Stessel, R. I. and Hodge, J. S. (1995). “Chemical resistance testing of geomembrane liners,” Journal of Hazardous Materials, Vol. 42, pp. 265-287

Takasumi, D. L., Green, K. R. and Holtz, R. D. (1991). “Soil-geosynthetics interface strength characteristics: a review of state-of-the-art testing procedures,” In Proceedings of Geosynthetics’91, Atlanta, USA, pp. 87-100

Tan, S. A., Chew, S. H. and Wong, W. K. (1998). “Sand-geotextile interface shear strength by torsional ring shear tests,” Geotextiles and Geomembranes, Vol. 16., pp. 161-174

Thurairajah, A. (1974). “Shear behavior of sand under stress reversal,” Proceedings of the 8th International Conference on Soil Mechanics and Foundation Engineering , Vol. 1.2, Moscow, pp. 439-445

Tisinger, L. G. and Giroud, J. P. (1993). “The durability of HDPE geomembranes,” Geotechnical Fabrics Report, Vol. 11, No. 6, pp. 4-8

US EPA 9090a. (1992). “Compatibility test for wastes and membrane liners,” www.epa.gov/osw/hazard/testmethods/sw846/pdfs/9090a.pdf

Vandervoort, J. (1992). “The use of extruded polymers in the containment of hazardous wastes,” Schlegel Lining Technology Inc., The Woodlands, TX

Weibull, W. (1951). “A statistical distribution function of wide applicability,” Journal of Applied Mechanics, Vol. 18, pp. 293-297

Zania, V., Tsompanakis, Y., Psarropoulos, P. N. (2010). “Seismic displacements of landfills and deformation of geosynthetics due to base sliding,” Geotextiles and Geomembranes, Vol. 28, pp. 491-502

Zehnder, A. J. B., Ingvorsen, K. and Marti, T. (1982). “Microbiology of methane bacteria,” Anaerobic Digestion, Vol. 45, Elsevier Biomedical Press B.V., Amsterdam, The Netherlands

Zornberg, J. G. and Christopher, B. R. (1999). “Geosynthetics,” Chapter 27, The Handbook of Groundwater Engineering, CRC Press, Inc., Boca Raton, Florida.

초 록

폐기물 매립장에 널리 사용되는 토목섬유는 보강, 여과, 배수, 보호 및 분리 등의 여러 기능을 담당한다. 따라서 토목섬유는 흙 입자와 직접 접촉하여 토목섬유-흙 접촉면을 형성하게 되며 이러한 접촉면의 공학적 거동 특성은 외력과 주위 조건에 의하여 영향을 받는다. 특히 접촉면의 전단 거동은 접촉면을 형성하는 재료의 고유 물성에 따라 복잡한 비선형 거동을 보인다. 최근의 연구는 이러한 토목섬유-흙 접촉면에서의 전단거동에 영향을 미치는 주변 조건, 즉 연직응력, 하중의 형태, 화학적 조건 등에 대하여 활발히 이루어지고 있다.

본 연구에서는 이러한 조건 중 폐기물 매립장 내 침출수에서 발생하는 산성 또는 염기성과 같은 화학성분이 토목섬유-흙 접촉면의 동적 전단거동에 미치는 영향을 실험적 연구를 통하여 파악하였다. 이를 위하여 반복단순전단시험을 수행할 수 있는 다기능 접촉면 전단시험기를 새로이 구축하고 보완하였다. *p*H 조건에 따라 총 72회의 반복단순전단시험을 수행하여 *p*H 조건이 접촉면 전단거동에 미치는 영향을 분석하였다. 토목섬유와 주문진 표준사를 산성, 중성 및 염기성 용액에 각각 30일 및 850일간 수침시켜 단기 및 장기거동을 각각 알아보고자 하였다. 시험 결과는 수침 용액의 *p*H 조건에 따라 전단응력 저감 정도에 현저한 차이를 보였으며, 이러한 전단응력 저감거동을 정량적으로 파악하기 위하여 교란상태개념 및 교란도 함수를 도입하였다. 또한 시험 결과에 따라 각 조건별로 교란도 함수의 새로운 파라메터인 A, Z 값을 새로이 제안하였다.

또한 화학적 조건에 의하여 서로 다른 교란도 함수 형태를 보이는 원인을 미세구조적 관점에서 파악하기 위하여 집속이온빔장치에 의한

전자현미경 관측을 수행하였다. 그 결과, 토목섬유-흙 접촉면 거동이 화학적 조건에 의하여 차이를 보이는 가장 큰 이유는 산성, 중성, 염기성에 수침된 흙 입자의 표면 손상형태가 다르기 때문임을 파악하였다.

실내시험 결과를 바탕으로 획득한 교란도 함수의 적정성을 검증하기 위하여 수치보간법에 의한 역해석을 수행하였다. 역해석을 통하여 반복 전단응력-변형율 거동을 재현하는 기법을 제시하고 이를 이용하여 재현된 전단응력-변형율 곡선이 시험 결과와 잘 일치함을 확인하였다.

결론적으로, 폐기물 매립장에서 화학적 영향을 고려한 토목섬유-흙 접촉면의 동적 전단거동을 정량적으로 파악하여 해석에 반영할 수 있는 일련의 방법론을 완성하였다..

주요어: 토목섬유-흙 접촉면, 화학조건, 다기능 접촉면 전단시험기, 반복단순전단시험, 교란상태개념, 집속이온빔장치, 역해석